

FINAL REPORT

PROCEDURES FOR CONTROLLING
THE EFFECT OF INCREASED TIRE PRESSURE
ON ASPHALT CONCRETE PAVEMENT DAMAGE

Ok-Kee Kim

Assistant Professor of Civil Engineering
Oregon State University

C.A. Bell

Associate Professor of Civil Engineering
Oregon State University

James E. Wilson

Assistant Engineer of Materials
Oregon Department of Transportation

FWWAOR-KD-83-01

June 1988

1. Report No. FHWA-OR-RD-88-01		2. Government Accession No.		3. Recipient's Catalog No.	
4. Title and Subtitle Procedures for Controlling the Effect of Increased Tire Pressure on Asphalt Concrete Pavement Damage				5. Report Date June 1988	
				6. Performing Organization Code	
7. Author(s) Ok-Kee Kim, C.A. Bell and James E. Wilson				8. Performing Organization Report No. TE-87-14	
9. Performing Organization Name and Address Oregon State University Department of Civil Engineering Corvallis, OR 97331-2302				10. Work Unit No. (TRAIS)	
				11. Contract or Grant No. HP&R 5168	
12. Sponsoring Agency Name and Address Oregon Dept. of Transportation U.S. Dept. of Trans. Materials & Research Section Fed. Hwy. Admin. Salem, OR 97310 Office of R&D Washington, D.C. 20590				13. Type of Report and Period Covered Final August 1985 - June 1988	
				14. Sponsoring Agency Code	
15. Supplementary Notes					
16. Abstract As the axle load increases, higher tire pressures become more popular for long-haul truck operators. In order to collect data on tire pressures and the types of tires in use, a survey was carried out at a weigh station located on Interstate 5 in Oregon during the summer of 1986. The data show that 87% of the tires surveyed were of radial construction. The average measured pressures (hot) of the radial and bias tires were 102 psi and 82 psi, respectively. This study investigates the influence of increased tire pressures on the fatigue and rutting performance (in terms of vertical compressive stress, tensile strain, and compressive strain) of asphalt-surfaced pavements, through use of elastic layer analysis (ELSYM5), for two typical state highways in Oregon. This theoretical analysis shows that the effect of increased tire pressure on vertical compressive stress is significant in the asphalt wearing layer. As tire pressure increases, the maximum tensile strain at the bottom of the asphalt layer increases. Theoretical equivalency factors for the two asphalt pavements (SN = 3.0 and 3.4) were developed using ELSYM5 to take into account tire pressures (80, 100, 125, and 150 psi) and number of tires per axle (2, 4, and 8 tires). A single axle with an 18-kip load, dual tires, and a tire pressure of 80 psi was used as a standard axle load and tire pressure. The results indicate that a 25% increase in tire pressure could result in a 40 to 60% increase in the equivalency factor for a dual-tired single axle with an 18-kip load or a tandem axle with a 34-kip load. However, this theoretical analysis needs to be verified by field studies. In order to evaluate current asphalt concrete specifications and mix design criteria, aggregate from four different sources were tested. Two of the aggregates were treated with 1% lime slurry prior to testing. Six different aggregate gradations, including Fuller maximum density gradation, were tested. In addition to the routine asphalt concrete mix tests, a simple creep test was run for 3 hours at 40°C with a compression stress of 0.1 MPa. In general, the creep stiffness decreased proportionally to the percentage of fines passing the #200 size sieve. The effect of the percentage of aggregates passing 1/4-in. or #10 sieve sizes on the creep stiffness is not clear. The results show that treating the aggregates with 1% lime slurry improves the resistance to deformation of the asphalt concrete mixes.					
17. Key Words Higher tire pressures, fatigue, rutting, asphalt pavements, ELSYM5, equivalency factor, aggregate gradation, creep test, lime slurry			18. Distribution Statement No Restrictions This report is available through the National Technical Information Service Springfield, VA 22161		
19. Security Classif. (of this report) Unclassified		20. Security Classif. (of this page) Unclassified		21. No. of Pages 162	22. Price

ABSTRACT

As the axle load increases, higher tire pressures become more popular for long-haul truck operators. In order to collect data on tire pressures and the types of tires in use, a survey was carried out at a weigh station located on Interstate 5 in Oregon during the summer of 1986. The data show that 87% of the tires surveyed were of radial construction. The average measured pressures (hot) of the radial and bias tires were 102 psi and 82 psi, respectively.

This study investigates the influence of increased tire pressures on the fatigue and rutting performance (in terms of vertical compressive stress, tensile strain, and compressive strain) of asphalt-surfaced pavements, through use of elastic layer analysis (ELSYM5), for two typical state highways in Oregon. This theoretical analysis shows that the effect of increased tire pressure on vertical compressive stress is significant in the asphalt wearing layer. As tire pressure increases, the maximum tensile strain at the bottom of the asphalt layer increases.

Theoretical equivalency factors for the two asphalt pavements (SN = 3.0 and 3.4) were developed using ELSYM5 to take into account tire pressures (80, 100, 125, and 150 psi) and number of tires per axle (2, 4, and 8 tires). A single axle with an 18-kip load, dual tires, and a tire pressure of 80 psi was used as a standard axle load and tire pressure. The results indicate that a 25% increase in tire pressure could result in a 40 to 60% increase in the equivalency factor for a dual-tired single axle with an 18-kip load or a tandem axle with a 34-kip load. However, this theoretical analysis needs to be verified by field studies.

In order to evaluate current asphalt concrete specifications and mix design criteria, aggregate from four different sources were tested. Two of the aggregates were treated with 1% lime slurry prior to testing. Six different aggregate gradations, including Fuller maximum density gradation, were tested. In addition to the routine asphalt concrete mix tests, a simple creep test was run for 3 hours at 40°C with a compression stress of 0.1 MPa. In general, the creep stiffness decreased proportionally to the percentage of fines passing the #200 size sieve. The effect of the percentage of aggregates passing 1/4-in. or #10 sieve sizes on the creep stiffness is not clear. The results show that treating the aggregates with 1% lime slurry improves the resistance to deformation of the asphalt concrete mixes.

KEY WORDS

Higher tire pressures, fatigue, rutting, asphalt pavements, ELSYM5, equivalency factor, aggregate gradation, creep test, lime slurry.

ACKNOWLEDGEMENTS

This report presents the results from a HP and R (Highway Planning and Research) study, conducted by the Oregon State Highway Division and Oregon State University in cooperation with the Federal Highway Administration.

The contribution of Glenn Boyle and his staff in obtaining materials and preparing mix designs was invaluable. Special appreciation is given to Ken Evert and his staff who collected tire pressure data (total of about 2700 tires) day and night during the summer of 1986.

The authors are indebted to Laurie Dockendorf and Peggy Offutt of the Engineering Experiment Station, Oregon State University, who typed the manuscript.

DISCLAIMER

The contents of this report reflect the views of the authors who are responsible for the facts and accuracy of the data presented. The contents do not necessarily reflect the official views or policies of either the Oregon State Highway Division or Federal Highway Administration at the time of publication.

This report does not constitute a standard specification or regulation.

TABLE OF CONTENTS

	<u>Page</u>
1.0 INTRODUCTION.	1
1.1 Problem Statement.	1
1.2 Objectives	1
1.3 Research Approach.	2
1.4 Significance of Study.	2
2.0 BACKGROUND.	4
2.1 Tire Pressure Distribution	7
2.2 Load Equivalency Factor.	9
2.3 Pavement Performance Analysis.	10
2.4 Mix Design	12
2.5 Tire Construction.	19
2.6 Creep Test	26
2.7 Other Considerations	29
3.0 EXPERIMENT DESIGN - TESTS ON ASPHALT CONCRETE MIXTURES.	31
3.1 Variables Considered	31
3.2 Specimen Preparation and Test Program.	33
3.3 Test Methods	33
3.3.1 Resilient Modulus	33
3.3.2 Creep Test.	37
4.0 RESULTS	39
4.1 Operating Characteristics of Oregon's Trucks	39
4.1.1 Preliminary Results	39
4.1.2 Truck Types	41
4.1.3 Tire Pressure	41
4.1.4 Tread Depth	41
4.1.5 Tire Size	57
4.1.6 Manufacturer.	57

	<u>Page</u>
4.2 Mix Designs.	57
4.3 Creep Test	65
4.4 Analysis of Pavement Structure	70
5.0 DISCUSSION.	75
5.1 Tire Pressure.	75
5.2 Mix Design	78
5.3 Creep Behavior of Mixes.	83
5.4 Analysis of Asphalt Concrete Pavement Structures	85
5.4.1 Pavement Analysis	85
5.4.2 Equivalency Factors	101
5.4.3 Rut Depth	111
6.0 CONCLUSIONS AND RECOMMENDATIONS	113
6.1 Summary.	113
6.2 Conclusions.	114
6.3 Recommendations.	116
7.0 REFERENCES.	118
APPENDIX A - CREEP TEST PROCEDURE.	123
APPENDIX B - TIRE PRESSURE DATA.	136
APPENDIX C - CALCULATION FOR EQUIVALENCY FACTORS	148
APPENDIX D - EQUIVALENCY FACTORS FOR PAVEMENTS A AND B IN FIGURE 4.6	152
APPENDIX E - PROCEDURE USING THE SHELL METHOD TO PREDICT THE RUT DEPTH IN ASPHALT CONCRETE PAVEMENTS	155

LIST OF TABLES

<u>Table</u>	<u>Page</u>
2.1 Incremental Incentives to Overweight (After Ref. 3)	6
2.2 Aggregate Gradations for Oregon's Asphalt Concrete and Fuller Maximum Density	16
2.3 Factors Influencing Tender Pavements (After Ref. 25).	18
2.4 Bias versus Radial Performance Testing (After Ref. 28).	23
3.1 Extracted Mix Aggregate Gradations (A through F).	32
3.2 Gradations Used in Mixtures for Each Aggregate Source	34
3.3 Physical Properties of Asphalt Cement	35
4.1 Number of Trucks in the Sample.	42
4.2 Mean Values of Manufacturer's Maximum Recommended Tire Pressure (Cold).	47
4.3 Mean Values of Measured Tire Pressure (Hot)	47
4.4 Mean Values of Measured Tread Depth (1/32-in.)	56
4.5 Tire Size Distribution.	58
4.6 Distribution of Tire Manufacturer (%)	60
4.7 Summary of Mix Design Data	
(a) Morse Brothers Pit	61
(b) Cobb Rock Quarry	62
(c) Hilroy Pit	63
(d) Blue Mountain Asphalt Pit.	64
4.8 Creep Test Results	
(a) Morse Brothers Pit	66
(b) Cobb Rock Quarry	67
(c) Hilroy	68
(d) Blue Mountain Asphalt Pit.	69
4.9 Effect of Increased Tire Pressure on Tensile Strain at the Bottom of the Asphalt Concrete Base Course	72
4.10 Effect of Increased Tire Pressure on Compressive Strain at the Top of the Subgrade	73

<u>Table</u>	<u>Page</u>
5.1 Mean Value of Tire Pressure Difference Between Maximum Recommended Pressure (Cold) and Measured Pressure (Hot)	76
5.2 Correlation Analysis	
(a) Correlations with log(Creep Stff., ksi).	79
(b) Correlations with log(Slope)	80
(c) Correlations with log(Intercept)	81
(d) Correlations with log(Stability)	82

LIST OF FIGURES

<u>Figure</u>	<u>Page</u>
2.1 Cargo Weight vs. Line Haul Cost (After Ref. 3).	5
2.2 Distribution of Truck Tire Inflation Pressures from Texas Studies (1984-85) (After Ref. 5).	8
2.3 Concentric Cylinder Pressure Distribution (After Ref. 9).	8
2.4 Classifications Used in Oregon's Weigh-in-Motion Study (After Ref. 15).	11
2.5 Variation of Vertical Stress with Depth, Boussinesq Problem (After Ref. 8).	13
2.6 Effect of Number of Wheels on Vertical Stress, Boussinesq Problem (After Ref. 8).	13
2.7 Rating Scale to Identify Tender Mixtures (After Ref. 25).	20
2.8 Cross-Bias Tire (After Ref. 27)	22
2.9 Break Layers in Cross-Bias Tire (After Ref. 27)	22
2.10 Radial Ply Rigid Breaker Tire (Radial Tire) (After Ref. 27)	23
2.11 Conventional vs. Low Aspect Ratio Comparison (After Ref. 28).	25
2.12 The Improvement in Creep Behavior Given by Substituting Crushed for Rounded Aggregate (After Ref. 32)	27
2.13 The Effects of Various Methods of Compaction on the Creep Behavior of an Asphaltic Concrete Mix (After Ref. 32)	27
3.1 Flowchart for Test Program.	36
4.1 Tire Pressure Data Collection Sheet	40
4.2 The Distribution of the Manufacturer's Maximum Recommended Tire Pressure (Cold)	43
4.3 The Distribution of the Measured Tire Pressure (Hot).	48
4.4 Distribution of Measured Tread Depth.	52
4.5 Tire Sizing Designations (After Ref. 41).	59
4.6 Typical Asphalt Concrete Pavement Structural Sections in Oregon	71
4.7 Axle and Tire Configurations for ELSYM5 Analysis.	74

<u>Figure</u>	<u>Page</u>
5.1 Effect of Asphalt Content on Creep Stiffness.	86
5.2 Vertical Compressive Stress Through the Pavement Structure.	89
5.3 Horizontal Strain in the Asphalt Concrete Pavement.	93
5.4 Vertical Compressive Strain Through the Pavement Structure.	97
5.5 Equivalency Factors for Pavement A.	102
5.6 Equivalency Factors for Pavement B.	107

1.0 INTRODUCTION

1.1 Problem Statement

The economics of truck transportation has tended to cause the average gross weight of trucks to increase such that the majority of trucks are operating close to the legal gross loads or axle loads (1). Many states, including Oregon, also issue permits for trucks to operate above normal legal load limits (2).

As the axle loads increase, the use of higher tire pressures has become more popular. Higher tire pressures decrease the tire-to-pavement contact area, resulting in reduced tire rolling friction, skid resistance, and increased potential for pavement damage under the high stress. The higher tire pressures contribute to greater deformation in flexible pavements which is manifested by high severity wheel track rutting. The higher tire pressures also tend to be accompanied by higher axle loads, and these pressures and loads tend to increase the severity of pavement fatigue cracking.

This study will assess the consequent impacts on flexible pavements due to the increased tire pressures used by trucks and present recommendations for dealing with the problem.

1.2 Objectives

The objectives of this study are:

- 1) To determine the existing operating characteristics of Oregon's long-haul trucks, including levels of tire pressure.
- 2) To develop the use of a simple method of creep testing and to use the Shell rut depth prediction method, in order to predict deformation in asphalt concrete pavements.

- 3) To evaluate the effectiveness of existing asphalt concrete mixture specifications and design methods of the Oregon Department of Transportation (ODOT) in limiting the excessive deformation caused by higher axle loads and tire pressures.
- 4) To recommend a comprehensive methodology to specify and design asphalt concrete mixtures and asphalt concrete pavements that minimize damage from higher tire pressures.

1.3 Research Approach

The research included a survey of existing truck operating characteristics in Oregon and the investigation of the damage to asphalt concrete pavements due to the increased tire pressures. This assessment of pavement damage due to higher tire pressure is a theoretical study. In addition, laboratory tests, specifications, mix design guidelines, and pavement structure design procedures were investigated to determine their effectiveness in providing pavements with adequate resistance to the effects of higher tire pressures.

1.4 Significance of Study

This study is very significant in view of the potential economic savings which could occur from improved selection of asphalt concrete mixtures. The effects of increased tire pressures on the fatigue performance of various thin asphalt bound layers may be of concern in both the pavement rehabilitation area and new design areas. The performance of the overlay will be analogous to performance of a new asphalt bound layer on a granular base. The strain levels developed will be assessed using established criteria for a new pavement and will indicate the likely performance of the overlay or asphalt

bound layers. In addition, the resulting reduction in rutting will provide safer pavements, since ruts cause an uneven pavement and can accumulate water and ice during harsh weather.

This study demonstrates the influence of tire pressures on the fatigue and rutting performance of asphalt surfaced pavements through the use of elastic layer analyses for a range of asphalt pavement structures.

This study provides an improved definition of the truck tire pressures used in Oregon. The effects of the observed levels of tire pressure are assessed and methods of dealing with pavement distress problems created by them are suggested. This will result in refinement of both paving mix design and pavement structure design methods. Hence, both material and design considerations are incorporated. For good field performance, pavements must be adequately constructed to satisfy the project specifications and design using the materials specified. The continuing refinement of the Oregon State Highway Division's (OSHD) specifications for the construction of asphalt pavement will help ensure optimum roadway performance.

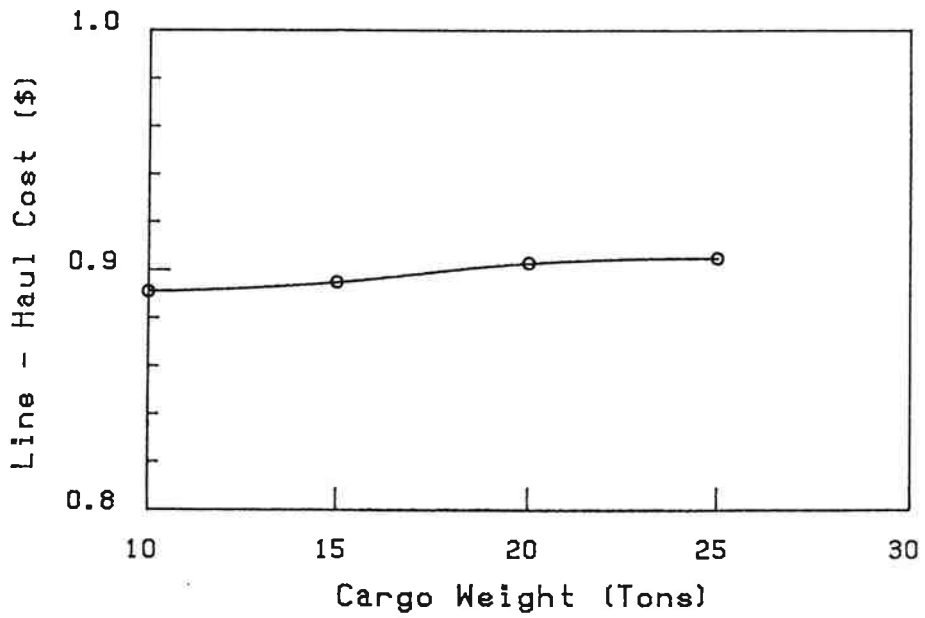
2.0 BACKGROUND

Economic incentives to the truck operator that often exceed the expected costs of overweighting are a major reason for increasing the cargo weights of trucks. The benefits that an operator gains from increasing the load capacity of a truck is the prospect of increased financial returns. This results as the cost per ton-mile decreases as the cargo weight increases (3). Figure 2.1 shows how the operating costs per ton-mile to the trucker decrease dramatically and costs per trip mile increase only slightly as the weight of the load increases. For example, a commodity with a rate of \$0.056/lb passing through a state with a 73,280 lb gross weight limit will provide the trucker with the estimated financial incentives given in Table 2.1. The cash incentive to load to 80,000 lbs gross weight is \$180, and the incentive increases as cargo weight increases. This illustrates the incremental financial advantage that a trucker gains as the amount of cargo weight increases.

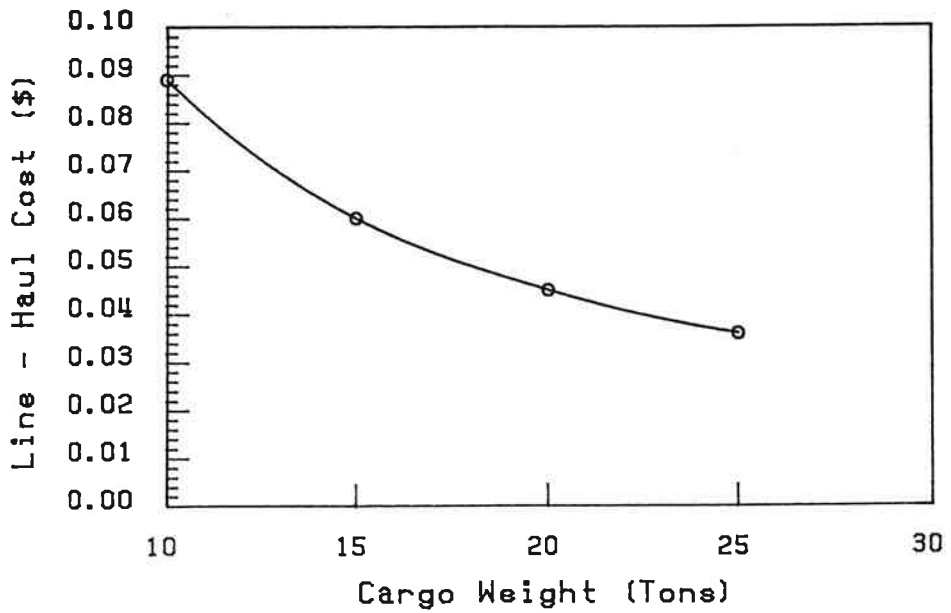
It should be noted that, while the operating cost to the trucker per mile increases only 1.5% as the load weight increases from 10 to 25 tons, the trucker's operating cost per ton-mile decreases 60%, as presented in Figure 2.1. Since fuel cost per mile traveled does not vary proportionately with the weights of trucks, as shown in the Mississippi and Oregon studies (1), the more a truck is loaded the greater the resulting financial benefit.

Consequently, the economics of long haul truck transportation has tended to cause the average gross weight of trucks to increase such that the majority of trucks are operating close to or above the legal gross load or axle load limits.

As axle loads have increased, the use of higher tire pressures has become more popular for long-haul truck operators and radial tires are



(a) Per Mile



(b) Per Ton-Mile

Figure 2.1. Cargo Weight vs. Line Haul Cost (After Ref. 3).

Table 2.1. Incremental Incentives to Overweight (After Ref. 3).

Vehicle Weight (lb)	Cargo Weight (lb)	Rate per Pound* (\$)	Resulting Rate (\$)	Incentive (\$)
73,000	45,000	0.056	2520	0
75,000	47,000	0.054	2540	20
80,000	52,000	0.052	2700	180
90,000	62,000	0.050	3100	580
100,000	72,000	0.048	3460	940

*A typical rate \$0.056; the decreases in rate per pound are given in an attempt to account for the rate reduction that might be offered by a trucker planning to overweight.

predominantly used. The radial tires commonly in use have one higher ply rating and 15 psi higher maximum cold inflation pressure than their older bias ply counterparts (4).

Recent studies in Texas (5) indicate that trucks typically operate with tire pressures (hot) of 100 psi in that state (Figure 2.2). A total of 1486 trucks were surveyed and 70 percent were 3-S2 18 wheelers. The tire pressures (hot) were measured soon after the truck was stopped. The same study indicated that the tire-to-pavement contact pressure resulting from a bias tire with an inflation pressure of 125 psi could be as high as 200 psi. This study showed that for legal axle loads, increasing the tire pressure from 75 to 125 psi in a bias ply tire (10.00-20) can cut the life of a typical thin asphalt concrete pavement used in Texas by amounts ranging from 30 to 80%. In addition to the decreased fatigue life of these pavements, a significant increase in the permanent deformation within the asphalt concrete surface layer should occur.

2.1 Tire Pressure Distribution

For the analysis of the impact of axle loads on flexible pavements using elastic theory, a number of methods for selecting contact areas and pressures for loading input have been used. Treybig and Von Quintus (6) divided tire pressure into four groups that encompass all loads. Terrel (7) assumed that the contact radius is half of the tire width and he varied the tire and contact pressure to account for changes in the magnitude of the wheel load.

However, the traditional approach has been to assume that the contact area is circular in shape (8). This assumption simplifies the equations used in the analysis. In addition, the contact pressure is assumed to be uniform

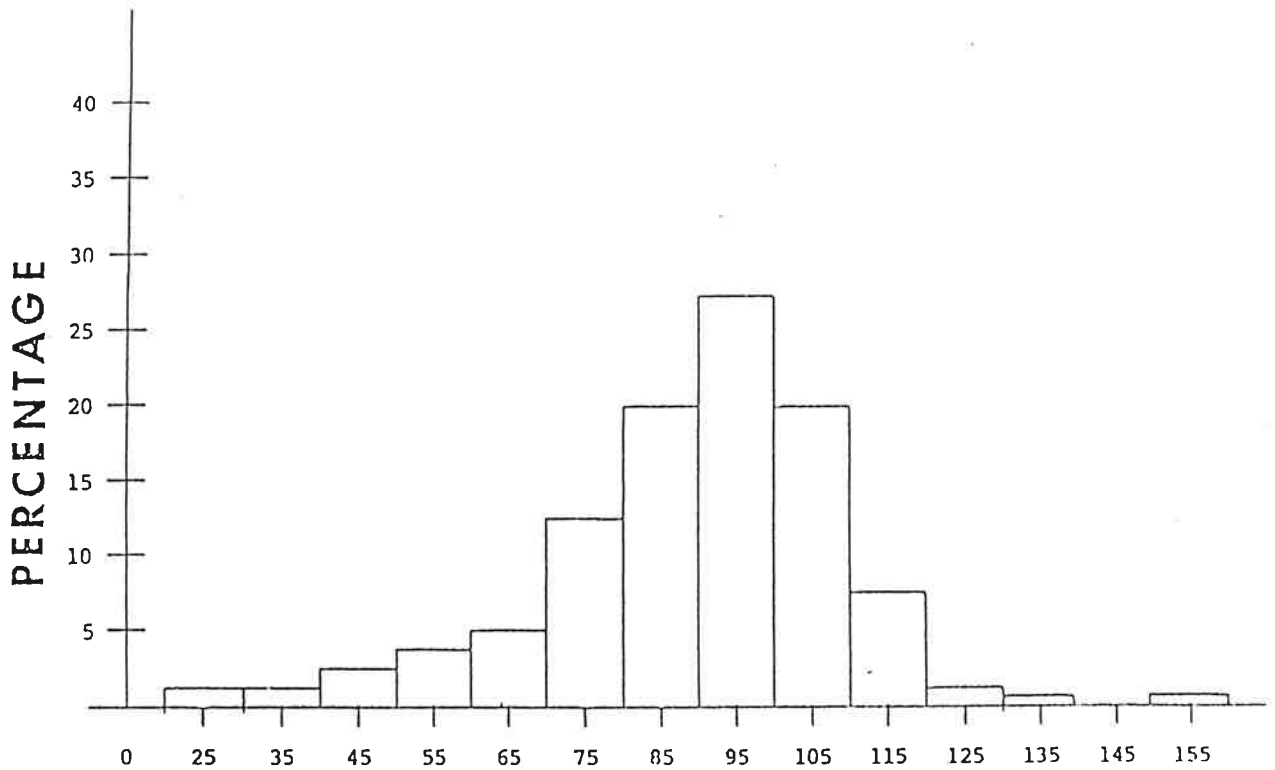


Figure 2.2. Distribution of Truck Tire Inflation Pressures from Texas Studies (1984-85) (After Ref. 5).

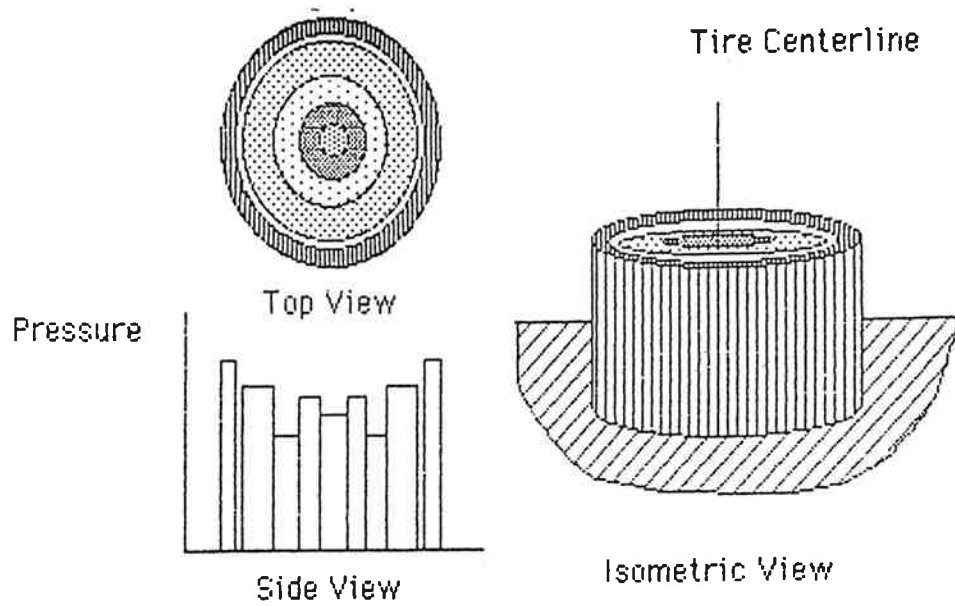


Figure 2.3. Concentric Cylinder Pressure Distribution (After Ref. 9)

throughout the circular area and to be equal in magnitude to the tire inflation pressure. Hence, the radius of contact is as follows:

$$a = [Q/(p \cdot 3.14)]^{1/2} \quad (2-1)$$

where a = radius of contact,
 Q = total load on the tire, and
 p = tire pressure.

Recently, Marshek et al. (9) employed a nonuniform concentric circular pressure model, as illustrated in Figure 2.3. Another study performed by Marshek et al. (10) shows that the tread pattern on a tire has a significant effect on the size of the contact area and the shape of the pressure profiles.

2.2 Load Equivalency Factor

One method of assessing the destructive effects of increased axle loads and tire pressures is through the use of the concept of load equivalency factors (6,11,12,13,14). The load equivalency factor of a given axle loading is defined as the number of applications of a standard load that is equivalent in its destructive effect on flexible pavement to one application of the load under consideration. An 18-kip (80 kN) single axle load is normally used as the standard. The previously listed studies included only different axle loads without considering tire pressure variables. The equivalency factors that are presented in the 1985 AASHTO pavement design guide are based mainly on data resulting from the AASHO road test, a test in which tire pressures (cold) of 70-80 psi were used. Therefore, it is necessary to investigate the effect of higher tire pressures on asphalt pavements.

The width of a tire controls the contact area between the tire and the pavement and, thus, is a factor limiting the stresses which are applied to the pavement. The number of tires and axles supporting a given load also influences the contact pressures and stresses induced in the pavement



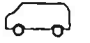



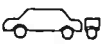



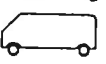




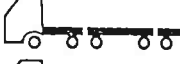
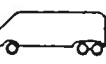










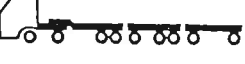

structure. Figure 2.4 shows the truck types used in Oregon's weigh-in-motion study (15). In addition, spacing between tires or between axles is important in calculating stresses, as the stress fields from adjacent tires may overlap and result in cumulative stresses at certain points within the pavement system.

2.3 Pavement Performance Analysis

Deacon (11), Havens et al. (16), Hicks et al. (17), and Patterson (18) have used multilayer elastic analyses to assess the relative effects of different axle configurations and loads on pavement performance.

Deacon used the maximum principal tensile strain on the bottom of the asphalt bound layer to arrive at equivalencies, and Havens et al., made use of the concept of strain energy density. Both studies were concerned with equivalencies based on fatigue in the asphalt bound layer. Hicks et al. used the horizontal tensile strain at the bottom of asphalt concrete layer as a measure of fatigue and the vertical compressive strain at the top of subgrade as a measure of rutting.

Patterson examined the effects of a range of tire pressures (58 to 116 psi) as well as axle loads. An important finding from his study was that increased tire pressure could have a more dominant effect on pavement performance than increased wheel load on pavements having asphalt bound layers over an untreated base. Barker and Chou (19) have used elastic analyses to evaluate different schemes of axle configurations in order to reduce damage to both asphalt surfaced and portland cement concrete pavements. For asphalt pavements, both fatigue in the asphalt bound layer and rutting as controlled by the subgrade strain were examined.

Vehicle Type		Vehicle Type	
1. 	Cars	13. 	(2-3) Other 5 Axle Combinations
	Panels		(3-2)
	Pickups	14. 	(3-51-2) 6 axle Combinations
2. 	Light Vehicles w/ trailers	15. 	(2-2-2)
3. 	2 axle, Single Units		(2-51-3)
4. 	2 axle Buses	16. 	(2-51-2-2) Triples
5. 	3 axle Single Units	17. 	(3-52-2) Other 7 Axle Combinations
6. 	(2-51) 3 axle Combinations		(2-2-3)
7. 	3 axle Buses		(3-2-2)
8. 	(2-52) 4 axle Combinations	18. 	(3-52-3) 8 axle Combinations
	(2-2)		(3-51-2-2)
9. 	(3-51)	19. 	(3-52-4) 9 axle or more Combinations
10. 	4 axle Single Units		(3-51-2-3)
11. 	(3-52) 5 axle Semis		(2-52-3-2)
12. 	(2-51-2) 5 axle Twins		

These are examples of configurations; there are other possible combinations not illustrated.

Figure 2.4. Classifications Used in Oregon's Weigh-in-Motion Study (After Ref. 15).

Figures 2.5 and 2.6 represent Boussinesq vertical pressures in an ideal soil mass due to various combinations of tire pressure and total load as shown by Yoder and Witczak (8). In Figure 2.5, one set of curves is for a tire pressure of 100 psi and loads of 4,000 and 80,000 pounds. The other set of curves is for identical gross wheel loads, but with a tire pressure of 200 psi. As seen on the curves, the effect of the high tire pressure is pronounced in the upper layers of the pavement, whereas at a depth of about 36 inches the stresses are about equal for both cases. High tire pressures, thus, necessitate high-quality materials in the upper layers of the pavement, but the required total depth of pavement is not affected appreciably by tire pressures, according to Yoder and Witczak. On the other hand, for a constant tire pressure, an increase in total load increases the vertical stress for all depths. Figure 2.6 shows the effect of dual wheels on stresses for constant tire pressures. Calculated stresses at the surface are not affected by the wheel configurations and are equal to the applied tire pressure. Dual wheels and tandem axles, however, result in increased stresses at greater depths, as the pressure bulbs of the tires overlap.

Southgate et al. (20) show a large increase in the pavement fatigue rate due to an unequal distribution of loads between the two axles of a tandem group as compared to the pavement fatigue rate under axles in a tandem group with evenly distributed loads.

2.4 Mix Design

The Marshall and Hveem methods of mix design have been widely used with satisfactory results. For each of these methods, mix design criteria have been developed by correlating the results of laboratory tests on compacted

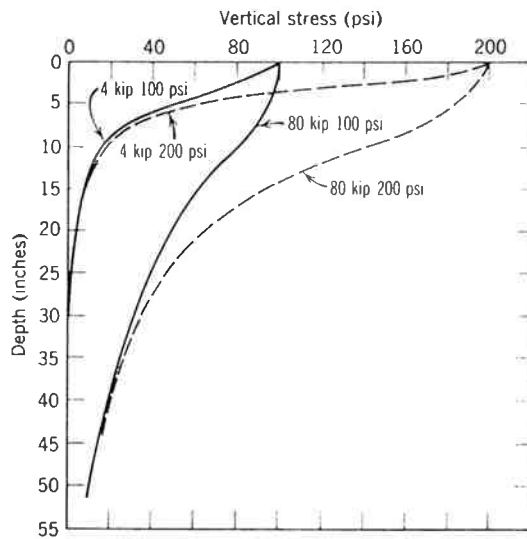


Figure 2.5. Variation of Vertical Stress with Depth, Boussinesq Problem (After Ref. 8).

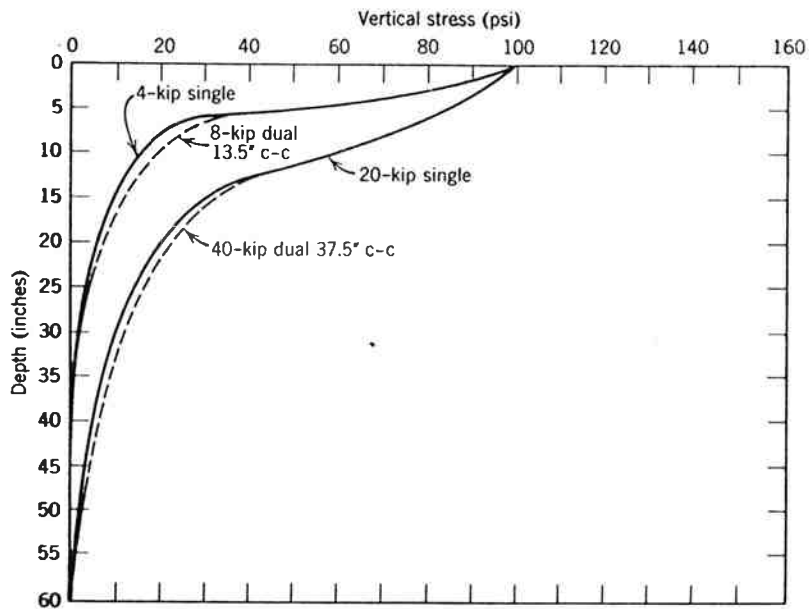


Figure 2.6. Effect of Number of Wheels on Vertical Stress, Boussinesq Problem (After Ref. 8).

Notes on Figure 2.6:

- (1) All tires have 100 psi inflation.
- (2) Depth at which interaction of dual wheels is significant is about equal to one-half the C-C spacing between tires.
- (3) Depth at which dual tires will act as a single tire is about two times the C-C spacing of the tires.
- (4) See Figure 4.7 for a definition of C-C spacing.

paving mixes with the performance of the paving mixes under actual roadway service conditions.

However, the limitations of empirically based methods of pavement mix design have become increasingly apparent in recent years as both traffic loads and the numbers of commercial vehicles have increased during a period when costs of materials and labor have also escalated.

Increasing demands on asphalt pavements from both higher traffic volumes and higher truck tire pressures have caused highway engineers to examine the basis of pavement specifications and asphalt concrete mix design guidelines and procedures in order to see how to best cope with these challenges. As truck tire pressures and truck traffic volumes increase, it is apparent that at some level the existing asphalt pavements constructed and designed to earlier standards will show increasing distress.

In Oregon, there have been several occurrences of excessive wheel track rutting which have been associated with the higher truck tire pressures prevailing during recent years. The rutting may be a function of deformation in all layers of the flexible pavement structure; however, with high tire pressures, deformation in the asphalt concrete mixture is the major contributor. Existing pavement specifications and mix design procedures may not produce mixtures capable of dealing with high tire pressures. Similarly, they may not identify highly deformable mixtures. Such a situation was identified by Finn et al. (21) in designing mixtures for heavy duty airfield pavements, where very high tire pressures occur. They utilized a simple creep test, similar to that developed by Shell researchers (22), to complement the Marshall and Hveem mix design procedures and to quantify deformation charac-

teristics of the mix. They also indicated a need to consider modified specifications and criteria in assessing mix designs.

Hicks and Bell (23) recently completed a study for Oregon State Highway Division (OSHD) to evaluate their current specifications and asphalt concrete mix design process. One area that was identified as a possible problem were the specifications for class "B" and class "C" dense-graded mixture aggregate gradations. In particular, the gradations specified for these mixtures do not satisfy the Fuller's maximum density gradation as presented in Table 2.2. The grain size distribution of an aggregate can be represented by the following equation.

$$p = 100*(d/D)**n \tag{2-2}$$

In this expression, d represents the sieve (particle size) in question, p is the percent by weight finer than the sieve, and D is the maximum size of the aggregate. Maximum density generally occurs when the exponent n equals 0.45.

Many researchers indicate the potential for constructing tender mix pavements with possible deformation problems increase if the percent passing values for a 3/4-in. maximum size mix are greater than the following (24):

Sieve	% Passing
#4	55
#10	37
#40	16
#200	3-7

Further, they indicate that gradation curves that cross back and forth over

Table 2.2. Aggregate Gradations for Oregon's Asphalt Concrete and Fuller Maximum Density.

Sieve Size (mm)		Percent Passing		Fuller Maximum Density Gradations*		
		Oregon Class "B"	Oregon Class "C"			
1-in.	25.4	100	100	100	100	100
3/4-in.	19	95-100	100	88	100	100
1/2-in.	12.5	81-93	95-100	73	83	100
3/8-in.	9.5	-	-	64	73	88
1/4-in.	6.3	52-72	60-80	54	61	73
#4	4.75	-	-	47	54	64
#8	2.36	-	-	34	39	47
#10	2.00	21-41	26-46	32	36	43
#16	1.18	-	-	25	29	34
#30	0.600	-	-	18	21	25
#40	0.425	8-24	9-25	16	18	21
#50	0.300	-	-	13	15	18
#200	0.075	2.0-7.0	3.0-8.0	7.2	8	9.9

*n = 0.45 in Eq. (2-2), for 1-, 3/4-, and 1/2-in. maximum size.

the maximum density curve, especially in the region of the No. 30 to No. 80 sieves, tend to produce tender mixes.

Reference 25 presents an excellent discussion on the causes of pavement performance problems, particularly from tender mixes. This report indicates the likely causes of tender mixes, as related to mix design, to be as follows:


- 1) Incorrect mix design,
- 2) Excessive middle sand size in the mix, characterized by a hump in the gradation curve for the material passing the No. 4 sieve,
- 3) Insufficient amounts of material passing the No. 200 sieve,
- 4) The grade of asphalt used in the mix is too soft, and
- 5) Excess fluids in the mix (asphalt plus moisture).

Table 2.3 indicates that mixtures which contain one or more of the following characteristics can result in pavements with tender or slow setting properties which are difficult to compact:

- 1) Large sand sizes (passing No. 4 sieve),
- 2) Small quantities of minus No. 200 material,
- 3) Small maximum size aggregates,
- 4) Smooth rounded aggregates,
- 5) Highly temperature susceptible asphalts,
- 6) Slow setting asphalts,
- 7) Less than anticipated hardening during hot mixing (i.e., low C-value), and
- 8) High fluids content.

Table 2.3. Factors Influencing Tender Pavements (After Ref. 25).

Material or Mixture Variable	Discussion
Aggregate Gradation	<ul style="list-style-type: none"> • Avoid large portions of sand-sized particles. • Minus No. 200 material should be greater than 4%. • Mineral filler can add stability to a mixture. • Small maximum-sized aggregate mixes have a greater tendency to be tender.
Aggregate Type	<ul style="list-style-type: none"> • Smooth, rounded aggregate particles are most likely to produce a tender mixture. • Sand-sized crushed particles can add stability to a mixture.
Asphalt Properties	<ul style="list-style-type: none"> • Highly temperature susceptible asphalts can aggravate tenderness problems. • Slow setting asphalts can cause tenderness problems. • Less than anticipated hardening of the asphalt during hot mix hardening can cause tenderness problems.
Asphalt Content	<ul style="list-style-type: none"> • High asphalt content can aggravate tenderness problems. • High fluids content (asphalt plus water) can cause tenderness problems.

Material or Mixture Variable										
	1	2	3	4	5	6	7	8	9	10
<u>Aggregate</u> Shape Texture Maximum Size * -#30 to + #100 -#200	Angular Very Round >3/4-inch Suitable >6%		Subangular Rough <5/8-inch 5%			Subrounded Smooth <1/2-inch Excessive 4%		<3/8-inch 3%		Rounded Polished <1/4-inch Large Excess <2%
<u>Asphalt Cement</u> Content Viscosity Penetration Hardening Index Temp. Susceptibility Setting Characteristic Asphaltene Content	Low High Low High Low Fast >20%					Optimum Medium Medium Medium Medium 10 to 20%				High Low High Low High Slow <10%
<u>Mixture</u> Softening Additives Moisture Content	None >0.5%					Some 1 to 2%				Much >2.5%
<u>Construction</u> Rolling Temperature C-value (41) Ambient Temperature	Low >50 <70					Medium 30 - 50		90		High <30 >100

* Suitable quantity depends upon design gradation. Rounded sand size particles can produce a critical mixture.

Figure 2.7. Rating Scale to Identify Tender Mixtures (After Ref. 25).

filaments with the direction of the cords in each layer laying at an angle to the principal axes of the tire. Half of the layers have the cords at a positive angle and half at a negative angle to the principal axis, as shown in Figure 2.8. In order to give increased protection to the casing under tread and/or to increase the casing strength in the crown region of a cross bias tire, one or two additional layers of cords are sometimes incorporated. These cords lay substantially parallel to the cords in the other plies and extend approximately the width of the tire tread. This is shown in Figure 2.9. Such layers are called breakers. If the cord angles in the breaker layers are substantially different from those in the main plies, and the breaker is made of either higher modulus cords than the casing or of more layers than the casing, the breaker construction has an important bearing on the mechanical properties of the tire. Tires of this type are known as bias belted tires (sometimes incorrectly called semiradial tires) (27).

In the 1970s, the trucking industry increased their use of radial truck tires (a more correct description is a rigid breaker, radial ply tire (27)) as tire service demands increased on medium and heavy trucks. In radial tires, the cords or filaments in the casing are disposed in a radial, or substantially radial, direction giving a 90° bias or crown angle in relation to the axis of rotation of the tire, as shown in Figure 2.10.

Testing done on bias and radial tires with similar tread designs from the same manufacturer has confirmed that the radial tire generally offered improvements over the bias tire, as presented in Table 2.4 (28). Cooper has described the usage trends which have taken place with heavy duty radial tires and also the potential for some future changes in their usage in Reference 28.

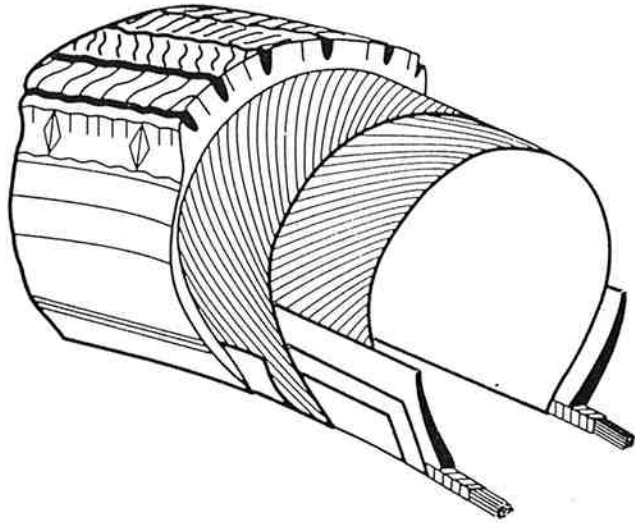


Figure 2.8. Cross-Bias Tire (After Ref. 27).

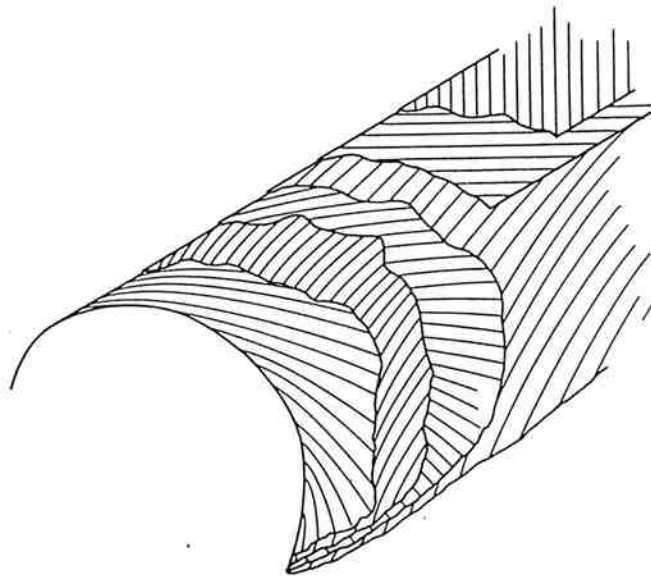


Figure 2.9. Break Layers in Cross-Bias Tire (After Ref. 27).

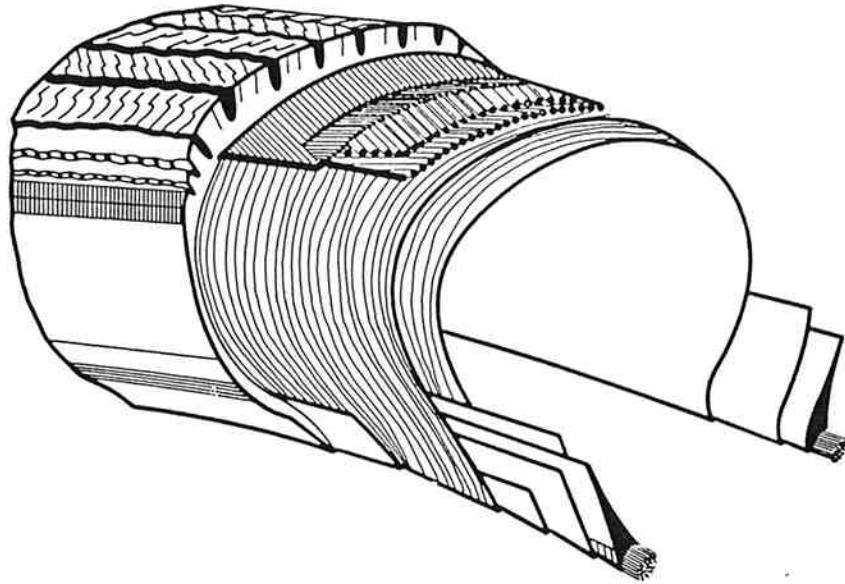


Figure 2.10. Radial Ply Rigid Breaker Tire (Radial Tire) (After Ref. 27).

Table 2.4. Bias versus Radial Performance Testing (After Ref. 28).

Property	Type Test	Bias Tire	Radial Tire
Wear Rate	Proving Grounds	Par	Better
Wear Regularity	Proving Grounds	Par	More Sensitive
Running Temperature	Laboratory	Par	Better (Lower)
Fuel Economy	Proving Grounds	Par	Better (6% Savings)
Tire Noise	SAE J57A	Par	Better (3 dBA Less)
Puncture Resistance	Commercial Fleet	Par	Better (40% Fewer)

Wong (29) indicated that under a radial ply tire on a hard surface, there is a relatively uniform ground pressure over the whole contact area. In contrast, the ground pressure under a bias ply tire varies greatly from point to point, as tread elements passing through the contact area undergo complex localized wiping motions.

In 1982, the federal government permitted an 80,000 pounds gross vehicle weight limit and a 34,000 pounds tandem-axle weight limit on trucks using interstate highways. This weight limit allowed a theoretical 12,000-lb load on the steering axle. Most states have invoked a restriction of 600 lbs maximum load per inch of tire width, i.e., two 10-in. wide tires could legally support a 12,000-lb axle load. According to Cooper, two bias tires in the commonly used sizes and standard 12-ply rating do not have the 12,000-lb capacity, but two standard 14-ply rating radial tires which allow higher inflation pressure necessary for a higher capacity rating do carry over 12,000 lbs. The improved loading capacity and the advantages presented in Table 2.4 can be some of the reasons which have led to increasing radial truck tire usage.

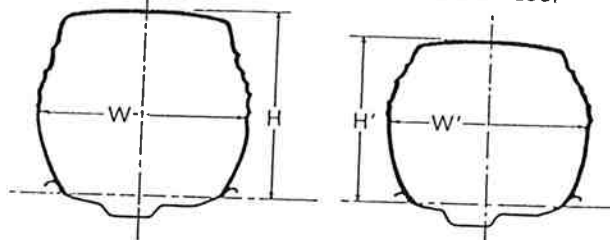
Recently, the trucking and tire industries have started to promote super single radials and new low profile (or low aspect ratio) tubeless tires (30). The concept of replacing dual tires with a wide single is not new but has gained popularity recently in the long haul market. New super single radial tires are claimed to have 10% or better tread mileage and 8 to 10% better fuel economy than conventional dual radials. Also, the lighter weight of the wide-base single tire assembly permits higher payloads. The reduced tire aspect ratio (section height/section width, Figure 2.11) decreases tire deflection, thereby improving vehicle handling and stability while increasing tread life

LOW ASPECT RATIO TIRES
24.5 INCH HIGHWAY SIZE

(USING TYPICAL DESIGN DIMENSIONS)

CONVENTIONAL ASPECT RATIO
(TUBELESS)

LOW ASPECT RATIO
(TUBELESS)



$$\frac{H}{W} = .85 \text{ (.86 ACTUAL)}$$

$$\frac{H'}{W'} = .75 \text{ (.77 ACTUAL)}$$

11R24.5

285/75R24.5

H = 0.24 METRES (9.5 INCHES)
W = 0.28 METRES (11.0 INCHES)
OD = 1.10 METRES (43.5 INCHES)

H' = 0.21 METRES (8.4 INCHES)
W' = 0.28 METRES (10.9 INCHES)
OD = 1.05 METRES (41.3 INCHES)

Figure 2.11. Conventional vs. Low Aspect Ratio Comparison (After Ref. 28).

and fuel economy. However, the effect of the super single tire on the performance of asphalt pavement is not well known.

2.6 Creep Test

In a major effort towards developing rational procedures for the design of asphalt concrete pavement mixes, an attempt has been made to develop a suitable test method to judge their stability properties. Van de Loo (31) defined the stability properties of an asphalt mix as the resistance of a mix to rutting in an actual pavement, i.e., under varying conditions of climate, traffic density, and traffic load.

Many researchers have carried out creep tests (static or repeated mode) as a relatively simple means of predicting rutting or permanent deformation of an asphalt concrete pavement.

In 1973, theoretical deformation models of asphalt concrete mixes were formulated by J.F. Hills (32). It was assumed that any deformations in the mix were the result of sliding displacements between adjacent mineral particles separated by a thin film of asphalt. He interpreted the results in terms of a mix stiffness (S_{mix}) as a function of bitumen stiffness (S_{bit}), as shown in Figures 2.12 and 2.13. Hills stated that, in addition to the effect of the volume concentration of the mineral aggregate, the gradation, shape, and surface texture of the aggregate, and the level of compaction have a strong influence on the mix behavior. The effect of substituting crushed for rounded aggregate is illustrated in Figure 2.12, which shows the creep behavior of two sandsheet mixes with similar gradations and asphalt contents. Figure 2.13 shows the effects of various methods of compaction on the creep behavior of an asphalt mix. Hills reported that strain in the mix as a

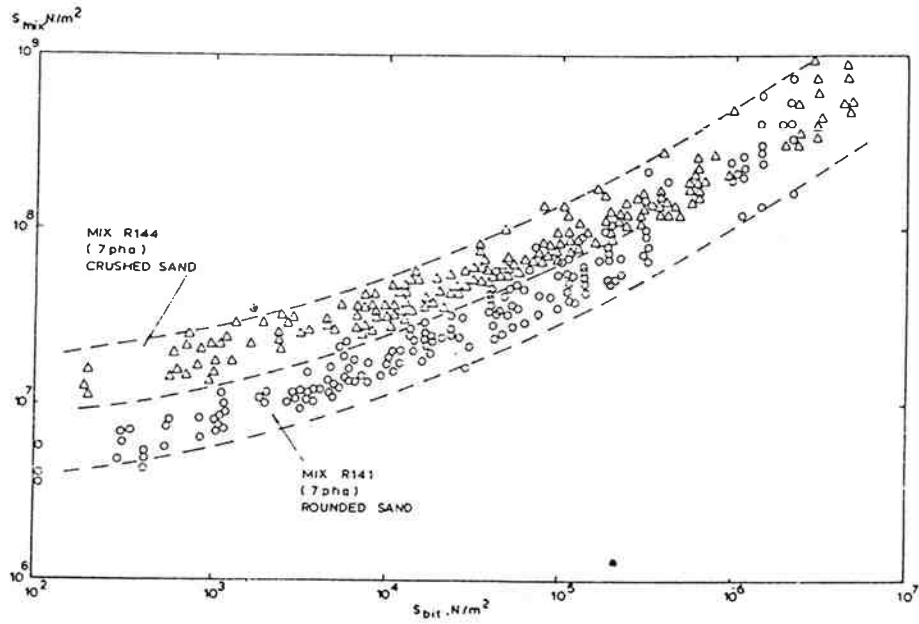


Figure 2.12. The Improvement in Creep Behavior Given by Substituting Crushed for Rounded Aggregate (After Ref. 32).

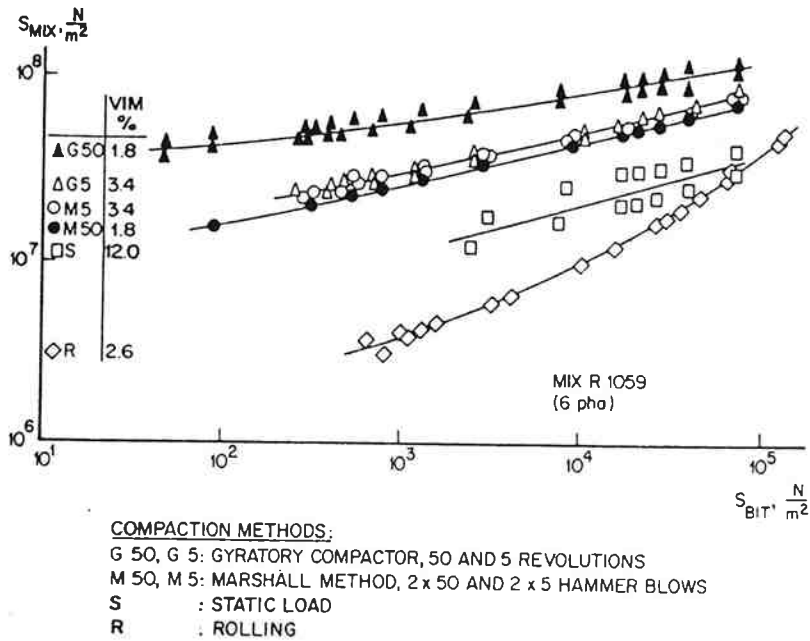


Figure 2.13. The Effects of Various Methods of Compaction on the Creep Behavior of an Asphaltic Concrete Mix (After Ref. 32).

function of loading time is independent of the shape and size of the specimens.

Reference 33 provides recommendations for performing the unconfined, statical creep test which was standardized during the Colloquium 1977 held in Zürich. These tests were performed in water on samples of the same size as normal Marshall specimens. In the test, the samples reached a temperature of 40°C before the test commenced. During the test a constant load of 0.1 MPa (14.5 psi) having a duration of one hour was applied without any impact. The loading time of one hour was arbitrary.

The deformation of an asphalt specimen is measured as a function of loading time at a fixed test temperature. This relationship is shown on the creep test curves; an example is presented in Figure E.1 of Appendix E. The general equation of the creep curve is:

$$\log \epsilon = c + n \log t \quad (2-3)$$

where ϵ = creep strain at time t and

c, n = constants.

The constants c and n are related to test conditions, such as uniaxial stress, temperature, asphalt cement content, and the factors indicated by Hills above.

The constant n represents the inclination of a linear approximation of the creep test curve. A relatively small n indicates a less viscous creep behavior; conversely, a relatively large n shows a predominately viscous creep behavior (33). It has been found that the level of the instantaneous response to loading increases with the amount of filler and bitumen in the sample (34). Furthermore, the time dependence of the vertical displacement

has been associated with the viscosity of the mortar, a factor which is related to the filler-binder ratio.

To carry out unconfined creep compression tests, Hills used a modified version of a soil consolidation apparatus. Snaith and Brown (35) used samples of 100 mm diameter and 150 mm length. The sample ends were cut off using a diamond-tipped blade. They used a special jig to ensure that the finished ends were flat and perpendicular to the axis of the sample. Van de Loo (31) used silicone grease and powdered graphite on the ends of the sample to minimize the lateral constrictional forces exerted by the compression apparatus plates.

To determine the relationship between creep behavior determined by either static or dynamic testing, parking tests (i.e., confined creep tests) with a static wheel were carried out on test track pavement by Van de Loo (31).

Bolk (36) has used a "semidynamic" creep test and compared the results to those obtained by a static creep test using the Shell method (37). Bolk found that his method, which uses a correction factor for unconfinement, generally produced equivalent or even distinctly better test results than the corrected (for temperature) Shell method. Bolk stated that the gradient of the calculated deformation curve after the initial stage agreed better with the behavior of the mixture in practice.

Creep test procedures used in this study are documented in Appendix A.

2.7 Other Considerations

The above review highlights the most significant causative factors and potential methods of counteracting the high levels of fatigue cracking and wheel track rutting associated with increased axle loads and higher tire pressures. However, the specifications for materials, along with the entire

mix design and pavement structure design process, must be considered in order to provide optimum pavement performance. As an example, pavement fatigue resistance and durability could be decreased in mixtures developed to provide high stability. All these factors must be considered in designing a pavement both with regard to environment and the function of each pavement layer.

3.0 EXPERIMENT DESIGN- TESTS ON ASPHALT CONCRETE MIXTURES

3.1 Variables Considered

Aggregate from four different sources were used for the laboratory mixture study. The sources of aggregate were:

- 1) Morse Brothers Pit (gravel),
- 2) Cobb Rock Quarry,
- 3) Hilroy Pit (gravel), and
- 4) Blue Mountain Asphalt Pit (gravel).

For the test mixtures with the aggregates from Cobb Rock Quarry and Blue Mountain Asphalt Pit, the aggregates were treated with a 1% lime slurry and mellowed for a minimum of 24 hours prior to use in the mixture.

The variables considered in the laboratory mixture preparations for the creep tests were:

- 1) Asphalt cement content: three levels,
- 2) Aggregate batched gradation: A through F (Table 3.1),
 - A) 65% passing 1/4-in., 32% passing #10, 5.0% passing #200,
 - B) 60% passing 1/4-in., 29% passing #10, 5.0% passing #200,
 - C) Fuller curve - 60% passing 1/4-in., 36% passing #10, 8.0% passing #200,
 - D) 60% passing 1/4-in., 35% passing #10, 5.0% passing #200,
 - E) 60% passing 1/4-in., 34% passing #10, 56% of the aggregate passing the #10 screen passing the 1/4-in. screen, 5.0% passing #200,
 - F) 60% passing 1/4-in., 34% passing #10, 56% of the aggregate passing the #10 screen passing the 1/4-in. screen, 8.0% passing #200.

Table 3.1. Extracted Mix Aggregate Gradations (A through F).
Percent Passing

Aggregate Gradation	Morse Brothers Pit			Cobb Rock Quarry			
	A	B	C	A	B	C	D
1-in.							
3/4-in.	100	100	100	100	100	100	100
1/2-in.	98	97	82	99	99	86	82
3/8-in.	86	83	72	82	78	73	72
1/4-in.	65	60	60	66	60	60	60
#10	32	30	37	32	29	37	37
#40	13	11	18	13	11	19	19
#200	4.7	4.3	6.8	6.7	6.0	9.0	6.9

Aggregate Gradation	Hilroy Pit						Blue Mountain Asphalt Pit				
	A	B	C	D	E	F	A	B	C	D	E
1-in.	100	100	100	100	100	100					
3/4-in.	99	98	99	99	98	98	100	100	100	100	100
1/2-in.	86	85	82	82	85	85	87	87	86	86	87
3/8-in.	76	72	72	72	72	72	77	74	73	73	73
1/4-in.	65	60	60	60	60	60	65	60	60	60	60
#10	33	31	37	37	34	34	32	29	36	36	34
#40	14	13	19	19	14	14	14	13	16	16	15
#200	4.5	4.2	5.9	4.3	5.0	6.9	5.0	4.5	7.0	5.0	5.2

Table 3.2 presents the aggregate gradation for each aggregate source.

The physical properties of the asphalt cement used in the fabrication of the test specimens are presented in Table 3.3.

3.2 Specimen Preparation and Test Program

Following the standard ODOT procedure (38) using a kneading compactor, 4-in. (100 mm) diameter by 2.5-in. (63 mm) high specimens were fabricated using aggregate from four different sources.

A flowchart of the test program followed in this study is given in Figure 3.1. The Oregon Department of Transportation (ODOT) testing program included the conventional mixture tests such as the Hveem Stability test (AASHTO T-246), the Index of Retained Strength (AASHTO T-165), the Rice Maximum Specific Gravity test (AASHTO T-209), the Bulk Specific Gravity test (AASHTO T-166), and the Repeated Load Diametral test for unconditioned and freeze-thaw conditioned resilient modulus. Oregon State University performed creep tests with 54 laboratory-fabricated specimens, as summarized in Section 3.3.2 and described in Appendix A.

3.3 Test Methods

After the completion of standard laboratory mix design tests, additional specimens were made for repeated load diametral and creep testing.

3.3.1 Resilient Modulus

The resilient modulus test was performed using the repeated load diametral test apparatus. The maximum load applied and the resulting horizontal elastic tensile deformation were recorded in order to determine the resilient modulus using the following equations:

Table 3.2. Gradations Used in Mixtures for Each Aggregate Source.

Aggregate Source	Aggregate Gradation					
	A	B	C	D	E	F
1. Morse Brothers Pit	X	X	X			
2. Cobb Rock Quarry (with 1% lime slurry)	X	X	X	X		
3. Hilroy Pit	X	X	X	X	X	X
4. Blue Mountain Asphalt Pit (with 1% lime slurry)	X	X	X	X	X	

Table 3.3. Physical Properties of Asphalt Cement.

	Morse Brothers Pit	Cobb Rock Quarry	Hilroy Pit	Blue Mountain Asphalt Pit
Grade	AR4000W	AR4000W	AR4000W	AC20
<u>Original</u>				
• Penetration, 77°F	68	68	68	61
• Absolute Viscosity, 140°F, Poises	1339	1349	1349	2111
• Kinematic Viscosity, 275°F, C.S.	261	248	248	352
• Flash Point, Open Cup, °F	600	605	605	580
<u>After the Rolling Thin Film Oven Test</u>				
• Penetration, 77°F	41	40	40	32
• Absolute Viscosity, 140°F, Poises	3033	3139	3139	5870
• Kinematic Viscosity, 275°F, C.S.	367	365	365	562
• Loss on Heating, %	0.45	0.52	0.52	0.65

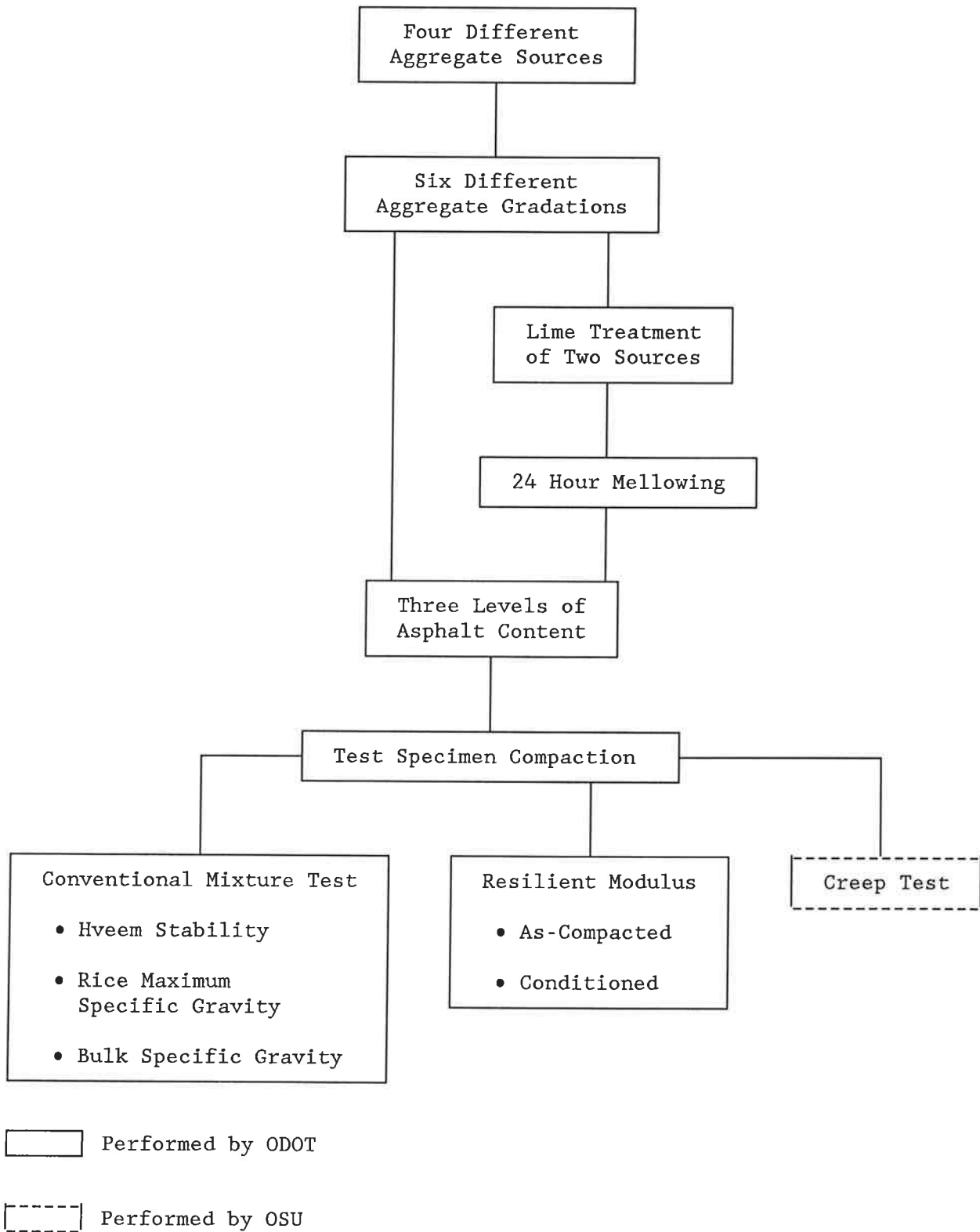


Figure 3.1. Flowchart for Test Program.

$$M_R = \frac{P}{\Delta H \cdot t} (0.2692 + 0.9974 \nu) \quad (3-1)$$

where: M_R = resilient modulus, psi;
 ΔH = horizontal elastic tensile deformation, inches;
 P = dynamic load, lbs;
 t = specimen thickness, inches; and
 ν = Poisson's ratio.

Poisson's ratio was assumed constant and equal to 0.35, which simplified Eq. (3.1) to:

$$M_R = \frac{0.6183 P}{\Delta H \cdot t} \quad (3-2)$$

During the test, the dynamic load duration was fixed at 0.1 sec and the load frequency at 60 cycles per minute. A static load of 10 pounds (4.5 kg) was applied to hold the specimen in place. The test was carried out at 77°F (25°C).

3.3.2 Creep Test

A simple creep test was developed and performed at Oregon State University.

For the creep test, a loading device for soil consolidation and a data acquisition/control unit with a personal computer were used. The creep test was run for 3 hours at 40°C and a compression stress of 0.1 MPa (14.5 psi) was applied. A summary of the creep test is as follows:

- 1) Place a loading device for soil consolidation testing in an environmental cabinet and connect the loading device to an external regulator. Place the test specimens and a dummy

specimen with a thermistor into the environmental cabinet. Set the loading device pressure regulator to 0.1 MPa.

- 2) Warm the inside of the environmental cabinet to 40°C and determine the temperature of the dummy specimen using the data acquisition system and thermistor.
- 3) After the temperature of the dummy specimen core reaches 40°C, place a preheated specimen on the load plate. Put an LVDT on the bottom plate and attach the thermistor to the specimen. Check the level of the bottom plate before running the test.
- 4) Wait for 5 to 10 minutes after closing the environmental cabinet door to be sure the specimen temperature is at 40°C.
- 5) Apply a pressure of 10 kPa to the specimen as a preload for 2 minutes.
- 6) Apply a pressure of 0.1 MPa to the sample and run the computer program.

Appendix A describes the apparatus and the procedure for sample preparation in detail. Also included in Appendix A are computer programs to monitor the temperature and measure the deformation of the specimen at regular time intervals throughout the duration of the creep test.

4.0 RESULTS

4.1 Operating Characteristics of Oregon's Trucks

A survey to evaluate long-haul truck tire inflation pressures and types of tires in use was carried out at a weigh station located on Interstate 5, near Woodburn, Oregon, from July 28 to July 30 and from August 25 to August 31 in 1986. A tire pressure data collection sheet is shown in Figure 4.1. One data collection form represents one truck. The data collection form consists of four parts, as follows:

- 1) Basic data: date, time, Public Utility Commission (PUC) safety inspection number, inspector, PUC plate number, and commodity.
- 2) Weather information, including air temperature and pavement temperature.
- 3) Truck classification used in Oregon's Weigh-in-Motion study (refer to the figure used in 2.4).
- 4) Tire data: axle number, dual/single tire, manufacturer, tire construction (radial/bias), tire size, tread depth, and tire manufacturer's maximum recommended inflation pressure (cold) and measured tire pressure (hot).

4.1.1 Preliminary Results

The data collected show that the majority of tires sampled were radials (87% of 2704 tires). The average measured pressures (hot) of radial and bias tires were 102 and 82 psi, respectively. The average recommended inflation pressure (cold) for radial tires was 102 psi, and for bias tires 81 psi. About 40% of all radial tires were operated with inflation pressures (hot)




TIRE PRESSURE DATA COLLECTION SHEET

BASIC DATA: Test No. (no entry required): _____ Date: _____ Start Time: _____
 PUC Safety Inspection No.: _____ Place of Inspection: _____ Inspector: _____
 PUC Plate No.: _____ Commodity: _____ Comments: _____

WEATHER: (tick one)
 Hot & Cool & Hot & Cool & Intermittent Frequent Persistent
 a) Sunny ___; b) Sunny ___; c) Cloudy ___; d) Cloudy ___; e) Showers ___; f) Showers ___; g) Rain ___
 *Air Temperature ___°F *Pavement Temperature ___°F *Record immediately after start time

TRUCK CLASSIFICATION: (tick one)

A. Single Units:

- ___ a) SU-2  ___ b) SU-3  ___ c) SU-4 







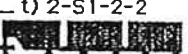
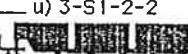
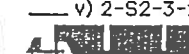
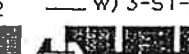
B. Trucks & Trailers:

- ___ d) 2-2  ___ e) 2-3  ___ f) 3-2  ___ g) 2-2-2  ___ h) 2-2-3  ___ i) 3-2-2 

C. Tractors & Semitrailers:

- ___ j) 2-S1  ___ k) 3-S1  ___ l) 2-S2  ___ m) 3-S2 

D. Tractors, Semitrailers & Trailers:

- ___ n) 2-S1-2  ___ o) 3-S1-2  ___ p) 2-S1-3  ___ q) 3-S2-2  ___ r) 3-S2-3 
 ___ s) 3-S2-4  ___ t) 2-S1-2-2  ___ u) 3-S1-2-2  ___ v) 2-S2-3-2  ___ w) 3-S1-2-3 

TIRE DATA:

A. Left Side - Outer Tires

Axle #	Twin/Single Tire	Mfr.		Rad/Bias (R/B)	Pressure (psi)	Tread Depth†
		Rec/Max Pressure (psi)	Rad/Bias (R/B)			
(1)						
(strg)						
(2)						
(3)						
(4)						
(5)						
(6)						
(7)						
(8)						
(9)						

B. Right Side - Outer Tires

Axle #	Twin/Single Tire	Mfr.		Rad/Bias (R/B)	Pressure (psi)	Tread Depth†
		Rec/Max Pressure (psi)	Rad/Bias (R/B)			
(1)						
(strg)						
(2)						
(3)						
(4)						
(5)						
(6)						
(7)						
(8)						
(9)						

*measured at beginning of inspection; ** measured at end of inspection; †1/32nd in.

Finish time: _____

Figure 4.1. Tire Pressure Data Collection Sheet.

above 110 psi. The sample included measurements on a total of 270 trucks, of which 56% were 18-wheelers (3-S2).

4.1.2 Truck Types

The total of 270 trucks surveyed were classified as shown in Figure 4.1. Based on data presented in Table 4.1, 55.9% were 3-S2, 7.4% were single axle unit trucks, and 13% were trucks with tractors, semitrailers, and trailers.

4.1.3 Tire Pressure

4.1.3.1 Recommended Maximum Tire Pressure. The tires surveyed were divided into three groups: 1) single tires used on steering axles, 2) single tires on non-steering axles, and 3) dual tires on non-steering axles.

Figure 4.2 shows the distribution of the manufacturer's recommended maximum tire pressure (cold) for three groups of radial and bias tires, and Table 4.2 presents the mean value and one standard deviation. The average recommended maximum pressures (cold) for dual radial and bias tires were 101 psi and 81 psi, respectively.

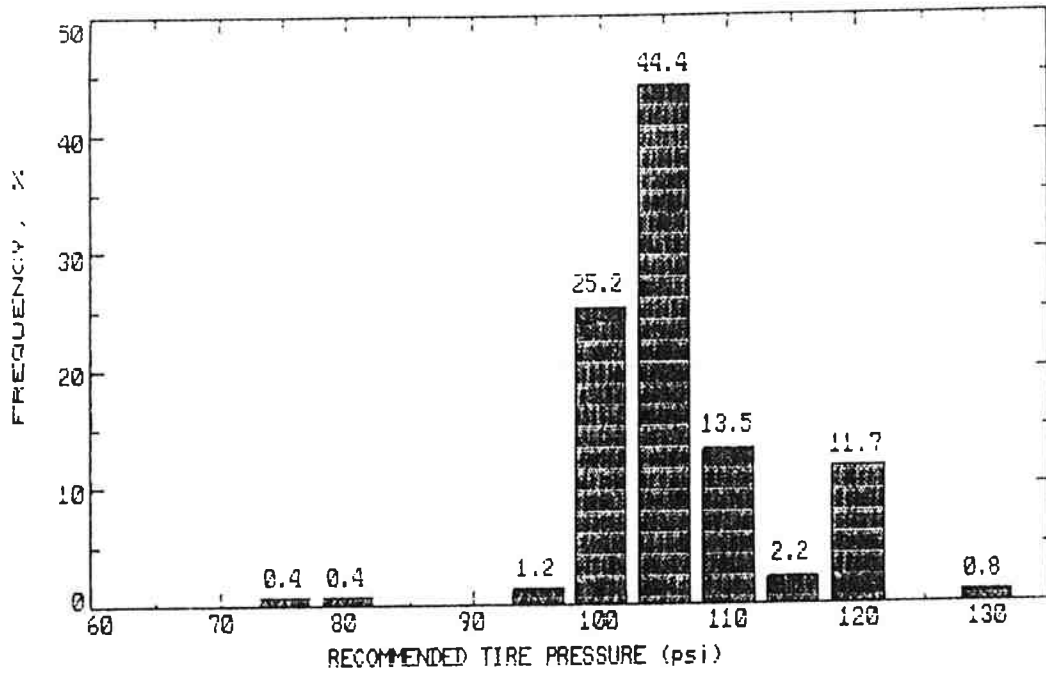
4.1.3.2 Measured Tire Pressure. Figure 4.3 shows the distribution of measured tire pressures (hot) for three groups of radial and bias tires. Table 4.3 presents the mean value and one standard deviation of the measured tire pressures (hot). The average measured pressures (hot) for dual radial and bias tires were 102 psi and 82 psi, respectively.

4.1.4 Tread Depth

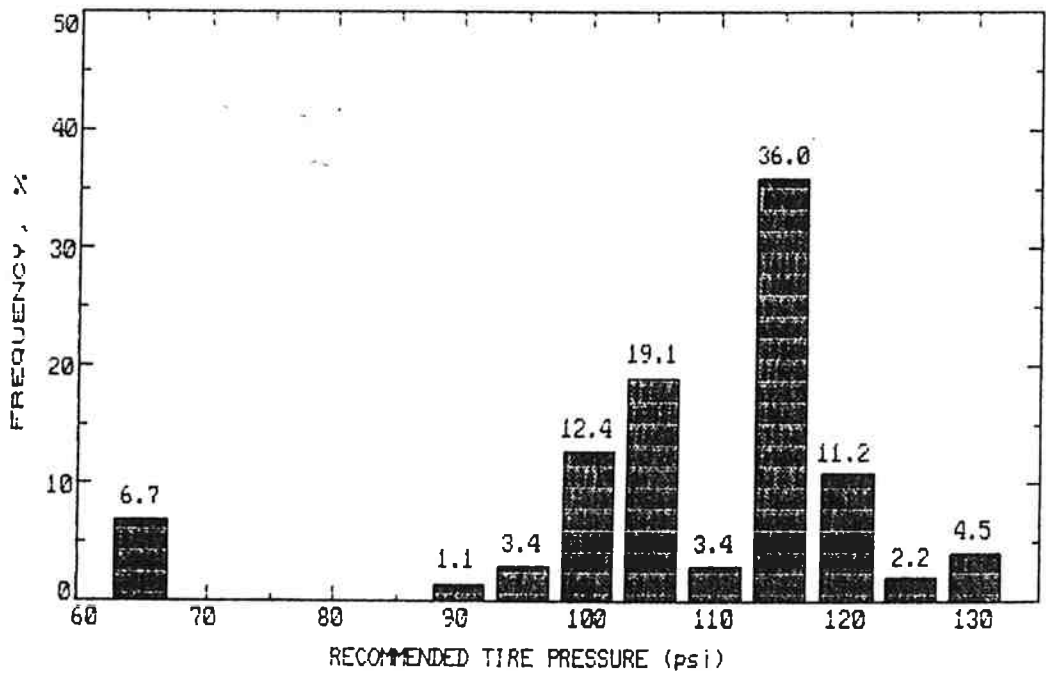
Figure 4.4 and Table 4.4 present the results of the tread depth survey. The average tread depth for radial tires used for steering axles was 13/32 in. This was the highest tread depth among the groups. The average tread depth

Table 4.1. Number of Trucks in the Sample.

	Truck Type	Frequency	%
Single Units	SU-2	11	4.1
	SU-3	9	3.3
Trucks and Trailers	2-3	2	0.7
	3-2	16	5.9
	3-3	4	1.5
	3-4	3	1.1
	4-4	1	0.4
Tractors and Semi-Trailers	2-S1	12	4.4
	3-S1	3	1.1
	2-S2	11	4.1
	3-S2	151	55.9
	4-S2	1	0.4
	2-S3	1	0.4
	3-S3	1	0.4
Tractors, Semi-Trailers and Trailers	2-S1-2	10	3.7
	3-S1-2	11	4.1
	3-S2-2	3	1.1
	3-S2-3	3	1.1
	3-S2-4	1	0.4
	2-S1-2-2	4	1.5
	3-S1-2-2	2	0.7
	2-S1-2-1	1	0.4
Unknown		9	3.3
TOTAL		270	100



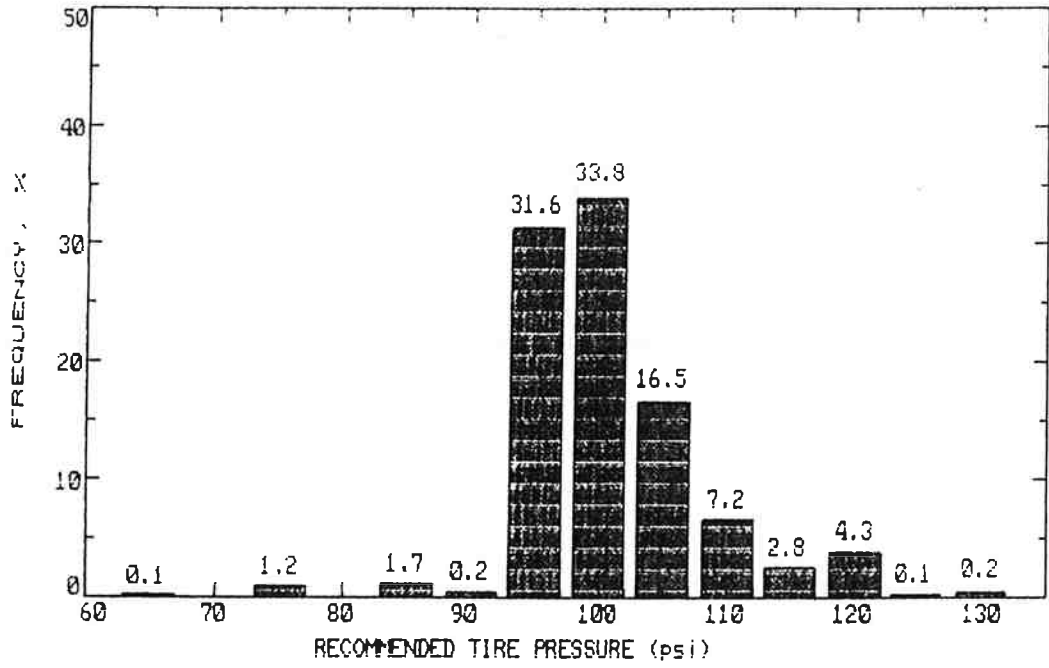
(1) Single Tire, Steering Axle



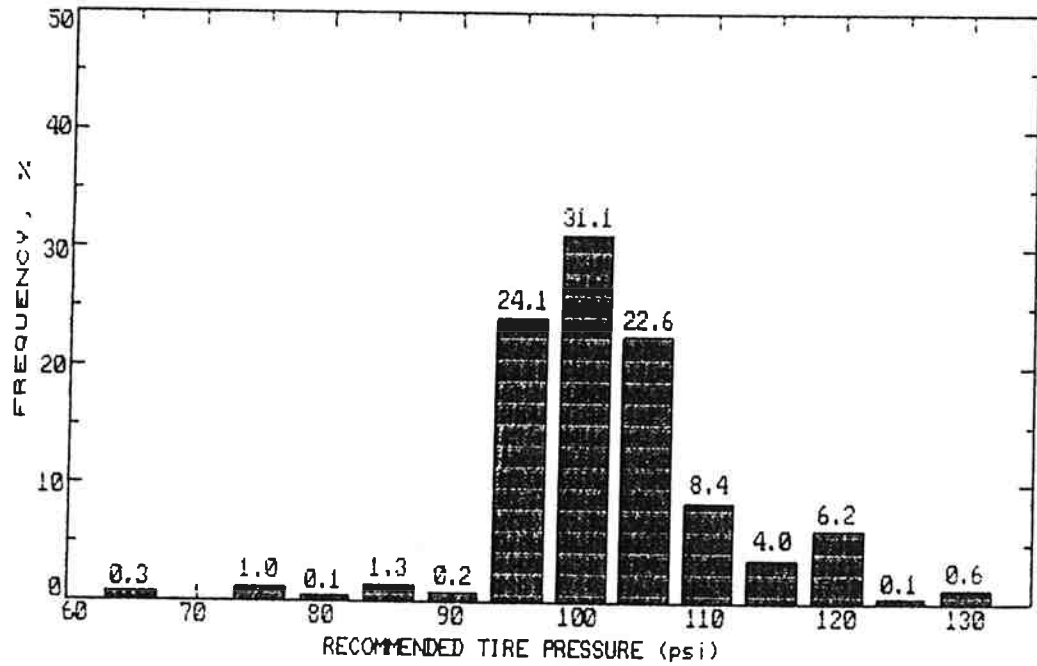
(2) Single Tire, Non-Steering Axle

(a) Radial Tire

Figure 4.2. The Distribution of the Manufacturer's Maximum Recommended Tire Pressure (Cold).



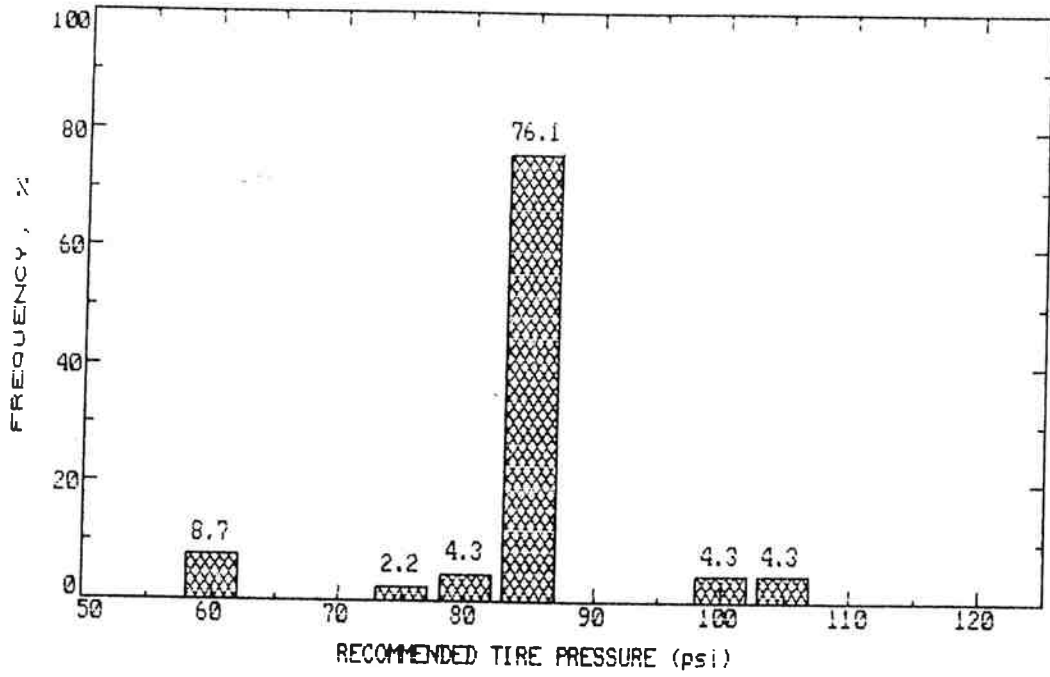
(3) Dual Tire, Non-Steering Axle



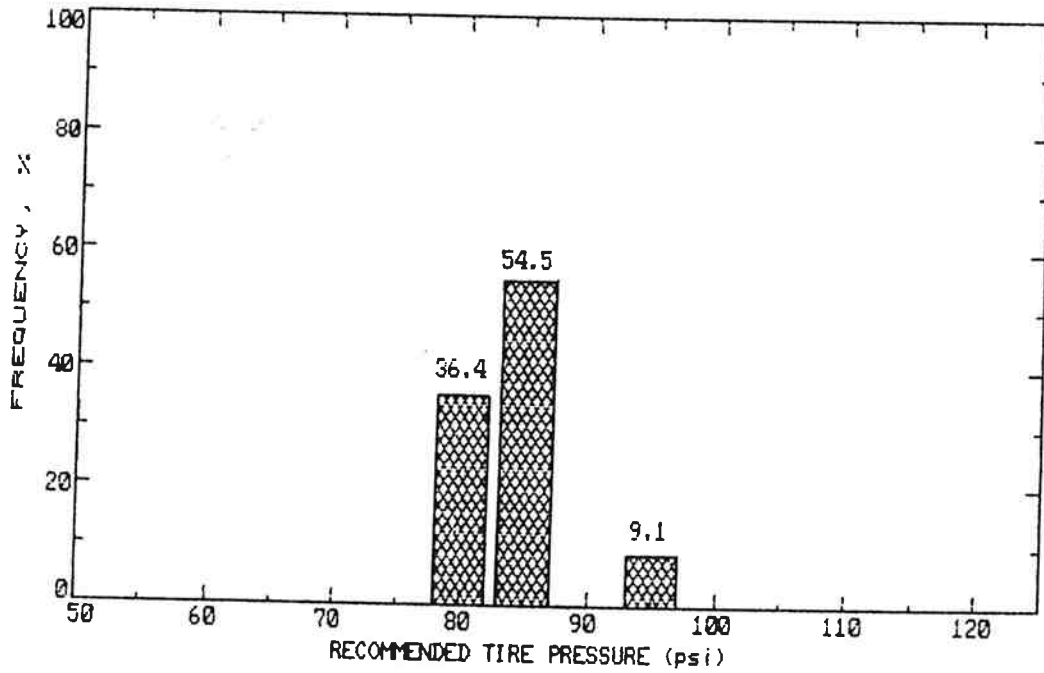
(4) Total Radial Tire

(a) Radial Tire

Figure 4.2. The Distribution of the Manufacturer's Maximum Recommended Tire Pressure (Cold) (Continued).



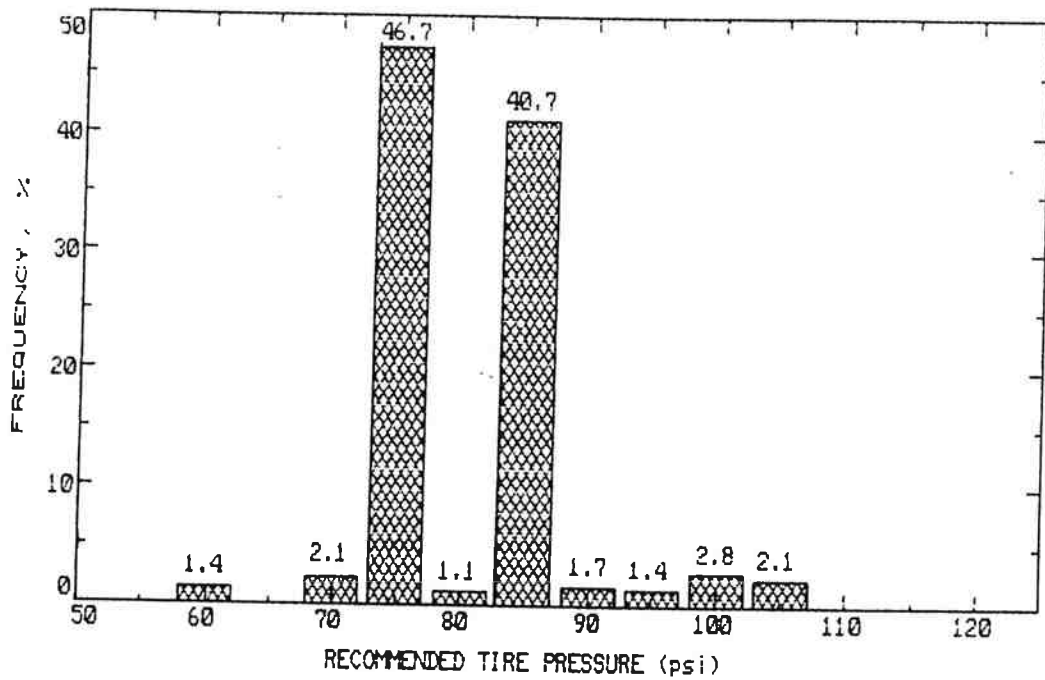
(1) Single Tire, Steering Axle



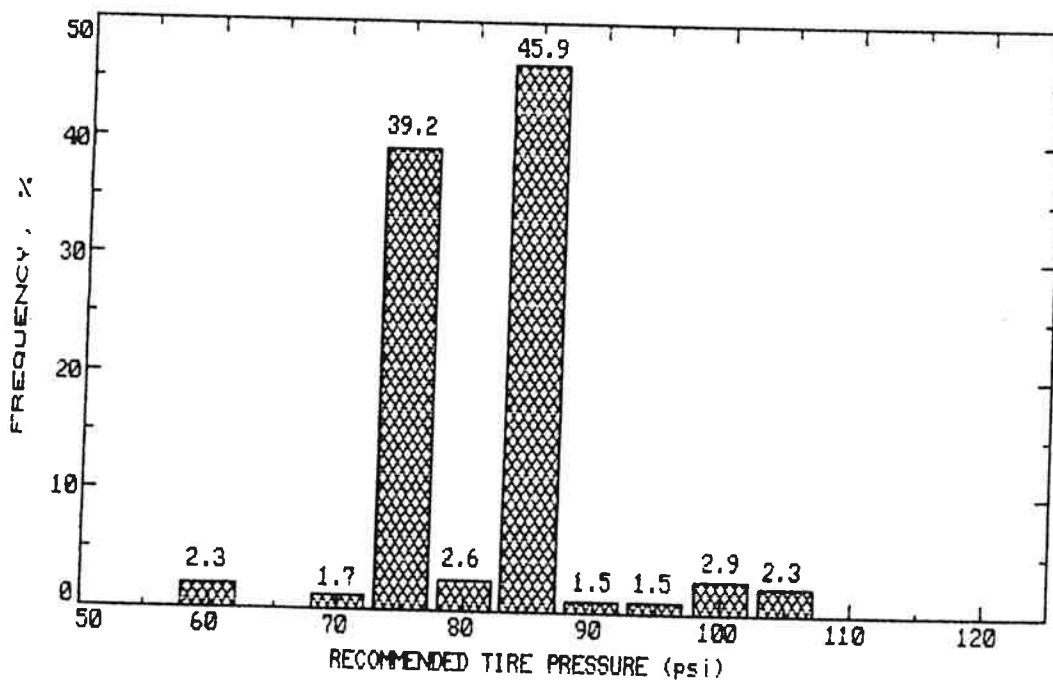
(2) Single Tire, Non-Steering Axle

(b) Bias Tire

Figure 4.2. The Distribution of the Manufacturer's Maximum Recommended Tire Pressure (Cold) (Continued).



(3) Dual Tire, Non-Steering Axle



(4) Total Bias Tire

(b) Bias Tire

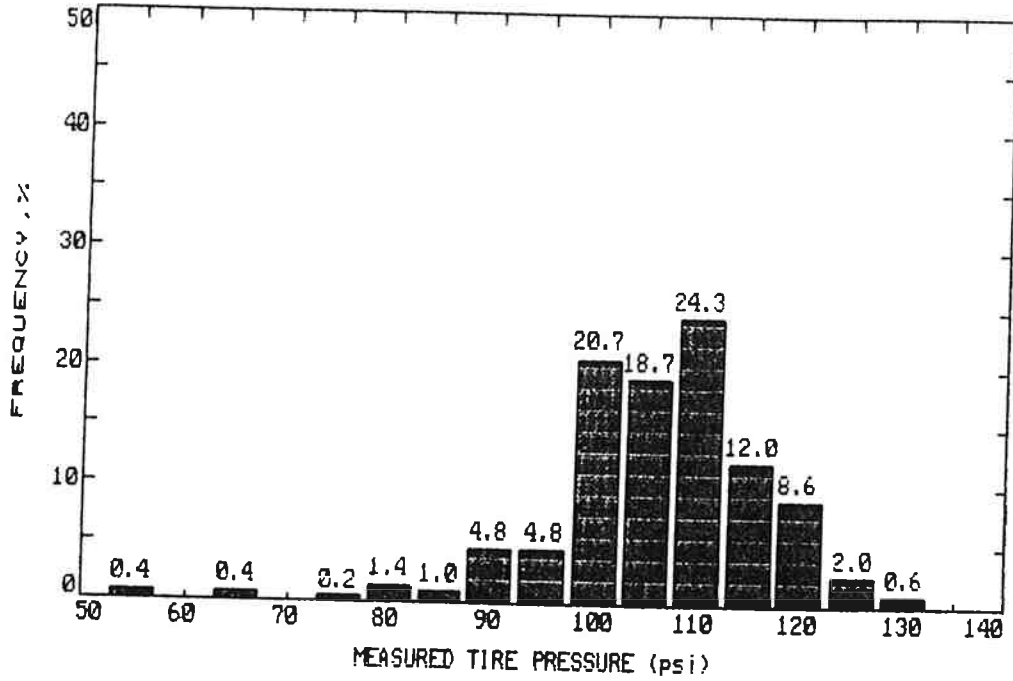
Figure 4.2. The Distribution of the Manufacturer's Maximum Recommended Tire Pressure (Cold) (Continued).

Table 4.2. Mean Values of Manufacturer's Maximum Recommended Tire Pressure (Cold).

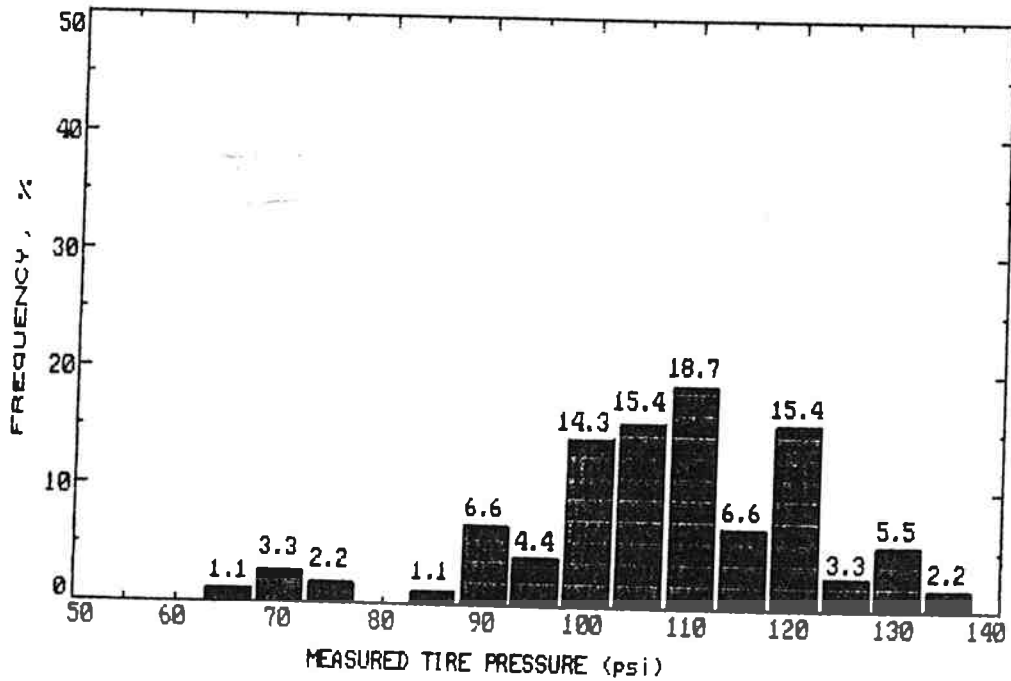
	Single Tire on Steering Axle		Single Tire on Non-Steering Axle		Dual Tire on Non-Steering Axle	
	Radial	Bias	Radial	Bias	Radial	Bias
Mean (psi)	106	84	108	84	101	81
Standard Deviation (psi)	7	9	14	4	8	8
Number in Sample	495	46	89	11	1735	285

Table 4.3. Mean Values of Measured Tire Pressure (Hot).

	Single Tire on Steering Axle		Single Tire on Non-Steering Axle		Dual Tire on Non-Steering Axle	
	Radial	Bias	Radial	Bias	Radial	Bias
Mean (psi)	106	86	107	93	102	82
Standard Deviation (psi)	10	17	15	10	12	15
Number in Sample	498	46	91	11	1755	292



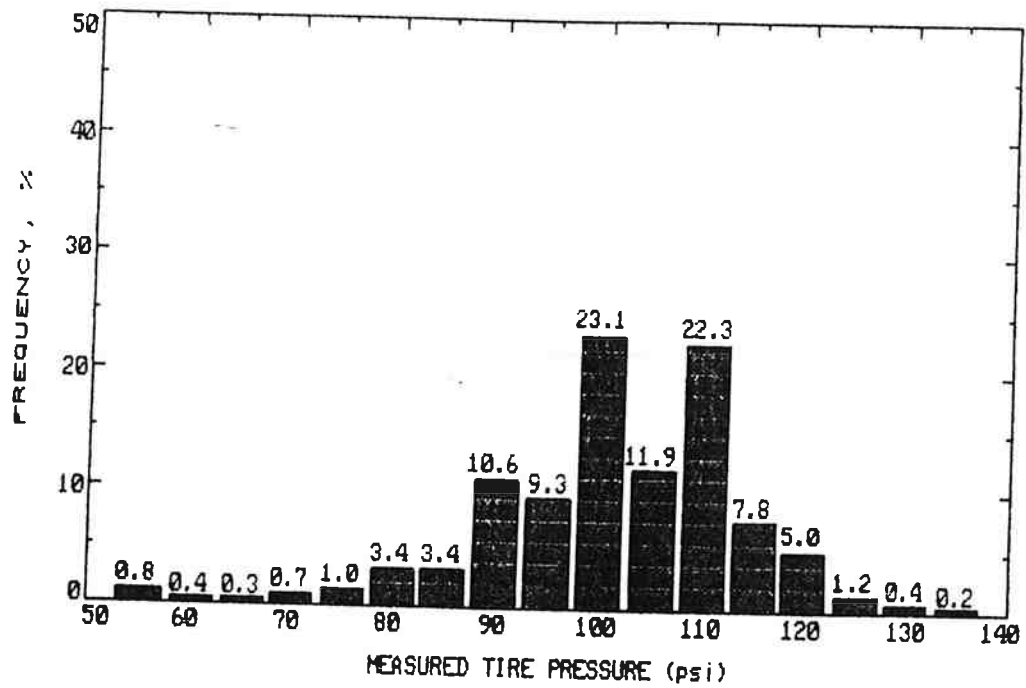
(1) Single Tire, Steering Axle



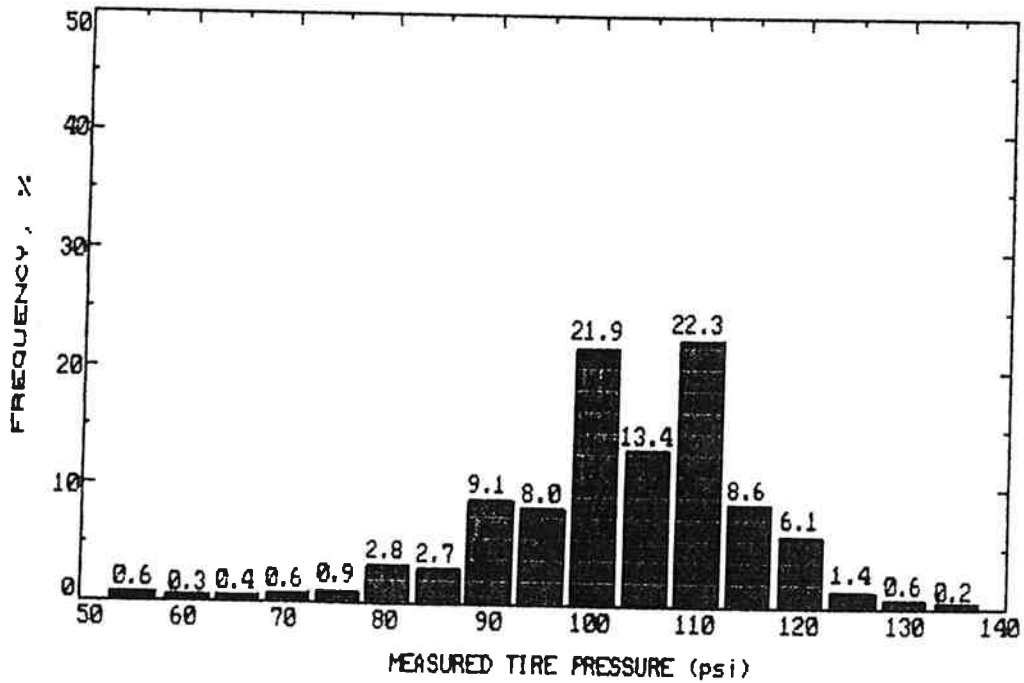
(2) Single Tire, Non-Steering Axle

(a) Radial Tire

Figure 4.3. The Distribution of the Measured Tire Pressure (Hot).



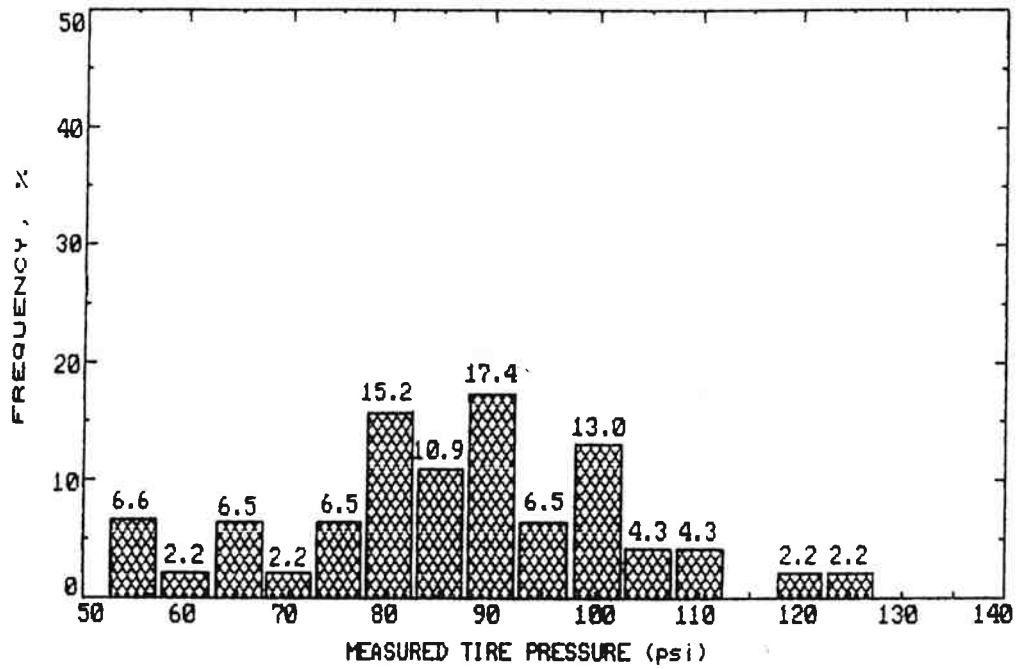
(3) Dual Tire, Non-Steering Axle



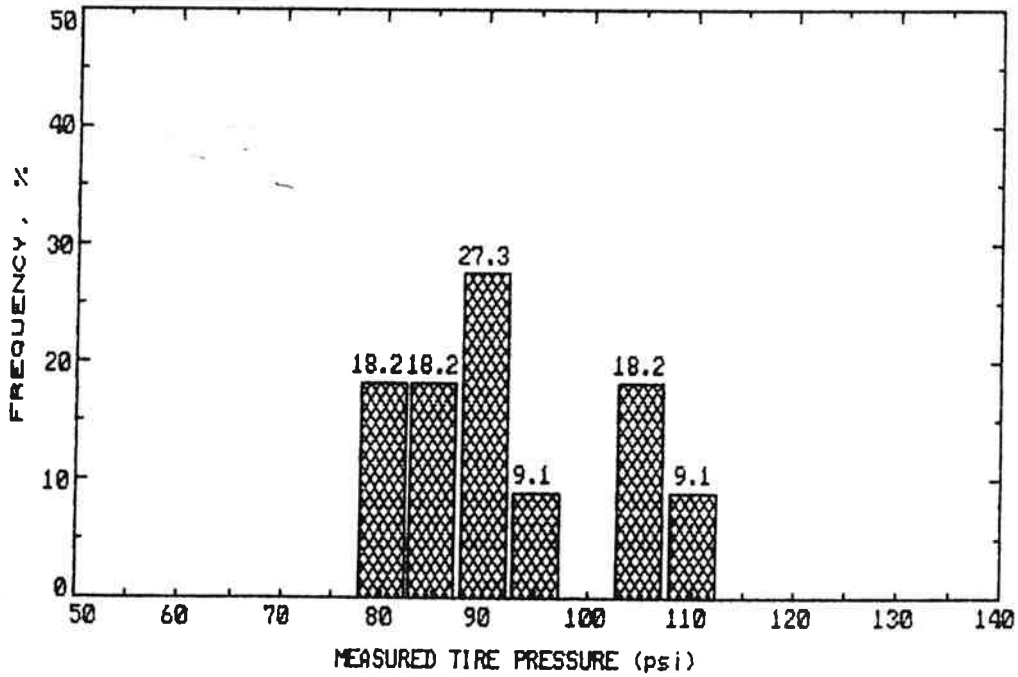
(4) Total Radial Tire

(a) Radial Tire

Figure 4.3. The Distribution of the Measured Tire Pressure (Hot) Continued).



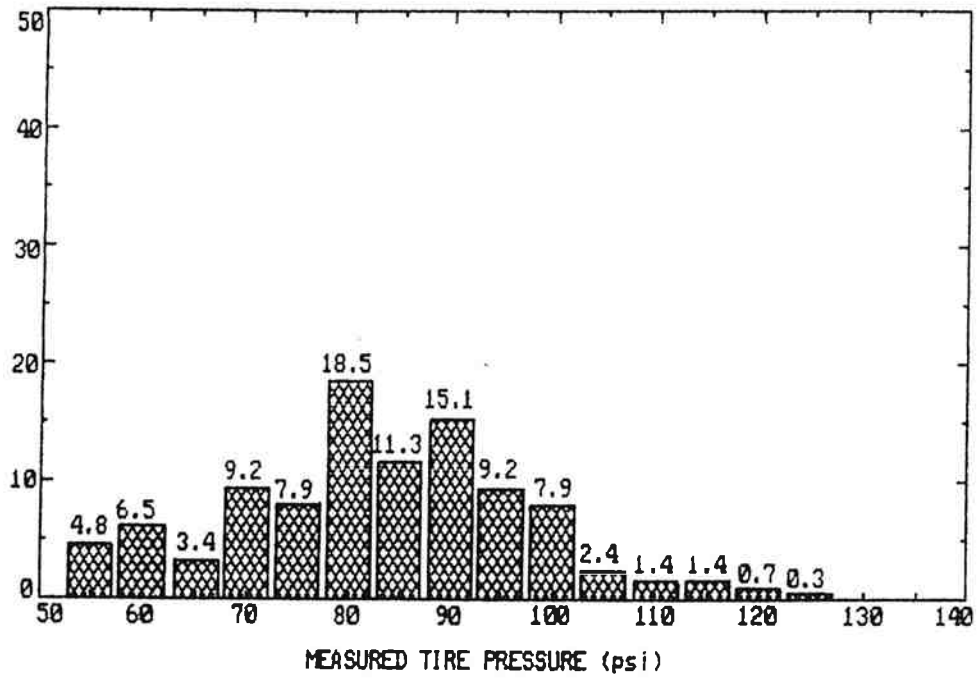
(1) Single Tire, Steering Axle



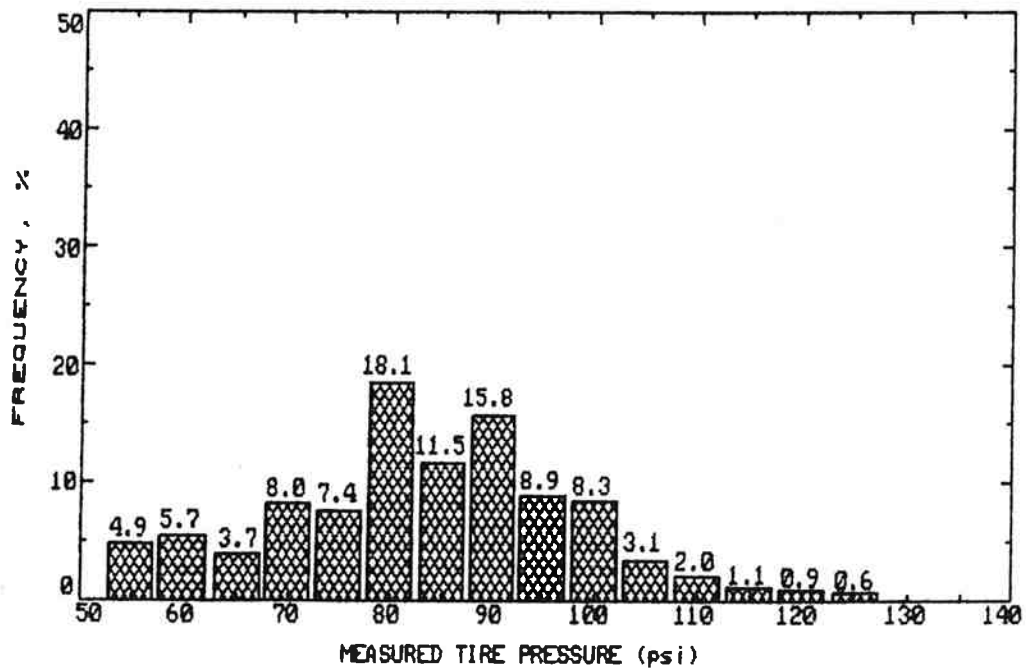
(2) Single Tire, Non-Steering Axle

(b) Bias Tire

Figure 4.3. The Distribution of the Measured Tire Pressure (Hot)
(Continued).



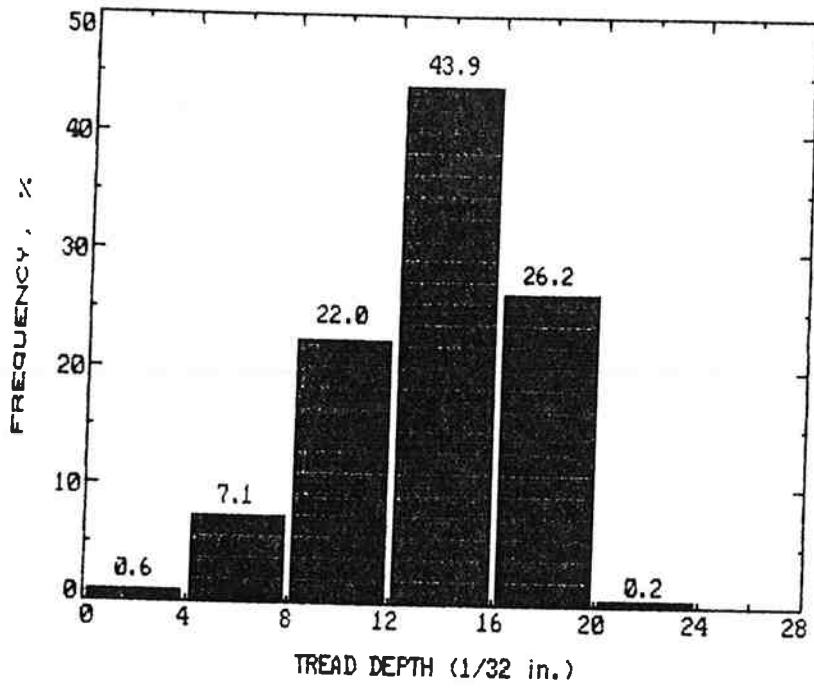
(3) Dual Tire, Non-Steering Axle



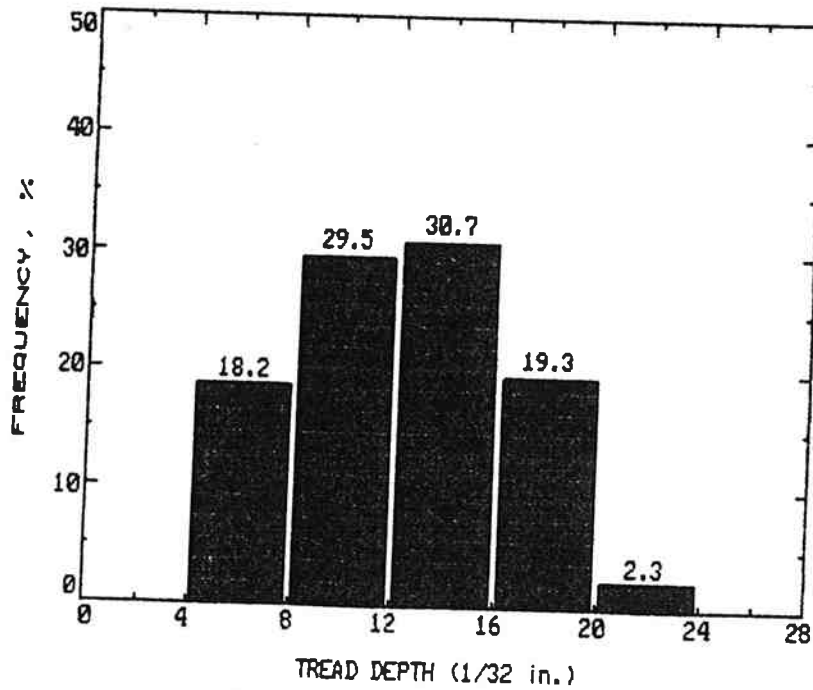
(4) Total Bias Tire

(b) Bias Tire

Figure 4.3. The Distribution of the Measured Tire Pressure (Hot)
(Continued).



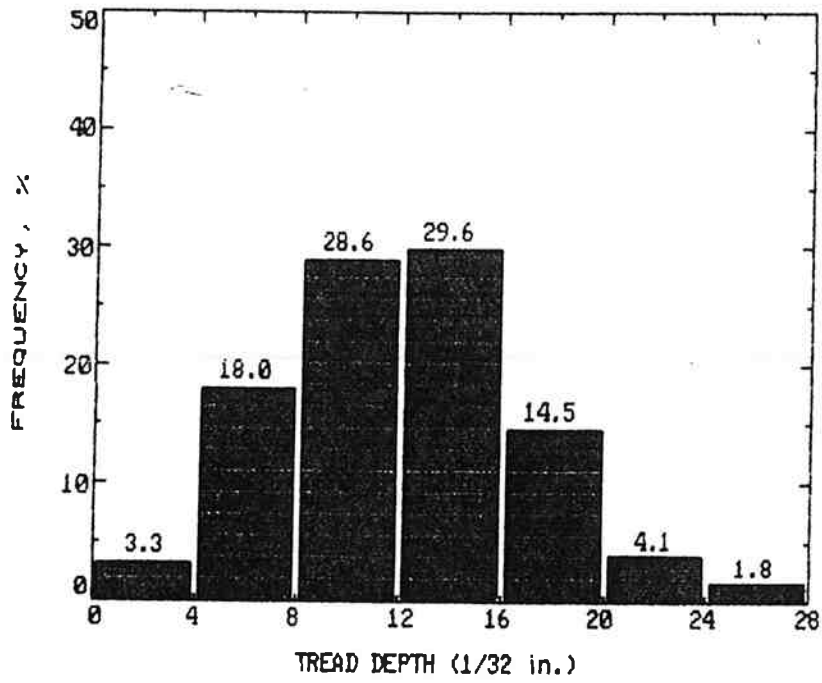
(1) Single Tire, Steering Axle



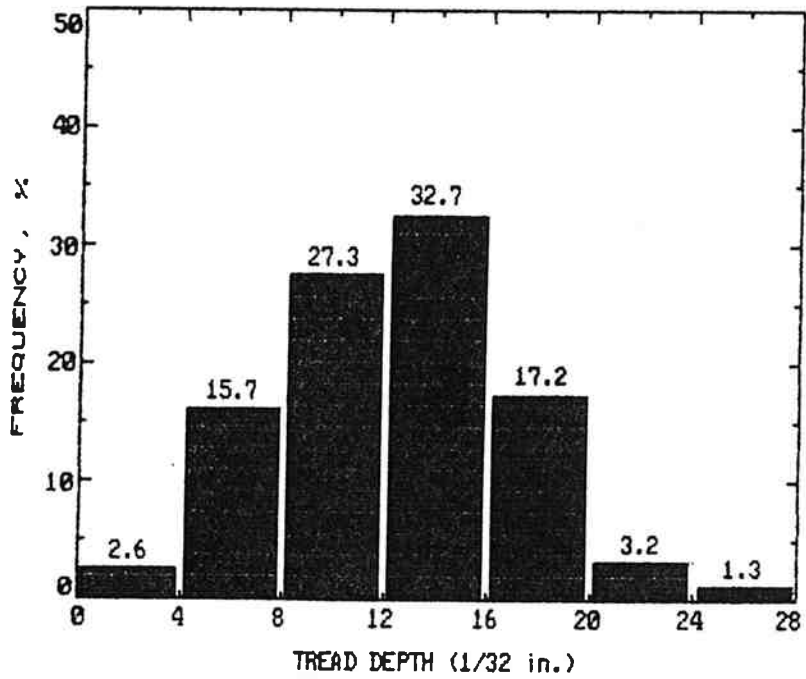
(2) Single Tire, Non-Steering Axle

(a) Radial Tire

Figure 4.4. Distribution of Measured Tread Depth.



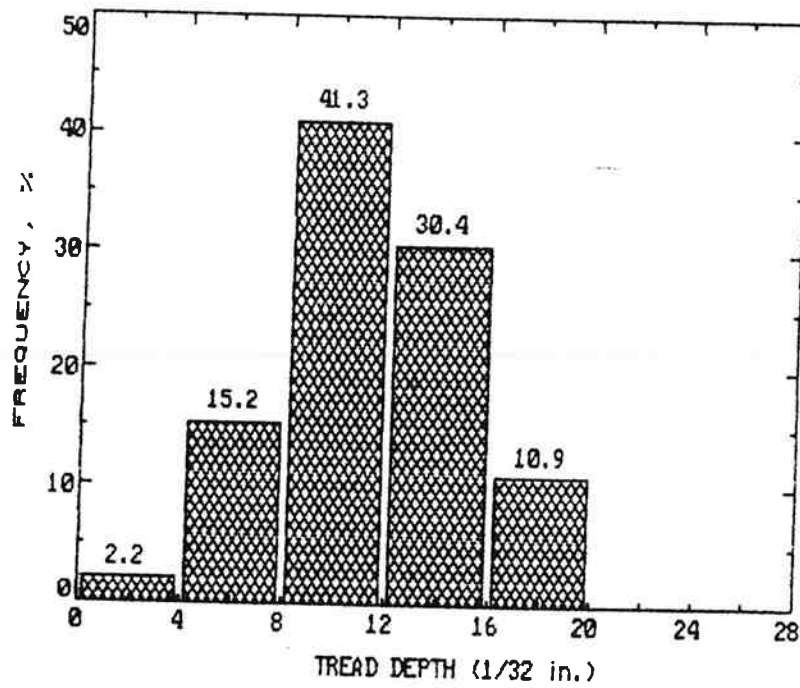
(3) Dual Tire, Non-Steering Axle



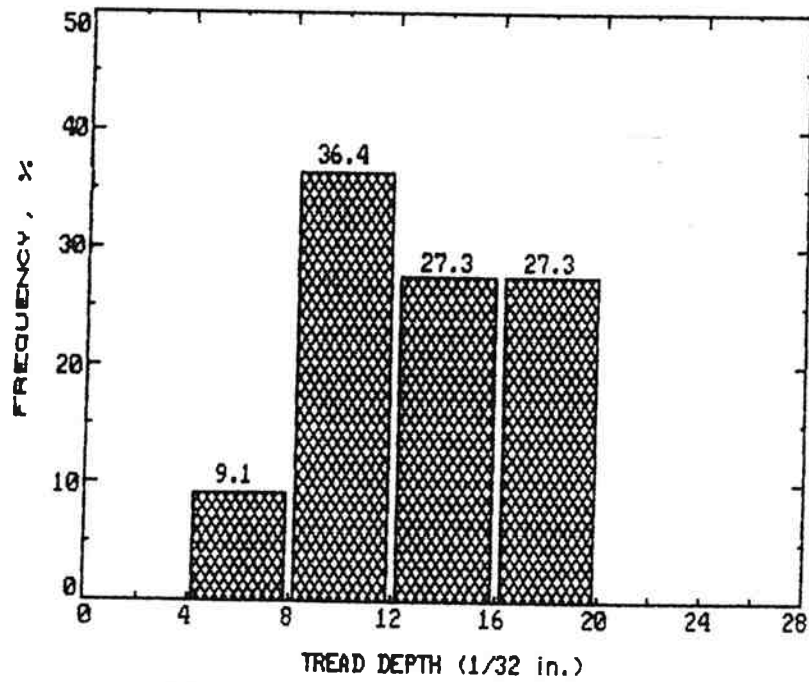
(4) Total Radial Tire

(a) Radial Tire

Figure 4.4. Distribution of Measured Tread Depth (Continued).



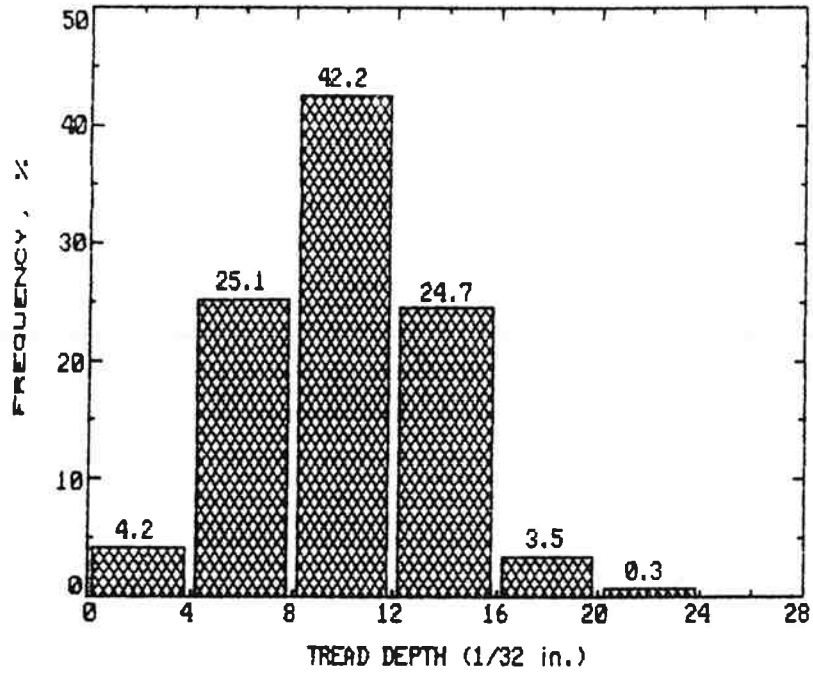
(1) Single Tire, Steering Axle



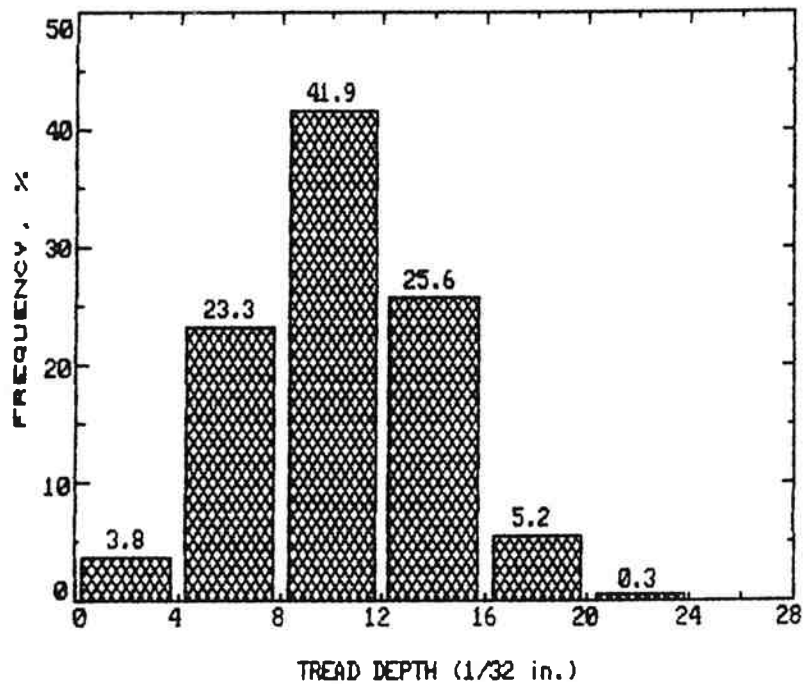
(2) Single Tire, Non-Steering Axle

(b) Bias Tire

Figure 4.4. Distribution of Measured Tread Depth (Continued).



(3) Dual Tire, Non-Steering Axle



(4) Total Bias Tire

(b) Bias Tire

Figure 4.4. Distribution of Measured Tread Depth (Continued).

Table 4.4. Mean Values of Measured Tread Depth (1/32-in.).

	Single Tire on Steering Axle		Single Tire on Non-Steering Axle		Dual Tire on Non-Steering Axle	
	Radial	Bias	Radial	Bias	Radial	Bias
Mean	13	11	12	12	11	9
Standard Deviation	3.4	3.7	4.3	3.7	4.9	3.4
Number in Sample	496	46	88	11	1746	287

for bias dual tires used for non-steering axles was 9/32 in. This was the lowest measured tread depth.

4.1.5 Tire Size

Table 4.5 presents the distribution of sizes for both the radial and bias tires in the sample. The major tire size for radials was 11/80R 24.5. However, for single tires on non-steering axles, the major size was 12 R 22.5, which was slightly wider than the 11/80 R 24.5. The major sizes for the bias tires were 11-24.5 and 10-20.00 as presented in Table 4.5b. It should be noted that 13.2% of the single tires used on non-steering axles were 15 R 22, i.e., 15 in. wide tires, which were wider than the major tire sizes. Figure 4.5 shows a description of the tire dimensional information used in truck tire size nomenclature.

More detailed data are presented in Appendix B.

4.1.6 Manufacturer

Table 4.6 presents the distribution, by manufacturer of both the radial and bias tires surveyed. It should be noted that one company, which supplied 28% of the radial tires in the survey, did not manufacture any of the bias tires.

More detailed data are presented in Appendix B.

4.2 Mix Designs

The summary of the mix design for each of the aggregate sources and different aggregate gradations is presented in Table 4.7. Table 4.7 includes the resilient modulus for unconditioned and freeze-thaw conditioned samples, and the minimum asphalt content for the retained modulus ratio of 0.7. The retained modulus ratio is defined by Eq. (4-1).

Table 4.5. Tire Size Distribution (%).

(a) Radial Tire

Tire Size	Single Tire on Steering Axle	Single Tire on Non-Steering Axle	Dual Tire on Non-Steering Axle
11/80 R 24.5	46.5	15.4	49.1
11 R 22.5	22.2	19.8	21.1
285/75 R 24.5	9.6	1.1	7.1
275/80 R 24.5	6.1	3.3	3.9
275/80 R 22.5	3.9	-	4.1
12 R 22.5	2.0	33.0	2.2
10.00 R 22	2.0	-	3.9
15 R 22.5	-	13.2	-
Others	7.7	14.2	8.6
Number in Sample	490	91	1737

(b) Bias Tire

Tire Size	Single Tire on Steering Axle	Single Tire on Non-Steering Axle	Dual Tire on Non-Steering Axle
11-24.5	30.8	-	30.8
10.00-20	15.4	36.4	29.8
10.00-22	11.5	18.1	21.2
11-22.5	17.3	-	9.9
9.00-20	3.8	45.5	2.6
Others	21.2	0.0	5.8
Number in Sample	52	11	302

NUMERIC (TWO PART):

7.00 R 15 LT
 Approx. Cross Section Width in Inches Radial Construction Rim Diameter in Inches Light Truck application

ALPHANUMERIC:

H R 78 - 15 LT
 Tire Size/Load Radial Const. Series (Aspect Ratio) Rim Diameter in Inches Light Truck application

METRIC:

LT 235 /85 R 16 E
 Light Truck Tire Section Width (MM) Aspect Ratio Radial Const. Rim Diameter Load Range

THREE PART (FLOTATION SIZING):

26 x 8.50 R 14 LT
 Overall Diam. in Inches Approx. Cross Section Width in Inches Radial Const. Rim Diam. in Inches Light Truck application

*Bias ply designated with a hyphen in place of "R".

Figure 4.5. Tire Sizing Designations (After Ref. 41).

4.6. Distribution of Tire Manufacturer (%).

(a) Radial Tire

	Single Tire on Steering Axle	Single Tire on Non-Steering Axle	Dual Tire on Non-Steering Axle
1. Michelin	25.0	36.3	28.4
2. Goodyear	22.0	11.0	22.7
3. Bridgestone	15.5	24.2	15.0
4. Toyo	9.7	15.4	9.6
5. Kelly	3.6	2.2	4.0
6. Yokohama	3.8	1.1	3.0
7. Firestone	2.2	1.1	2.8
8. OHTSU	3.6	1.1	1.7
Others	14.6	7.6	12.8
Number in Sample	496	91	1755

(b) Bias Tire

	Single Tire on Steering Axle	Single Tire on Non-Steering Axle	Dual Tire on Non-Steering Axle
1. Goodyear	10.9	30.0	23.2
2. Firestone	6.5	-	9.5
3. Goodrich	10.9	20.0	6.7
4. Bridgestone	-	-	7.7
5. General	-	10.0	7.0
6. Multimile	8.7	-	3.5
7. Dunlop	4.3	0	3.9
8. OHTSU	8.7	20.0	2.1
Others	50.0	20.0	36.4
Number in Sample	46	10	284

Table 4.7. Summary of Mix Design Data.

(a) Morse Brothers Pit, Gravel, Chevron AR-4000W, "C" a/c

Sample ID*	Max. Sp.Gr.	Bulk Sp.Gr.	Air Voids (%)	Asphalt Content (%)	VMA (%)	Hveem Stability	IRS ¹ (%)	M _r (ksi) Uncond. ²	M _r (ksi) Cond. ³	M _r Ratio ⁴	Min. A/C to .7 MRRT ⁵ (%)	Optimum A/C (%)
A32	2.484	2.26	9.0	5.0	15.9	33	60	258	146	0.56		
A33	2.455	2.30	6.3	6.0	14.7	35	82	227	197	0.87	5.5	6.6
A34	2.408	2.32	3.6	7.0	13.5	31	93	224	189	0.84		
B29	2.463	2.28	7.4	5.0	14.8	35	68	186	102	0.55		
B30	2.446	2.30	6.0	6.0	14.3	32	86	187	139	0.75	5.8	6.6
B31	2.423	2.33	3.8	7.0	13.8	33	92	194	133	0.69		
C26	2.489	2.34	6.0	4.5	12.4	36	49	492	161	0.33		
C27	2.466	2.37	3.9	5.5	11.8	37	77	447	349	0.78	5.3	5.1
C28	2.440	2.40	1.6	6.5	11.2	19	96	303	237	0.78		

*A, B, C = aggregate gradation type.

¹Index of Retained Strength (AASHTO T-165)

²M_r Uncond. = resilient modulus at 25°C, before conditioning

³M_r Cond. = resilient modulus at 25°C, after vacuum saturation and freeze-thaw conditioning

⁴M_r Ratio = $\frac{\text{resilient modulus after conditioning}}{\text{resilient modulus before conditioning}}$

⁵Min A/C .7 MRRT = minimum asphalt content for the retained modulus ratio (M_r Ratio) of 0.7

Table 4.7. Summary of Mix Design Data (Continued).
 (b) Cobb Rock Quarry, 1% Lime Slurry, Chevron AR-4000W, "C" a/c

Sample ID*	Max. Sp.Gr.	Bulk Sp.Gr.	Air Voids (%)	Asphalt Content (%)	VMA (%)	Hveem Stability	IRS ¹ (%)	M _r (ksi) Uncond. ²	M _r (ksi) Cond. ³	M _r Ratio ⁴	Min. A/C to .7 MRRT ⁵ (%)	Optimum A/C (%)
A11	2.514	2.25	10.5	4.5	15.1	41	62	361	172	0.48		
A12	2.476	2.29	7.5	5.5	14.5	37	75	320	346	1.08	4.9	6.3
A13	2.433	2.33	4.2	6.5	13.9	37	91	320	312	0.97		
B09	2.506	2.26	9.8	4.5	14.7	33	61	312	127	0.41		
B10	2.471	2.30	6.9	5.5	14.1	30	74	240	120	0.50	6.5	6.2
B11	2.433	2.34	4.2	6.5	13.5	37	87	266	187	0.70		
C09	2.512	2.33	7.2	4.5	12.0	39	42	465	301	0.65		
C10	2.471	2.37	4.1	5.5	11.5	31	63	392	501	1.28	4.6	5.3
C11	2.428	2.41	0.1	6.5	10.9	5	75	282	374	1.33		
D29	2.541	2.31	9.1	4.0	12.3	45	37	205	76	0.37		
D30	2.497	2.35	5.9	5.0	11.8	38	56	404	242	0.60	5.2	5.3
D31	2.459	2.39	2.8	6.0	11.2	33	69	232	302	1.30		

*A, B, C, D = aggregate gradation type.

¹Index of Retained Strength (AASHTO T-165)

²M_r Uncond. = resilient modulus at 25°C, before conditioning

³M_r Cond. = resilient modulus at 25°C, after vacuum saturation and freeze-thaw conditioning

⁴M_r Ratio = $\frac{\text{resilient modulus after conditioning}}{\text{resilient modulus before conditioning}}$

⁵Min A/C .7 MRRT = minimum asphalt content for the retained modulus ratio (M_r Ratio) of 0.7

Table 4.7. Summary of Mix Design Data (Continued).
(c) Hilroy Pit, Gravel, Chevron AR-4000W, "B" a/c

Sample ID*	Max. Sp.Gr.	Bulk Sp.Gr.	Air Voids (%)	Asphalt Content (%)	VMA (%)	Hveem Stability	IRS ¹ (%)	M _r (ksi) Uncond. ²	M _r (ksi) Cond. ³	M _r Ratio ⁴	Min. A/C to .7 MRRT ⁵ (%)	Optimum A/C (%)
A30	2.501	2.27	9.2	4.5	15.3	38	52	362	94	0.26		
A31	2.465	2.31	6.3	5.5	14.7	38	75	252	115	0.46	6.4	6.1
A32	2.429	2.34	3.7	6.5	14.5	36	88	239	180	0.75		
B21	2.493	2.27	8.9	4.5	15.3	36	59	364	93	0.26		
B22	2.459	2.29	6.9	5.5	15.5	35	64	280	150	0.54	6.9	6.2
B23	2.422	2.33	3.8	6.5	14.9	34	84	265	176	0.66		
C24	2.523	2.33	7.7	4.0	12.6	39	54	541	66	0.12		
C25	2.477	2.37	4.3	5.0	12.1	44	67	438	159	0.36	5.8	4.9
C26	2.437	2.41	1.1	6.0	11.5	35	87	384	302	0.79		
D27	2.474	2.33	5.8	5.0	13.5	40	54	391	142	0.36		
D28	2.431	2.37	2.5	6.0	13.0	41	67	403	260	0.65	6.3	5.3
D29	2.414	2.40	0.6	7.0	12.8	18	95	329	284	0.87		
E29	2.519	2.29	9.1	4.0	14.1	40	58	752	175	0.23		
E30	2.482	2.34	5.7	5.0	13.2	37	83	401	199	0.50	7.0	5.5
E31	2.443	2.35	3.8	6.0	13.7	40	84	396	239	0.60		
F09	2.519	2.30	8.7	4.0	13.8	37	40	420	89	0.21		
F10	2.482	2.38	4.1	5.0	11.7	39	68	429	293	0.68	5.3	4.9
F11	2.452	2.40	2.1	6.0	11.9	36	102	374	272	0.74		

*A, B, C, D, E, F = aggregate gradation type.

¹Index of Retained Strength (AASHTO T-165)

²M_r Uncond. = resilient modulus at 25°C, before conditioning

³M_r Cond. = resilient modulus at 25°C, after vacuum saturation and freeze-thaw conditioning

⁴M_r Ratio = $\frac{\text{resilient modulus after conditioning}}{\text{resilient modulus before conditioning}}$

⁵Min A/C .7 MRRT = minimum asphalt content for the retained modulus ratio (M_r Ratio) of 0.7

Table 4.7. Summary of Mix Design Data (Continued).

(d) Blue Mountain Asphalt Pit, Gravel, 1% Lime Slurry, Chevron AC-20, "B" a/c

Sample ID*	Max. Sp.Gr.	Bulk Sp.Gr.	Air Voids (%)	Asphalt Content (%)	VMA (%)	Hveem Stability	IRS ¹ (%)	M _r (ksi) Uncond. ²	M _r (ksi) Cond. ³	M _r Ratio ⁴	Min. A/C to .7 MRRT ⁵ (%)	Optimum A/C (%)
A38	2.583	2.33	9.8	4.5	17.9	29	81	437	214	0.49		
A39	2.545	2.37	6.9	5.5	17.4	30	88	404	291	0.72	5.4	6.3
A40	2.504	2.41	3.8	6.5	16.9	30	103	371	289	0.78		
B32	2.590	2.36	8.9	4.5	16.8	37	88	465	294	0.63		
B33	2.548	2.40	5.8	5.5	16.3	37	96	425	346	0.81	4.9	5.9
B34	2.510	2.44	2.8	6.5	15.8	38	101	374	346	0.92		
C29	2.607	2.37	9.1	4.0	16.0	39	70	679	339	0.5		
C30	2.565	2.41	6.0	5.0	15.5	38	85	630	353	0.56	5.4	5.4
C31	2.517	2.45	2.7	6.0	15.0	27	95	601	536	0.89		
D35	2.617	2.36	9.8	4.0	16.4	40	69	650	317	0.49		
D36	2.568	2.40	6.5	5.0	15.9	38	81	592	292	0.49	6.0	5.6
D37	2.530	2.44	3.6	6.0	15.4	33	86	523	372	0.71		
E37	2.607	2.32	11.0	4.0	17.8	37	77	836	496	0.59		
E36	2.574	2.39	7.1	5.0	16.2	35	82	728	737	1.01	4.3	5.7
E35	2.528	2.44	3.5	6.0	15.4	33	88	753	499	0.66		

*A, B, C, D, E = aggregate gradation type.

¹Index of Retained Strength (AASHTO T-165)

²M_r Uncond. = resilient modulus at 25°C, before conditioning

³M_r Cond. = resilient modulus at 25°C, after vacuum saturation and freeze-thaw conditioning

⁴M_r Ratio = $\frac{\text{resilient modulus after conditioning}}{\text{resilient modulus before conditioning}}$

⁵Min A/C .7 MRRT = minimum asphalt content for the retained modulus ratio (M_r Ratio) of 0.7

$$\text{Retained Modulus Ratio} = \frac{\text{Resilient Modulus after Conditioning}}{\text{Resilient Modulus before Conditioning}} \quad (4-1)$$

4.3 Creep Test

Table 4.8 presents the creep test results after a regression analysis; including the intercept (I), slope (S), creep stiffness after 60 min., and the coefficients of determination (R^2). The regression analysis was performed on data taken at loading times 1 min. to 90 min. (see Figure E.1 in Appendix E).

The intercept and the slope of the creep test curves for each sample were obtained by the following equations:

$$\log (\text{strain, \%}) = \log (I) + S * \log (\text{time,sec}) \quad (4-2)$$

or

$$\text{strain, \%} = (I) * (\text{time,sec}) ** S \quad (4-3)$$

The creep strain and creep stiffness were determined by the following equations:

$$\epsilon = \frac{\Delta h}{h} \quad (4-4)$$

where ϵ = creep strain

Δh = deformation at time t , and

h = thickness of specimen.

$$S_{\text{mix}} (T, t) = \frac{\sigma}{\epsilon (T, t)} \quad (4-5)$$

where $S_{\text{mix}} (T, t)$ = creep stiffness at temperature T and time t ,

σ = compressive stress, and

$\epsilon (T, t)$ = creep strain at temperature T and time t .

The creep stiffness of each sample as presented in Table 4.8, is the

Table 4.8. Creep Test Results.

(a) Morse Brothers Pit, Gravel, Chevron AR-4000W, Class "C" Mix

Sample ID*	Asphalt Content (%)	S_{mix}^1 (ksi)	I^2	S^3	R^2
A32	5.0	3.47	0.098	0.177	0.961
A33	6.0	3.93	0.132	0.126	0.957
A34	7.0	3.14	0.116	0.169	0.996
B29	5.0	4.14	0.126	0.124	0.929
B30	6.0	6.37	0.084	0.122	0.930
B31	7.0	2.83	0.146	0.153	0.983
C26	4.5	3.57	0.142	0.129	0.951
C27	5.5	4.85	0.117	0.114	0.977
C28	6.5	5.24	0.069	0.170	0.973

*A, B, C = aggregate gradation type

¹ S_{mix} = predicted creep stiffness at 60 min., after regression

² I = interception; strain, % at 1 sec

³ S = slope; strain, % = $I * (time, sec) ** S$

⁴ R^2 = coefficient of determination

Table 4.8. Creep Test Results (Continued).

(b) Cobb Rock Quarry, 1% Lime Slurry, Chevron AR-400W, Class "C" Mix

Sample ID*	Asphalt Content (%)	S_{mix}^1 (ksi)	I^2	S^3	R^*R^4
A11	4.5	4.76	0.135	0.099	0.940
A12	5.5	3.68	0.171	0.102	0.929
A13	6.5	5.40	0.105	0.115	0.997
B09	4.5	5.15	0.096	0.134	0.940
B10	5.5	3.33	0.206	0.091	0.931
B11	6.5	7.33	0.069	0.128	0.948
C09	4.5	3.95	0.075	0.194	0.998
C10	5.5	2.80	0.114	0.185	0.985
C11	6.5	1.47	0.307	0.143	0.962
D29	4.0	5.03	0.107	0.121	0.942
D30	5.0	3.81	0.093	0.172	0.964
D31	6.0	3.73	0.113	0.151	0.985

*A, B, C, D = aggregate gradation type

$^1S_{mix}$ = predicted creep stiffness at 60 min., after regression

2I = interception; strain, % at 1 sec

3S = slope; strain, % = $I * (time, sec) ** S$

$^4R^*R$ = coefficient of determination

Table 4.8. Creep Test Results (Continued).
(c) Hilroy Pit, Gravel Chevron AR-4000W, Class "B" Mix

Sample ID*	Asphalt Content (%)	S _{mix} ¹ (ksi)	I ²	S ³	R*R ⁴
A30	4.5	5.06	0.127	0.099	0.898
A31	5.5	3.50	0.128	0.143	0.929
A32	6.5	2.05	0.073	0.277	0.983
B21	4.5	6.07	0.058	0.173	0.889
B22	5.5	4.85	0.064	0.188	0.944
B23	6.5	3.75	0.051	0.247	0.938
C24	4.0	4.05	0.101	0.155	0.960
C25	5.0	4.62	0.056	0.210	0.979
C26	6.0	3.59	0.091	0.182	0.984
D27	5.0	5.72	0.058	0.180	0.990
D28	6.0	8.06	0.046	0.167	0.945
D29	7.0	2.70	0.135	0.169	0.973
E29	4.0	5.90	0.027	0.271	0.977
E30	5.0	7.52	0.018	0.292	0.964
E31	6.0	7.77	0.018	0.283	0.976
F09	4.0	4.87	0.025	0.303	0.971
F10	5.0	4.70	0.020	0.336	0.980
F11	6.0	4.58	0.130	0.109	0.803

*A, B, C, D, E, F = aggregate gradation type

¹S_{mix} = predicted creep stiffness at 60 min., after regression

²I = interception; strain, % at 1 sec

³S = slope; strain, % = I * (time,sec) ** S

⁴R*R = coefficient of determination

Table 4.8. Creep Test Results (Continued).
 (d) Blue Mountain Asphalt Pit, Gravel, 1% Lime Slurry,
 Chevron AC-20, Class "B" Mix

Sample ID*	Asphalt Content (%)	S _{mix} ¹ (ksi)	I ²	S ³	R*R ⁴
A38	4.5	5.34	0.137	0.084	0.939
A39	5.5	4.91	0.182	0.059	0.922
A40	6.5	2.31	0.148	0.176	0.991
B32	4.5	2.24	0.270	0.107	0.942
B33	5.5	2.99	0.188	0.116	0.945
B34	6.5	2.57	0.175	0.143	0.984
C29	4.0	2.61	0.182	0.137	0.965
C30	5.0	2.42	0.243	0.110	0.984
C31	6.0	1.48	0.358	0.123	0.970
D35	4.0	3.90	0.094	0.169	0.956
D36	5.0	2.17	0.206	0.143	0.968
D37	6.0	2.88	0.190	0.119	0.967
E38	4.0	5.01	0.031	0.273	0.943
E39	5.0	5.86	0.027	0.269	0.941
E40	6.0	4.25	0.012	0.409	0.952

*A, B, C, D, E = aggregate gradation type

¹S_{mix} = predicted creep stiffness at 60 min., after regression

²I = interception; strain, % at 1 sec

³S = slope; strain, % = I * (time, sec) ** S

⁴R*R = coefficient of determination

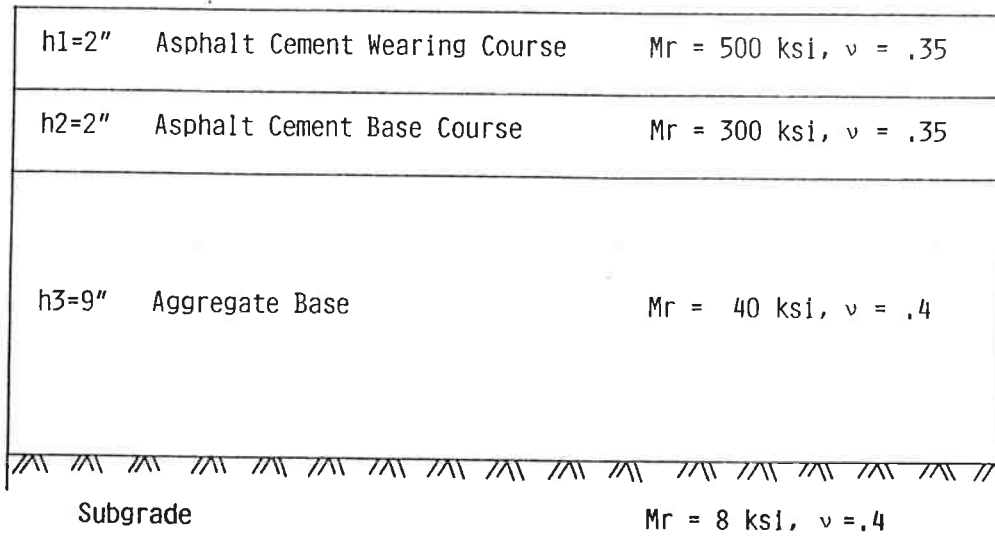
predicted value after a regression analysis. It is not the measured creep stiffness.

4.4 Analysis of Pavement Structure

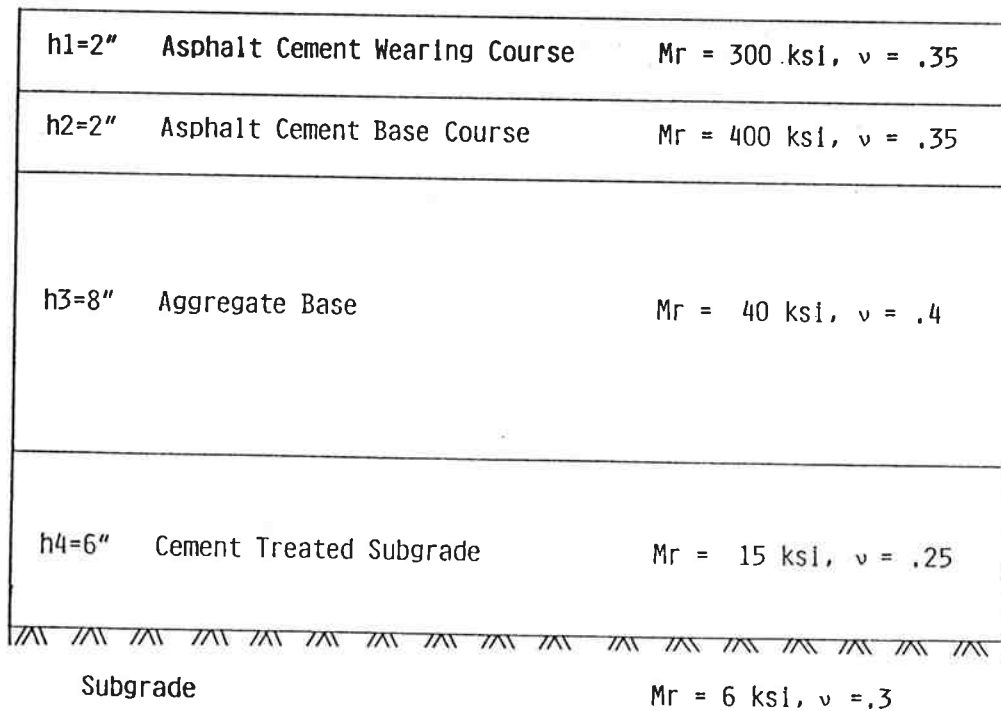
In order to investigate the effects of the increased tire pressures and axle loads on asphalt concrete pavements, ELSYM5 (42) (a computer program distributed by FHWA for microcomputers) was used for the analysis of two typical asphalt concrete pavement structural sections found on state highways in Oregon (Figure 4.6). Reasonable values of the input parameters (moduli, and Poisson's ratio) of each course were assumed. The structural numbers (SN) for each pavement were 3.0 and 3.4.

The tire pressures used for ELSYM5 were 80, 100, 125, and 150 psi. The maximum tensile strain at the bottom of the asphalt concrete base course and the maximum compressive strain at the top of the subgrade are presented in Tables 4.9 and 4.10 and are shown in Figures 4.6 (a) and (b), respectively.

Figure 4.7 shows the dimensions for the axle and tire configurations used in the computer program input.



(a) Asphalt Concrete Pavement A (SN = 3.0)



(b) Asphalt Concrete Pavement B (SN = 3.4)

Figure 4.6. Typical Asphalt Concrete Pavement Structural Sections in Oregon.

Table 4.9. Effect of Increased Tire Pressure on Tensile Strain at the Bottom of Asphalt Concrete Base Layer.

(a) Pavement Type A in Figure 4.6 ($\times 10^6$ Strain)

Axle Load (kips)	Single Axle			Single Axle			Tandem Axle			Tandem Axle		
	80	100	125	80	100	125	80	100	125	80	100	125
2	86.9	90.6	93.9	96.2	53.1	54.3	55.3	55.9	--	--	--	--
6	186.3	203.4	219.7	232.3	132.0	138.9	145.1	149.7	--	--	--	--
10	243.7	272.8	302.1	325.7	189.8	203.6	216.5	226.3	167.1	180.9	193.8	203.5
14	281.8	320.8	361.1	394.6	235.2	255.6	275.4	290.8	203.5	223.9	243.6	259.0
18	309.1	356.2	406.0	448.1	272.6	299.1	325.4	346.3	232.0	258.3	284.6	305.5
22	329.5	383.4	441.3	491.1	304.4	336.4	368.8	395.1	255.0	286.8	319.0	345.2
26	345.1	405.0	469.9	526.4	342.0	369.2	407.2	438.5	274.0	310.7	348.5	379.6
30	357.1	422.3	493.5	556.0	380.4	402.8	441.6	477.6	290.0	331.1	374.0	409.8
34	366.6	436.3	513.2	581.1	417.4	442.1	472.9	513.2	303.7	348.9	396.4	436.5
38	373.9	447.7	529.7	602.6	451.6	480.2	508.5	546.0	315.5	364.4	416.3	460.4
42	--	--	--	--	--	517.2	547.7	576.4	325.8	378.1	434.0	481.9
46	--	--	--	--	--	552.1	586.1	614.1	334.7	390.2	449.9	501.4
50	--	--	--	--	--	584.4	623.6	653.4	342.6	401.0	464.3	519.1

(b) Pavement Type B in Figure 4.6 ($\times 10^6$ Strain)

Axle Load (kips)	Single Axle			Single Axle			Tandem Axle			Tandem Axle		
	80	100	125	80	100	125	80	100	125	80	100	125
2	85.1	89.2	92.7	95.3	51.8	53.1	54.1	54.8	--	--	--	--
6	176.2	194.1	211.4	224.7	125.8	133.0	140.0	144.9	--	--	--	--
10	225.3	254.8	284.9	309.5	177.7	192.2	205.9	216.4	158.7	173.2	187.0	197.5
14	256.4	295.0	335.6	369.7	217.0	238.1	258.8	275.2	190.5	211.6	232.3	248.6
18	277.8	323.6	372.8	415.1	248.5	275.5	302.7	324.7	214.6	241.6	268.7	290.6
22	293.2	345.0	401.4	450.6	274.9	307.1	340.1	367.3	233.6	265.6	298.6	325.7
26	304.4	361.4	424.0	479.2	305.4	334.3	372.6	404.6	249.0	285.5	323.6	355.5
30	312.7	374.1	442.2	502.6	338.9	360.3	401.4	437.9	261.6	302.1	345.0	381.3
34	318.7	384.0	456.9	522.1	371.2	394.5	427.3	467.8	272.1	316.2	363.4	403.8
38	323.0	391.7	469.0	538.4	401.0	427.7	454.7	495.0	281.0	328.4	379.5	423.6
42	--	--	--	--	--	460.1	488.8	520.0	288.5	338.9	393.7	441.2
46	--	--	--	--	--	490.4	522.3	549.1	295.0	348.1	406.2	456.9
50	--	--	--	--	--	518.4	555.1	583.2	300.4	356.2	417.3	471.1

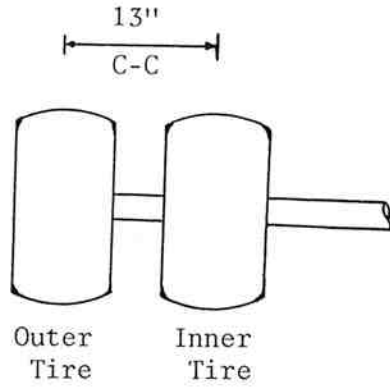
Table 4.10. Effect of Increased Tire Pressure on Compressive Strain at the Top of Subgrade.

(a) Pavement Type A in Figure 4.6 ($\times 10^{-6}$ Strain)

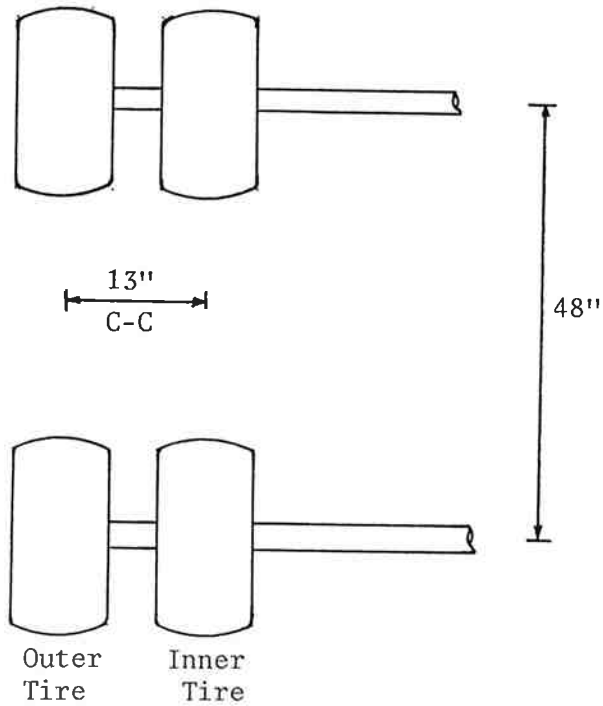
Axle Load (kips)	Single Axle			Tandem Axle			Tandem Axle				
	80	100	125	80	100	125	80	100	125		
2	117.4	119.7	122.6	125.2	88.9	90.4	92.0	93.5	150	150	150
6	337.2	339.0	340.9	342.9	260.9	261.5	261.9	262.2	285.4	286.9	288.9
10	550.4	556.6	560.9	563.6	431.9	433.4	434.6	435.4	402.4	400.5	402.4
14	751.3	765.0	775.2	781.3	600.5	603.4	605.8	607.3	508.6	511.9	514.2
18	940.6	963.5	981.6	993.0	766.7	771.5	775.4	778.0	503.9	508.6	511.9
22	1119	1153	1180	1198	930.5	937.7	943.5	947.4	608.7	616.5	622.1
26	1289	1334	1371	1397	1092	1102	1110	1115	722.0	730.5	735.5
30	1450	1507	1555	1589	1251	1264	1275	1282	809.3	825.0	844.3
34	1604	1673	1733	1775	1408	1425	1439	1448	905.2	925.6	941.5
38	1751	1833	1905	1956	1562	1583	1601	1612	998.5	1024	1044
42	--	--	--	--	--	1740	1761	1775	1089	1120	1145
46	--	--	--	--	--	1895	1920	1937	1178	1213	1243
50	--	--	--	--	--	2048	2078	2097	1264	1305	1340

(b) Pavement Type B in Figure 4.6 ($\times 10^{-6}$ Strain)

Axle Load (kips)	Single Axle			Tandem Axle			Tandem Axle				
	80	100	125	80	100	125	80	100	125		
2	99.7	102.6	105.9	108.8	83.2	84.9	86.6	88.0	150	150	150
6	278.4	280.1	282.7	285.9	239.9	240.3	240.6	240.9	240.9	240.9	240.9
10	459.5	461.6	463.5	465.3	397.5	398.7	399.6	400.2	240.9	242.9	246.1
14	636.2	641.4	644.9	647.0	553.3	555.5	557.3	558.6	334.8	336.3	338.5
18	806.7	816.9	823.9	827.9	707.3	711.0	713.9	715.9	428.6	430.3	432.1
22	971.1	987.4	999.4	1006	859.5	864.9	869.4	872.3	521.5	524.1	526.1
26	1130	1153	1171	1182	1010	1017	1024	1028	613.0	617.2	620.0
30	1283	1314	1339	1354	1159	1169	1177	1182	703.0	709.3	713.5
34	1431	1470	1502	1523	1306	1318	1329	1336	791.5	800.2	809.5
38	1575	1623	1662	1689	1451	1467	1480	1488	878.5	889.9	898.0
42	--	--	--	--	--	1614	1629	1640	963.9	978.4	989.0
46	--	--	--	--	--	1759	1778	1791	1048	1066	1079
50	--	--	--	--	--	1904	1925	1940	1130	1152	1168



(a) Single Axle, Dual Tire



(b) Tandem Axle, Dual Tire

Figure 4.7. Axle and Tire Configurations for ELSYM5 Analysis.

5.0 DISCUSSION

5.1 Tire Pressure

For single tires on both steering and non-steering axles, the mean manufacturer's maximum recommended cold inflation pressure was higher than the corresponding pressure for dual tiers, as shown in Table 4.2. The same trend appears in the measured tire pressures (hot) distribution as presented in Table 4.3. Therefore, the data show that truck operators tended to have higher tire pressures in single tires than dual tires.

For the small sample of bias single tires on non-steering axles, the mean measured pressure (hot) was 10 psi higher than the mean manufacturer's maximum recommended cold inflation pressure as shown in Table 5.1. In addition, for the various categories of bias tiers sampled, the mean measured inflation pressures (hot) were between 2.2 and 10.0 psi higher than the mean maximum manufacturer's recommended cold inflation pressures. As there can be a 10 to 20 psi increase in hot over cold inflation pressure in a bias tire (4), the data indicate that many truck operators who use bias ply tires have cold tire pressures close to the manufacturer's maximum recommended cold values.

For radial tires the mean measured inflation pressure (hot) is very close to the mean manufacturer's recommended maximum cold tire pressure, as shown in Table 5.1. There can be a 5 to 15 psi increase in hot over cold tire pressure in a radial tire (4). Consequently, a significant number of trucks in the radial tire sample had a cold inflation pressure lower than the manufacturer's maximum recommended cold pressure.

Radial tires in the sample had both mean measured hot inflation and mean maximum recommended cold inflation pressures about 20 psi higher than the respective pressures in the bias tire sample, as shown in Tables 4.2 and 4.3.

Table 5.1. Mean Value of Tire Pressure Difference Between Maximum Recommended Pressure (Cold) and Measured Pressure (Hot).*

	Single Tire on Steering Axle		Single Tire on Non-Steering Axle		Dual Tire on Non-Steering Axle	
	Radial	Bias	Radial	Bias	Radial	Bias
Mean (%)	0.3	2.5	-0.2	10.0	1.3	2.2
Standard Deviation (%)	10.7	14.6	8.0	9.6	12.9	19.9
Number of Tires	495	44	89	11	1734	285

* $\frac{\text{Measured Pressure} - \text{Recommended Pressure}}{\text{Recommended Pressure}} \times 100\%$

If government agencies which to control tire pressures, it would be expedient to control the manufacturer's maximum recommended cold inflation pressure. This would ensure reasonable control, as the data collected in this study for radial tires shows that the mean measured (hot) and mean manufacturer's recommended cold tire pressures are similar. Radial tires comprised both the bulk of the sample tested and the majority of tires running high tire pressures.

It can be assumed that cold tire pressures of 75 to 80 psi were used in the 1959 AASHO road test (43), and that a 10 to 20 psi increase in pressure could occur in a hot bias ply tire. Consequently, it is probable that the maximum cold tire pressure used in the AASHO road test was near 80 psi and the maximum hot pressure near 100 psi.

Of the tires sampled in this study, 67% had measured tire pressures (hot) over 100 psi and 93% had manufacturer's maximum recommended cold inflation pressures exceeding 80 psi, as determined from analysis of data shown in Tables I and II of Appendix B.

The earlier tire pressures, such as those used in the AASHO tests, were almost exclusively for bias ply tiers. The higher tire pressures currently in use are predominantly found in radial tires.

The percentage of tires running higher tire pressures, as described above, and the mean pressure values in the Texas study (5), indicate that higher tire pressures are in use than the 80 psi pressure commonly used in pavement design.

In general, tires with higher pressures had deeper tread depths. This implies that truck operators may use higher pressures with newer tires.

When designing pavements, caution is needed to be sure that the design standards are current. Procedures and standards used should reflect the high pressure radial tires currently in use rather than the lower pressure bias ply tires of the 1960's.

5.2 Mix Design

Table 4.7 summarizes the test results of laboratory fabricated and compacted mixes. The Hveem stability was considered to be most significant test result in relation to this study. ODOT mix design guidelines use a minimum Hveem stability of 30. The stability is not varied with traffic, which is contrary to recommendations published by the Asphalt Institute (39). In the past, ODOT required an Index of Retained Strength (IRS) value of 70% at the minimum design asphalt content. However, in 1984 ODOT increased the required IRS to 75%. The IRS and Resilient Modulus Ratio tests are made to determine the pavement's resistance to damage from moisture and freeze-thaw effects.

As presented in Table 5.2(d), the correlation between $\log(\text{Hveem Stability})$ and $\log(\text{Creep Stiffness})$ is not strong except for the Cobb Rock Quarry mixes. According to the results of the creep tests, it is not always true that a mix with a high Hveem stability value resists pavement deformation better than one with low stability.

It is noted that the gradation "C" mix (Fuller maximum density gradation) requires the least amount of optimum asphalt content for rock from each aggregate source on the basis of the existing mix design guidelines. Mixtures with the Fuller maximum density gradation showed low stiffness and had unacceptable low voids in mineral aggregate (VMA) values. Also, these mixtures had durability characteristics based on the Index of Retained Strength and/or Resilient Modulus Ratio lower than the acceptable minimum. The Fuller maximum density gradation may not be acceptable for use in asphalt concrete paving mixtures subject to high tire pressures and loads.

Table 5.2. Correlation Analysis.

(a) Correlations with log(Creep Stff.,ksi)

Variables	Morse Brothers Pit	Cobb Rock Quarry	Hilroy Pit	Blue Mountain Asphalt Pit
log(Stability)	-0.3141	0.8176	0.4878	-0.0482
log(M_R ;As-Comp.,ksi)	0.0636	-0.0859	0.5004	-0.2771
log(M_R ;Cond.,ksi)	0.2664	-0.4886	-0.1981	-0.7012
log(M_R Ratio)	0.2428	-0.5353	-0.3665	-0.3592
log(A/C,%)	-0.0906	-0.2440	-0.4839	-0.3310
log(Max.Sp.Gr.)	0.1638	0.2542	0.4825	0.3015
log(Air Voids,%)	-0.1736	0.7529	0.3890	0.5625
log(VMA)	N/A	0.5805	0.0615	0.7465
log(Pass 1/4-in.,%)	-0.4197	0.2196	-0.4026	0.5609
log(Pass #10,%)	0.1970	-0.5034	0.0897	-0.1731
log(Pass #200,T)	-0.3141	-0.6766	-0.1416	-0.3799
log(Intercept)	-0.6955	-0.7780	-0.3532	-0.7038
log(Slope)	-0.4395	-0.2410	-0.3908	-0.5329

Table 5.2. Correlation Analysis (Continued).
 (b) Correlations with log(Slope)

Variables	Morse Brothers Pit	Cobb Rock Quarry	Hilroy Pit	Blue Mountain Asphalt Pit
log(Stability)	-0.5737	-0.1073	-0.0163	0.4056
log(Creep Stff.,ksi)	-0.4395	-0.2410	-0.3908	-0.5329
log(M _R ;As-Comp.,ksi)	-0.1814	0.5060	-0.3602	0.2600
log(M _R ;Cond.,ksi)	-0.0878	0.4838	0.3963	0.2604
log(M _R Ratio)	0.0993	0.3077	0.4671	-0.0078
log(A/C,%)	0.3817	-0.0476	0.5256	0.0436
log(Max.Sp.Gr.)	-0.3476	0.0459	-0.4687	0.0079
log(Air Voids,%)	-0.3252	-0.2107	-0.2363	-0.2589
log(VMA)	N/A	-0.7506	-0.0819	-0.4468
log(Pass 1/4-in.,%)	0.4420	-0.5647	-0.2625	-0.4437
log(Pass #10,%)	-0.0317	0.6751	-0.0743	0.2183
log(Pass #200,%)	-0.5737	0.6777	-0.0215	0.0439
log(Intercept)	-0.3388	-0.4176	-0.5332	-0.2156

Table 5.2. Correlation Analysis (Continued).
(c) Correlations with log(Intercept)

Variables	Morse Brothers Pit	Cobb Rock Quarry	Hilroy Pit	Blue Mountain Asphalt Pit
log(Stability)	0.7761	-0.7241	-0.3974	-0.2351
log(Creep Stff.,ksi)	-0.6955	-0.7780	-0.3532	-0.7038
log(M _R ;As-Comp.,ksi)	0.0714	-0.2807	-0.1320	0.1409
log(M _R ;Cond.,ksi)	-0.2211	0.1370	-0.4243	0.5916
log(M _R Ratio)	-0.3393	0.3109	-0.2871	0.3855
log(A/C,%)	-0.2007	0.2766	-0.1660	0.2983
log(Max.Sp.Gr.)	0.0961	-0.2882	0.0705	-0.2930
log(Air Voids,%)	0.4335	-0.6008	0.1323	-0.4049
log(VMA)	N/A	-0.0696	0.2844	-0.5163
log(Pass 1/4-in.,%)	0.0795	0.1491	0.5427	-0.3455
log(Pass #10,%)	-0.1846	0.0341	-0.1375	0.0135
log(Pass #200,%)	0.7761	0.1812	-0.1531	0.4049
log(Slope)	-0.3388	-0.4176	-0.5332	-0.2156

Table 5.2. Correlation Analysis (Continued).
(d) Correlations with log(Stability)

Variables	Morse Brothers Pit	Cobb Rock Quarry	Hilroy Pit	Blue Mountain Asphalt Pit
log(Creep Stff., ksi)	-0.3141	0.8176	0.4878	-0.0482
log(M_R ;As-Comp., ksi)	0.0471	0.1153	0.3026	0.3061
log(M_R ;Cond., ksi)	-0.2101	-0.3435	-0.2735	0.0017
log(M_R Ratio)	-0.2987	-0.4685	-0.3810	-0.3332
log(A/C, %)	-0.4433	-0.4636	-0.4805	-0.4824
log(Max.Sp.Gr.)	0.3579	0.5197	0.4139	0.5657
log(Air Voids, %)	0.7820	0.9546	0.6501	0.3984
log(VMA)	N/A	0.4529	0.0179	-0.0909
log(Pass 1/4-in., %)	0.1302	0.2283	0.0664	-0.6330
log(Pass #10, %)	-0.2928	-0.2220	0.0104	-0.0017
log(Pass #200, %)	1.0000	-0.4696	0.2500	-0.1198
log(Intercept)	0.7761	-0.7241	-0.3974	-0.2351
log(Slope)	-0.5737	-0.1073	-0.0163	0.4056

In general, the optimum asphalt content for the existing mix design guidelines is higher than that for the retained modulus ratio (MRRT) of 0.7, except for the mixes from Hilroy Pit aggregate.

It seems to be necessary that current mix design guidelines and specifications be studied further to determine the optimum aggregate gradation and asphalt content of mixtures to provide pavements with improved resistance to rutting and moisture damage.

Target gradations for the design of Oregon Class "B" and "C" dense-graded asphalt concrete mixtures should be modified. The percentages of aggregate passing the 1/2-in. and 1/4-in. sieves should be equal to or less than the Fuller maximum density gradation. This will require a change in the asphalt concrete mixture specification grading requirements. Changes are needed for both the 3/4-in. to 1/4-in. stockpiled coarse aggregates and the percentage of rock passing the 1/2-in. screen.

5.3 Creep Behavior of Mixes

The asphalt concrete mixtures investigated in this study were tested for creep strain and creep stiffness. The creep test procedures detailed in Appendix A were used. The creep test results were used to: 1) develop a correlation between creep behavior and mix design properties, and 2) to provide input into the rut depth calculations using the Shell method, as detailed in Appendix E.

For each sample, a linear regression was performed on the creep test data. This regression provided the creep stiffness, the creep test regression line slope, and the creep test regression line intercept. These values are given in Table 4.8.

Correlation analyses were performed between each of the creep properties listed in the previous paragraph, the Hveem stability values, and the other mix design test results. The results of these correlations are shown in

Table 5.2. In these tables, a positive correlation number indicates a positive slope on the correlation curve. A correlation value near 1.000 shows a good correlation. Conversely, a value near zero indicates a poor correlation.

A limited number of tests were used to develop these relationships. As a result, these correlations are not very reliable.

Tests made on all mixture with variation in gradation, asphalt content, and aggregate source indicate that creep stiffness increases when: the voids in the mineral aggregate (VMA) increase; the asphalt content decreases; the percentage passing the #200 sieve decreases; the creep regression line intercept decreases; or the creep regression line decreases. The positive correlation relationship between creep properties and both the VMA and the percentage passing #200 sieve are likely the result of the increased coarse aggregate interlock that occurs when the voids in the mix increase. Likewise, when the asphalt content is decreased, the improved interlock of the coarse aggregate also results in increased stiffness. The negative correlations for the log (intercept) and log (slope) show the results of these mixtures higher resistance to deformation and slower rates of deformation during the initial stages of loading.

The results of tests made on the mixtures without lime-treated aggregate, rock from the Morse Brothers Pit and Hilroy Pit, show that creep stiffness increases when: the percentage passing the 1/4-in. sieve decreases; or the percentage passing the #10 sieve increases. These relationships indicate that larger amounts of coarse aggregate (retained on the 1/4-in. screen) and of fine aggregate (passing the #10 sieve) provide improved aggregate interlock and mix stiffness. The gradations which produced stiffer mixes were near the Fuller's maximum density gradation.

For tests made on mixtures containing lime-treated aggregate, rock from the Cobb Rock Quarry and the Blue Mountain Asphalt Pit, there is some indication that creep stiffness increases when: the percentage passing the 1/4-in. sieve increases; or the percentage passing the #10 sieve decreases. These differences in correlation relationships from mixes made with rock from the two other aggregate sources could be the result of changes in the coarse and fine aggregate surface properties due to lime treatment.

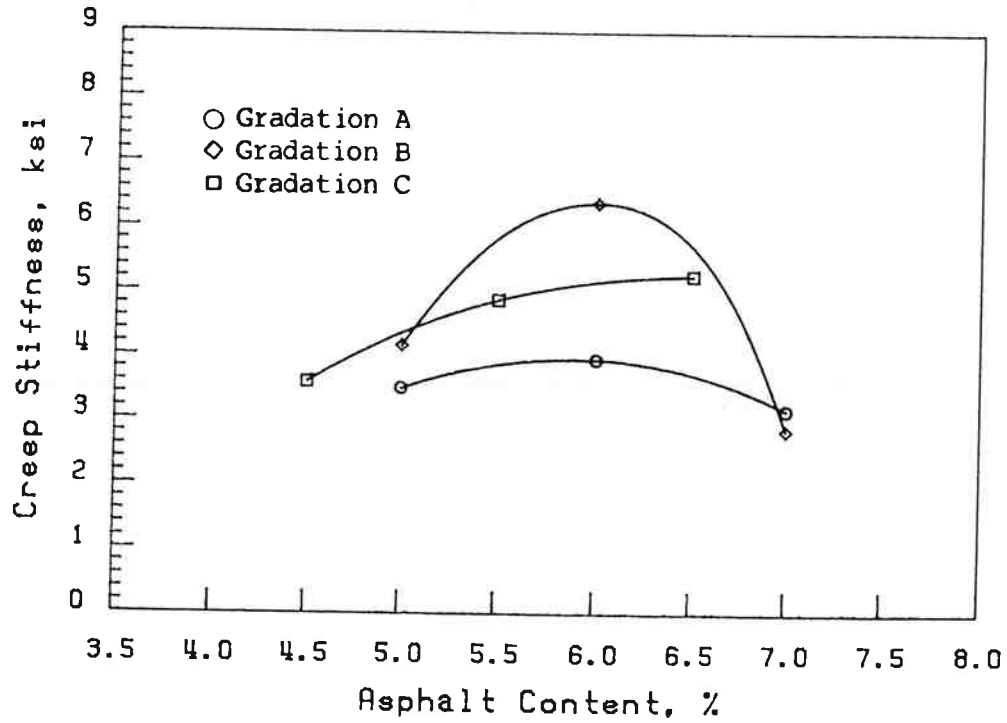
The correlation analysis for all Hveem stabilometer test values show that the stability increases when: the resilient modulus ratio decreases; the asphalt content decreases; or the air voids increase. These relationships are as expected for mixtures with the increased aggregate interlock that results from increased air voids in the mix. It should be noted that little or no correlation is obtained between mix stability and creep value.

Creep stiffness tests made on mixtures with variations in gradation, asphalt content, and aggregate source show that creep values at the optimum design asphalt content are generally highest when: the percentage passing the #200 sieve is low; the percent passing the 1/4-in. sieve is low; or the percent passing the #10 screen is high. Stiffness values are generally near their higher levels at the optimum or lower design asphalt contents.

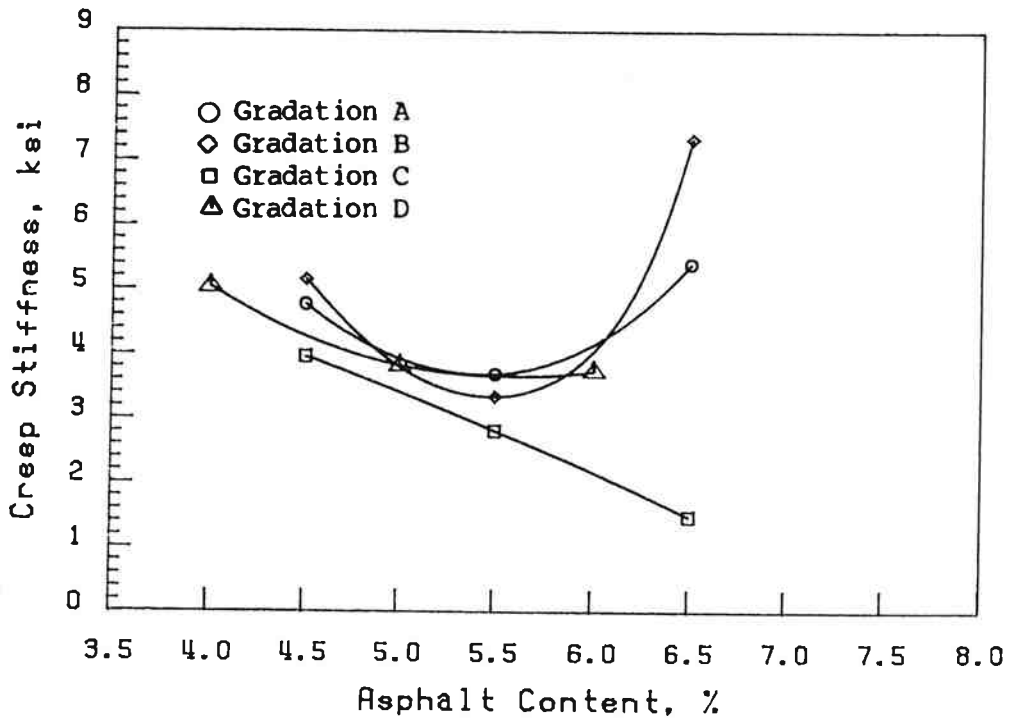
5.4 Analysis of Asphalt Concrete Pavement Structures

5.4.1 Pavement Analysis

In order to investigate the effect of increased axle loads and tire pressures on asphalt concrete pavements, as shown in Figure 4.6: 18-kip and 22-kip loads were used with single axles and dual tires; 34-kip and 42-kip loads were used with tandem axles dual tiers; and in all cases 80 psi and 125 psi tire pressures were analyzed. For the evaluation parameters, the vertical compressive stress through the pavement structure, the horizontal strain in the asphalt concrete wearing course and base course, and the vertical

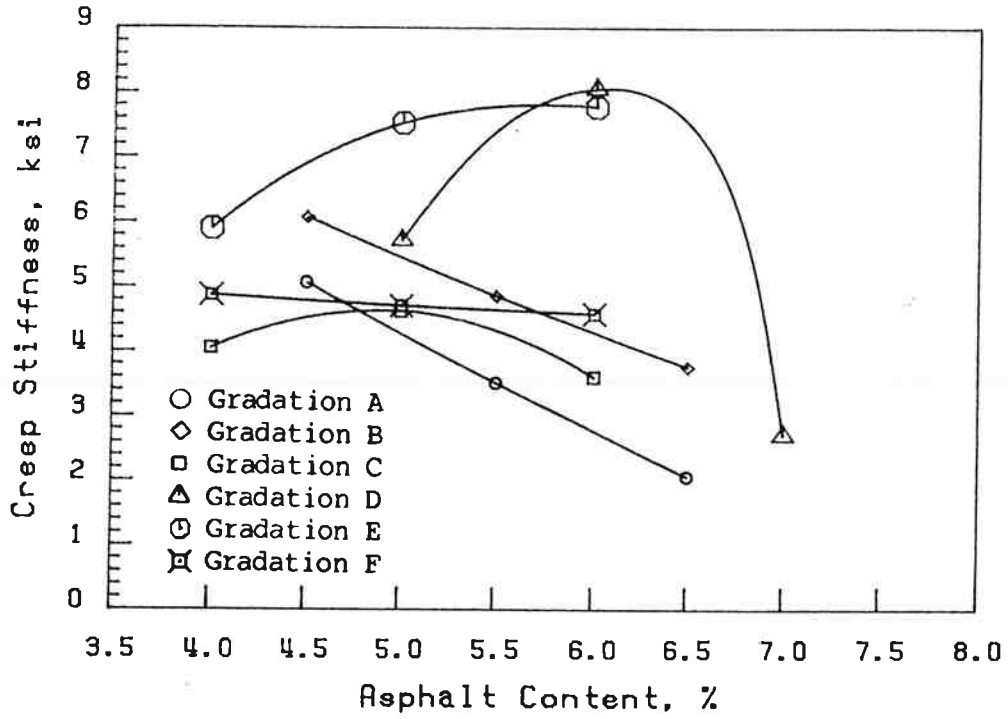


(a) Morse Brothers Pit

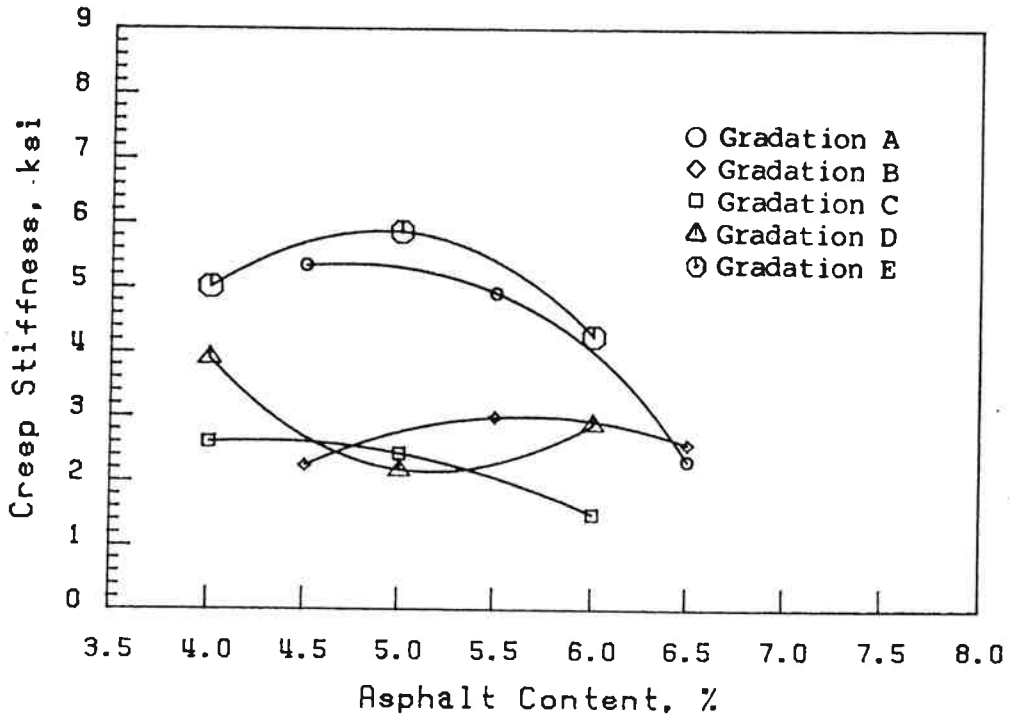


(b) Cobb Rock

Figure 5.1. Effect of Asphalt Content on Creep Stiffness.



(c) Hilroy Source



(d) Blue Mountain Asphalt Pit

Figure 5.1 Effect of Asphalt Content on Creep Stiffness (Continued).

compressive strain through the pavement structure at the point below the wheel load were used, and are shown in Figures 5.2, 5.3, and 5.4.

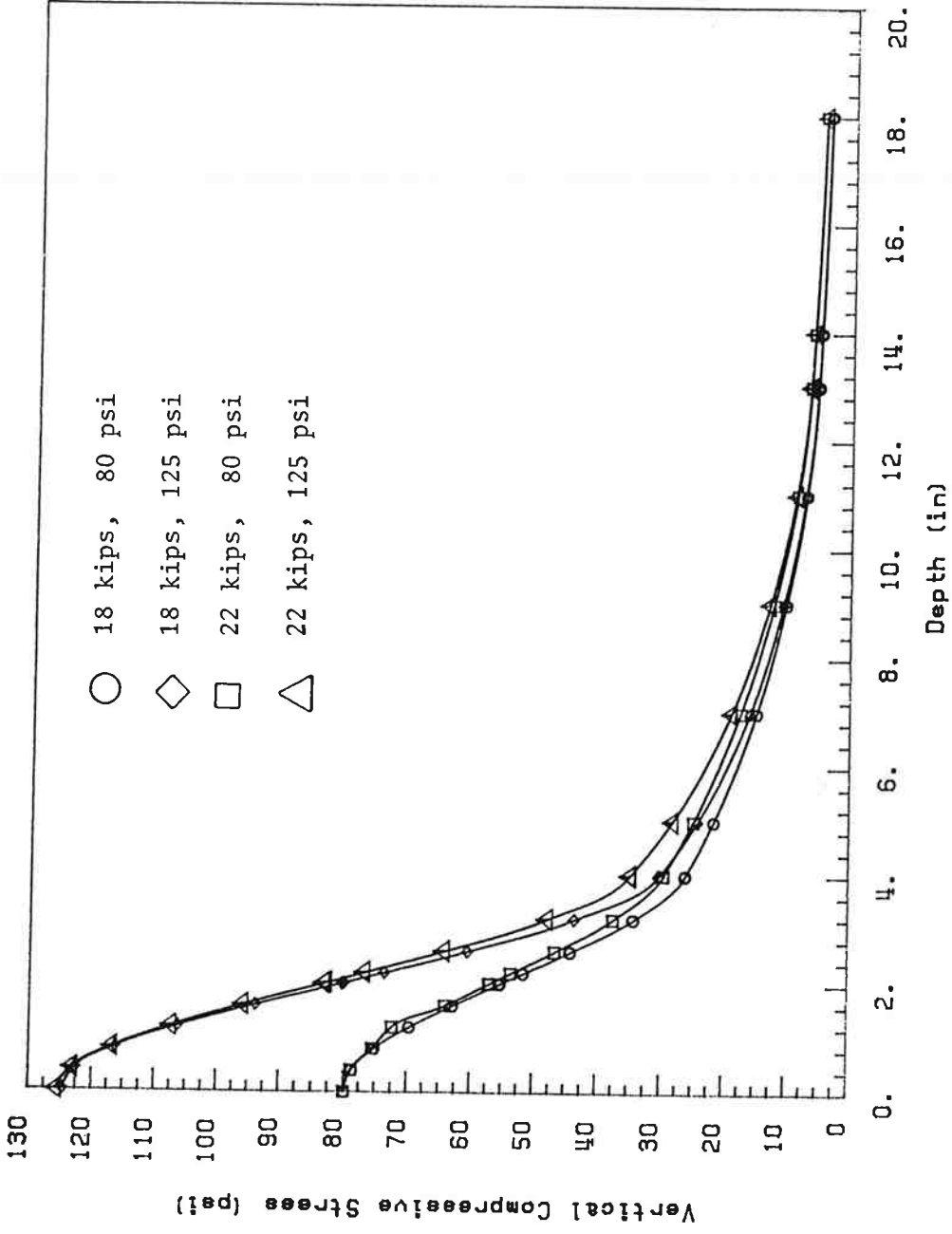
The data from the vertical compressive stress analysis will be used for the calculation of the predicted rut depth in the asphalt concrete layers according to the Shell method (22). As presented in Figure 5.2, the effect of high tire pressures created by every wheel and axle combination is significant in the asphalt wearing layer of both pavement structures, as reviewed in Section 2.3. However, at a depth of about 15 in., the vertical compressive stresses are about equal for both pavement structures and for both tire pressures.

As presented in Figure 5.3 and Figure 5.4, point of change from compressive strain to tensile strain in the asphalt concrete layer is shifted towards the pavement surface as the tire pressure increases and/or axle load decreases. However, in general, the magnitude of the maximum horizontal tensile strain in the asphalt concrete layer is the greatest for the heaviest axle load and highest tire pressure.

As presented in Figure 5.3, the maximum horizontal tensile strain at the bottom of the asphalt concrete base layer of Pavement B (the base layer is stiffer than the surface layer) is less than that of Pavement A (the base layer is of a lower stiffness level than the surface layer).

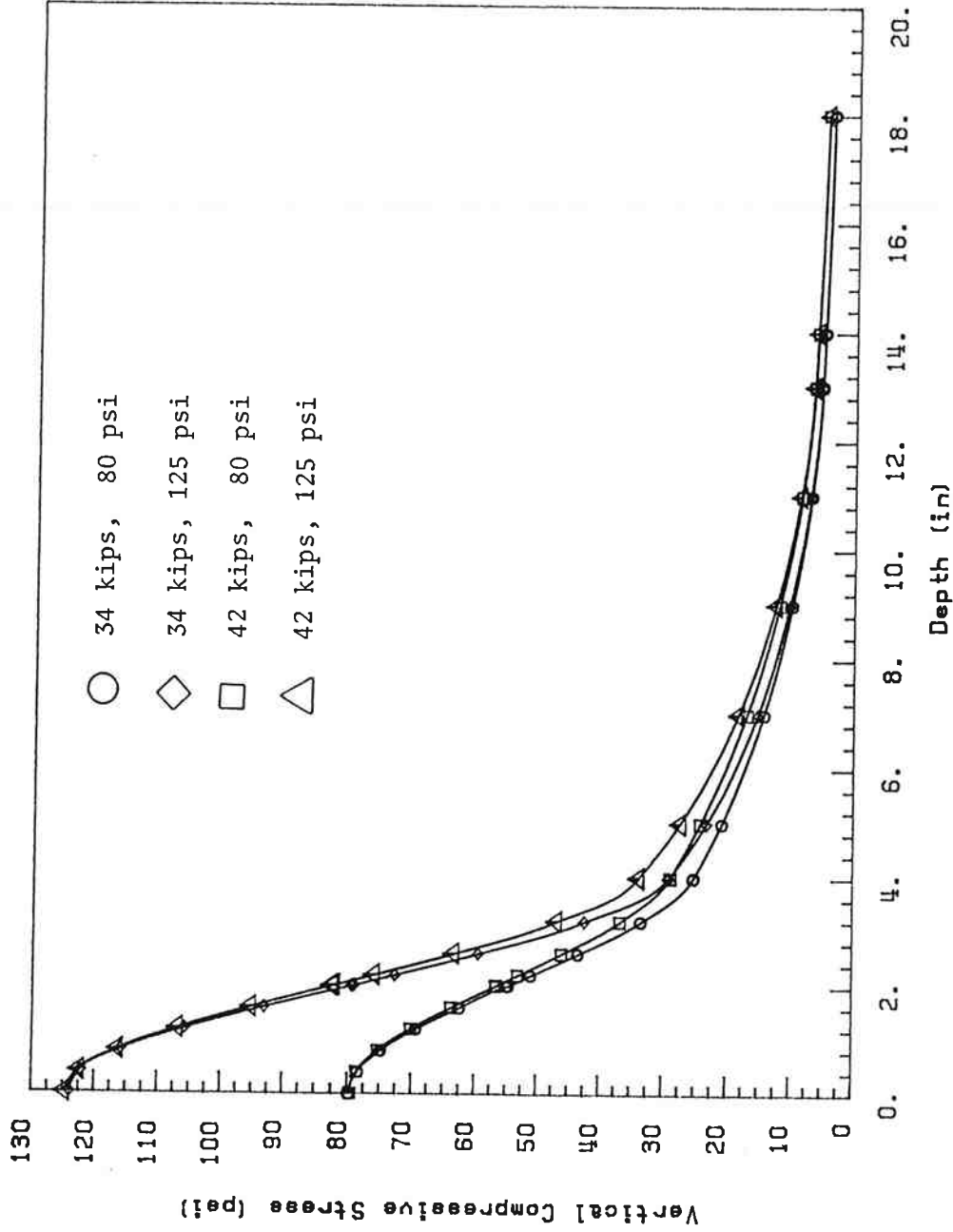
For both pavement structures, the tandem axles with dual tires and a 34-kip load created less tensile strain in the asphalt concrete layers than the single axle with dual wheels and the smaller 18-kip load.

Figure 5.4 shows the vertical compressive strain profiles through the pavement structures that are given in Figure 4.6. For the same load, the effect of increases in tire pressure on the vertical compressive strain at



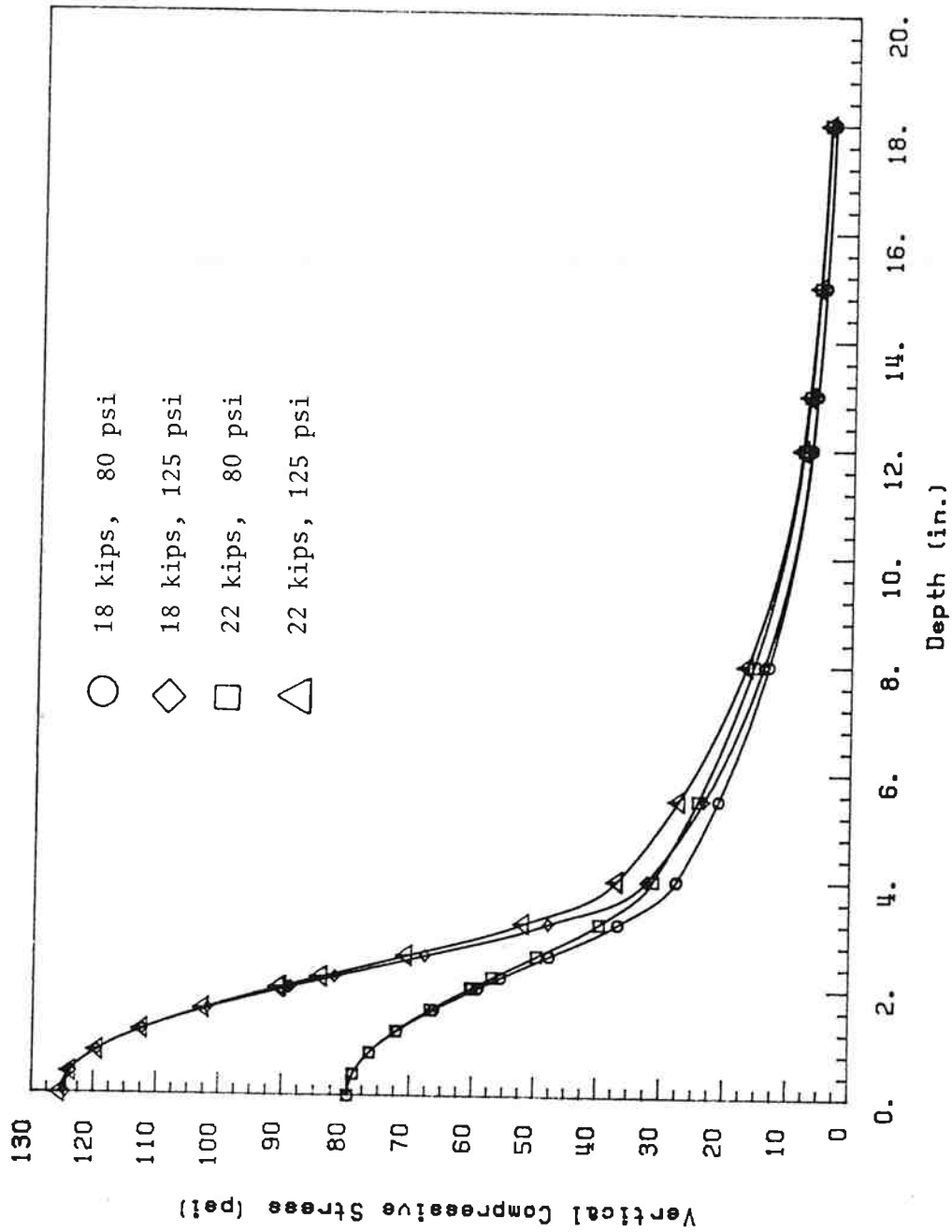
(a) Single Axle, Dual Tire - Pavement A Described in Figure 4.6

Figure 5.2. Vertical Compressive Stress Through the Pavement Structure.



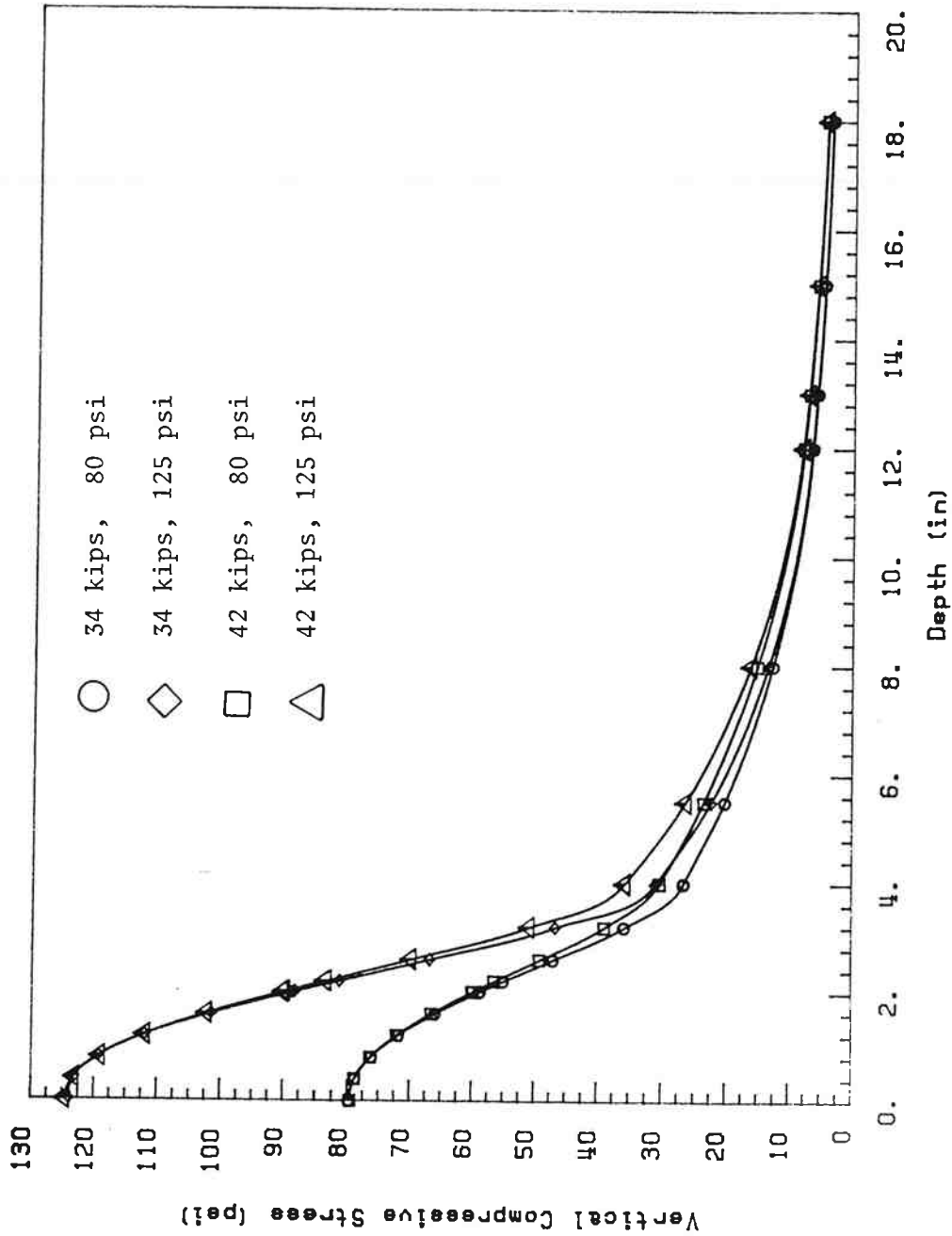
(b) Tandem Axle, Dual Tire - Pavement A Described in Figure 4.6

Figure 5.2. Vertical Compressive Stress Through the Pavement Structure (Continued).



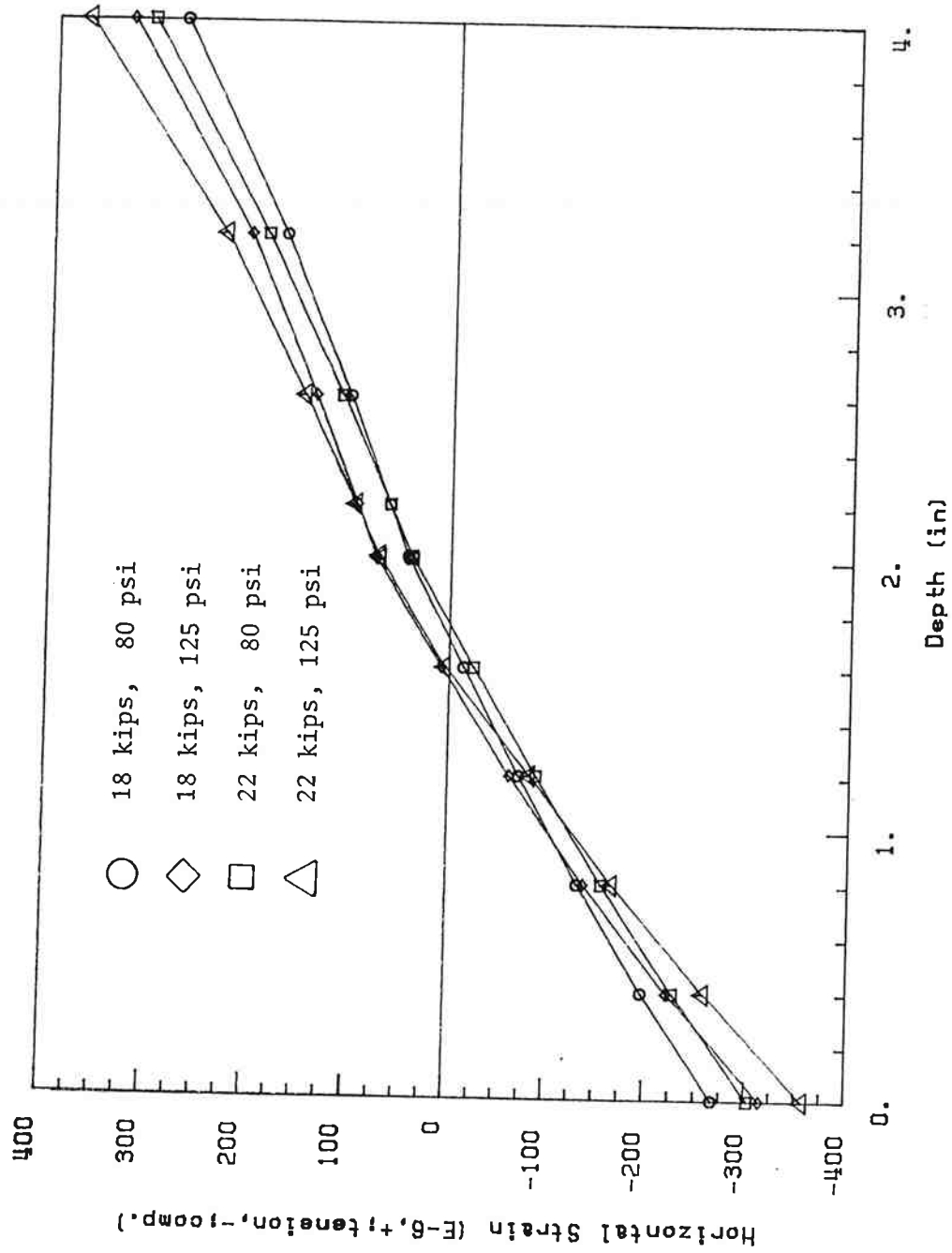
(c) Single Axle, Dual Tire - Pavement B Described in Figure 4.6

Figure 5.2. Vertical Compressive Stress Through the Pavement Structure (Continued).



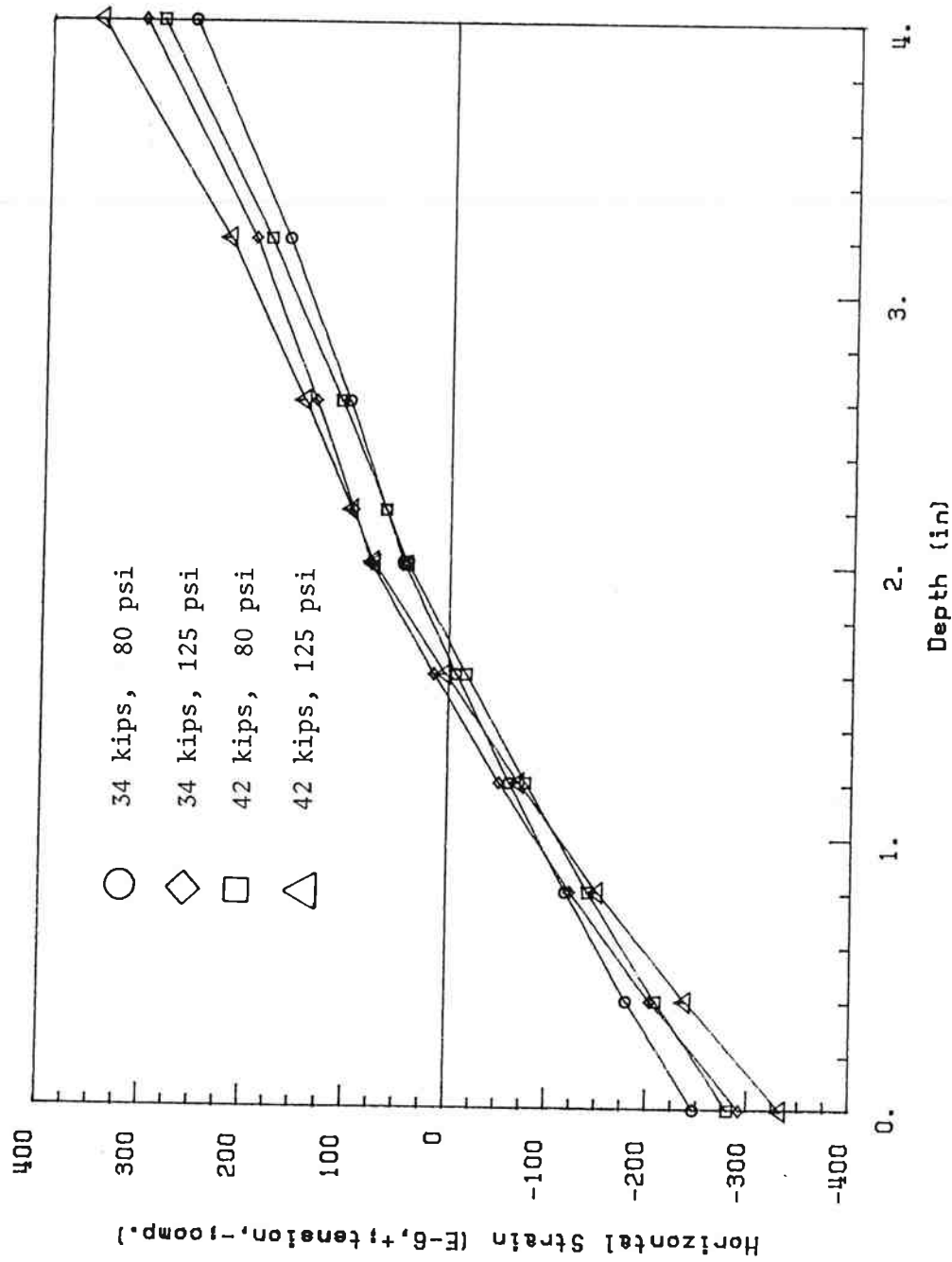
(d) Tandem Axle, Dual Tire - Pavement B Described in Figure 4.6

Figure 5.2. Vertical Compressive Stress Through the Pavement Structure (Continued).



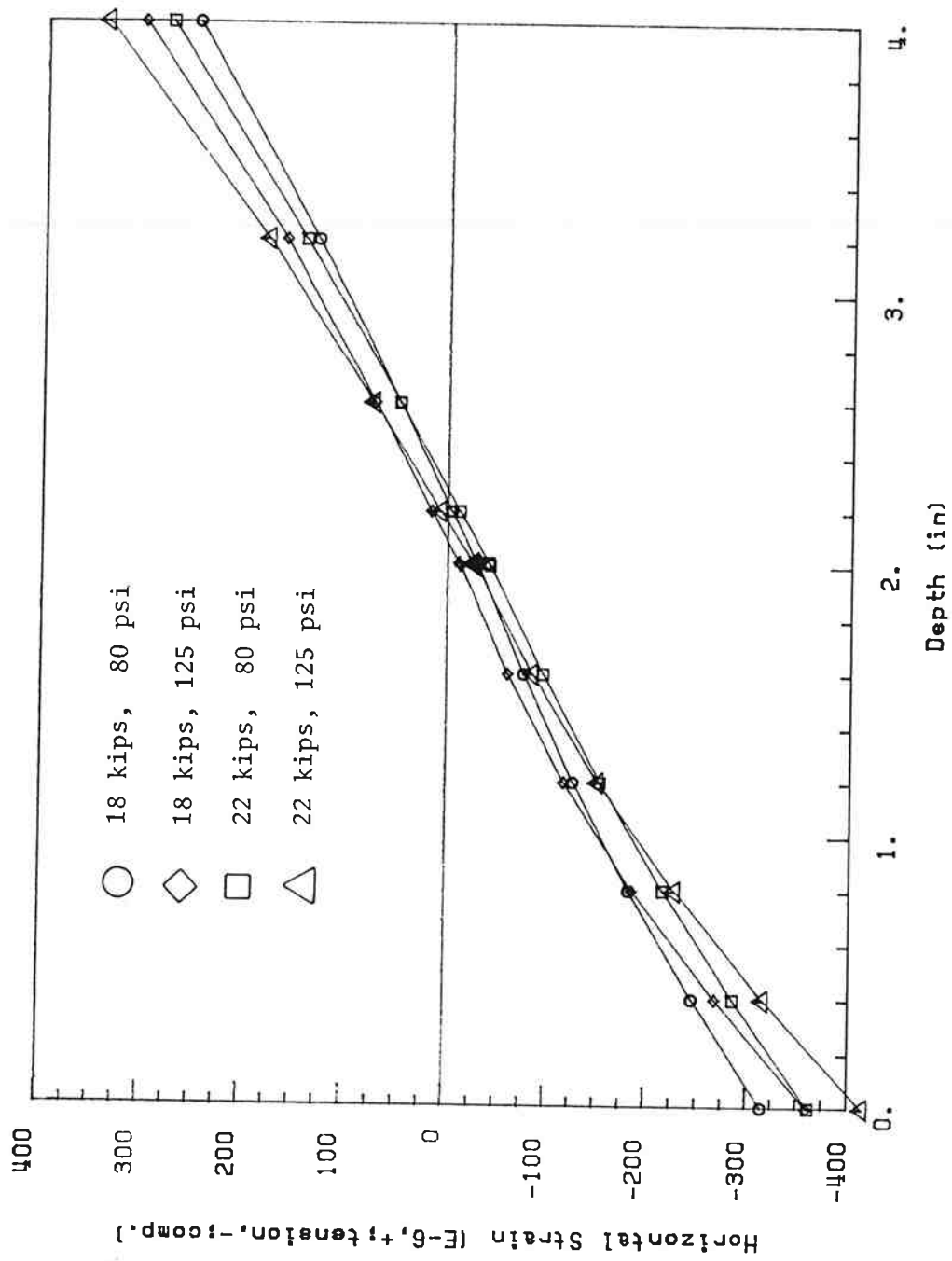
(a) Single Axle, Dual Tire - Pavement A Described in Figure 4.6

Figure 5.3. Horizontal Strain in the Asphalt Concrete Pavement.



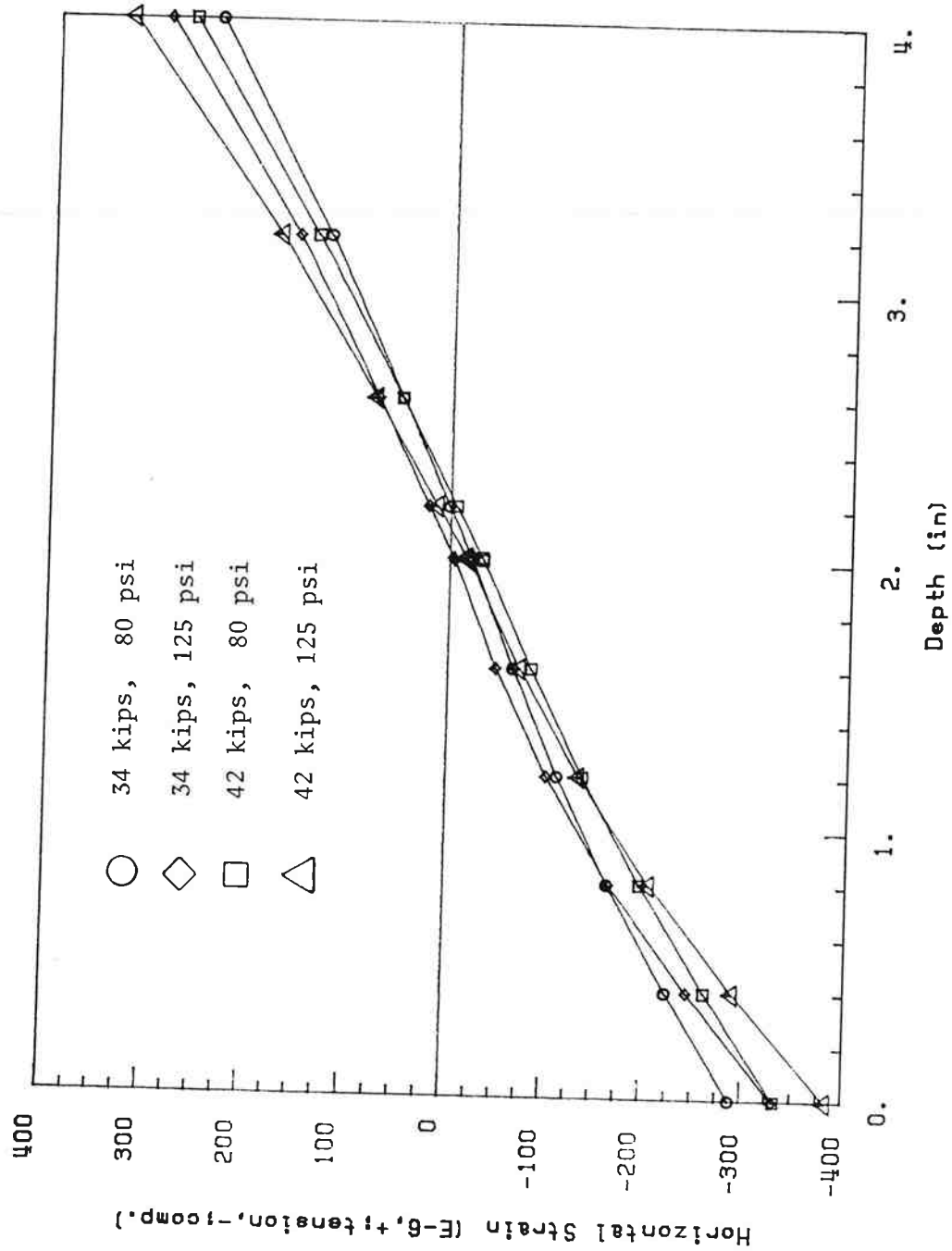
(b) Tandem Axle, Dual Tire - Pavement A Described in Figure 4.6

Figure 5.3. Horizontal Strain in the Asphalt Concrete Pavement (Continued).



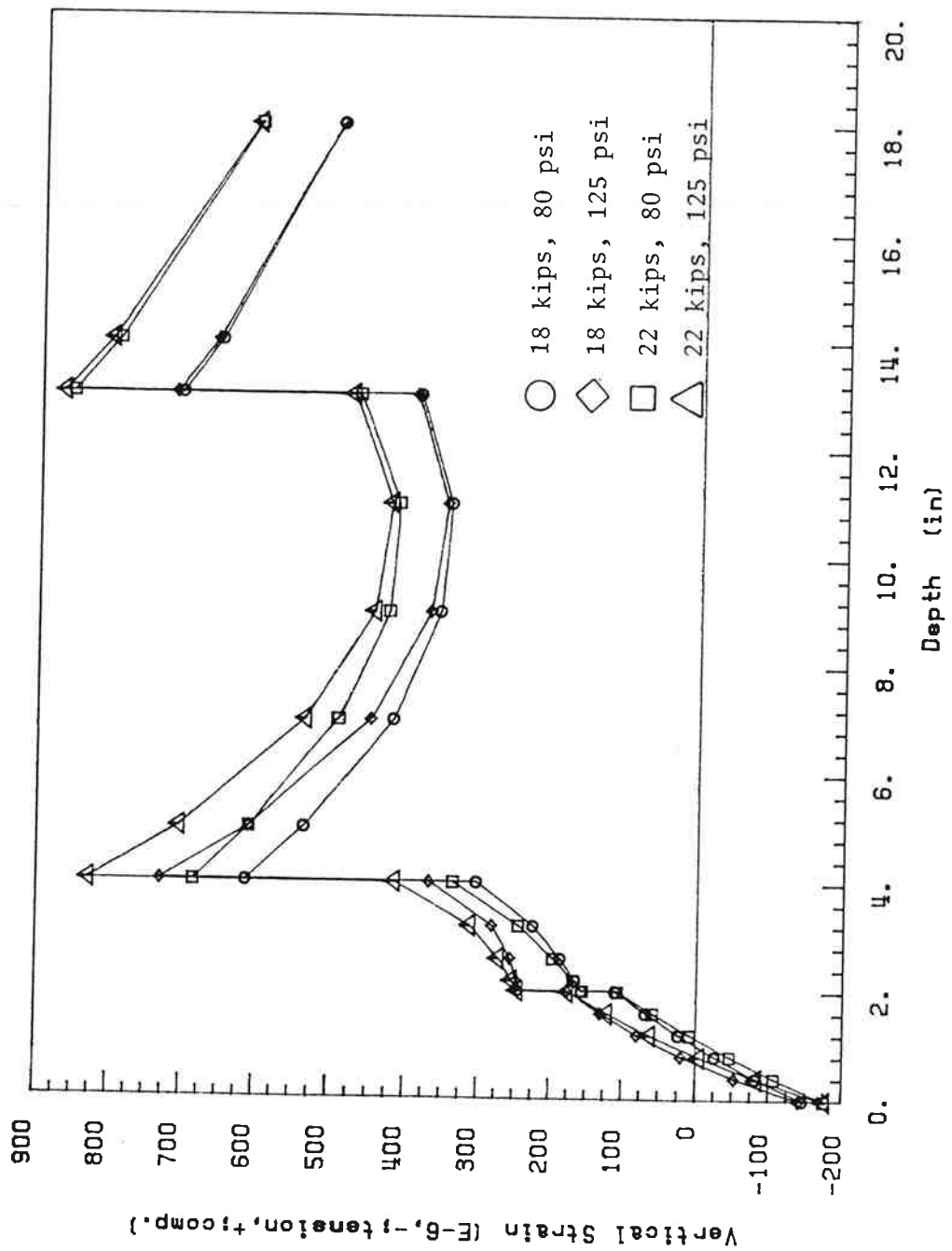
(c) Single Axle, Dual Tire - Pavement B Described in Figure 4.6

Figure 5.3. Horizontal Strain in the Asphalt Concrete Pavement (Continued).



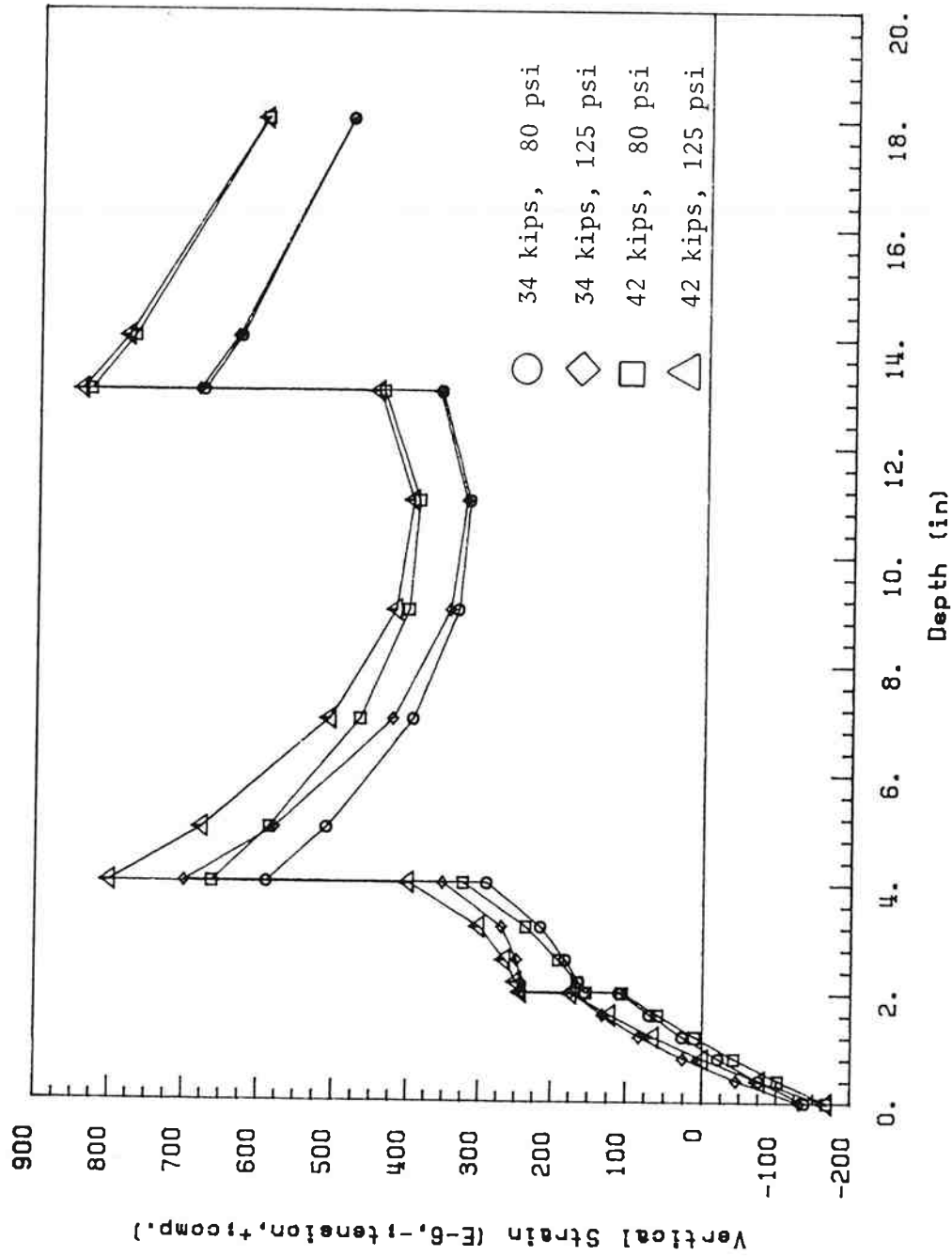
(d) Tandem Axle, Dual Tire - Pavement A Described in Figure 4.6

Figure 5.3. Horizontal Strain in the Asphalt Concrete Pavement (Continued).



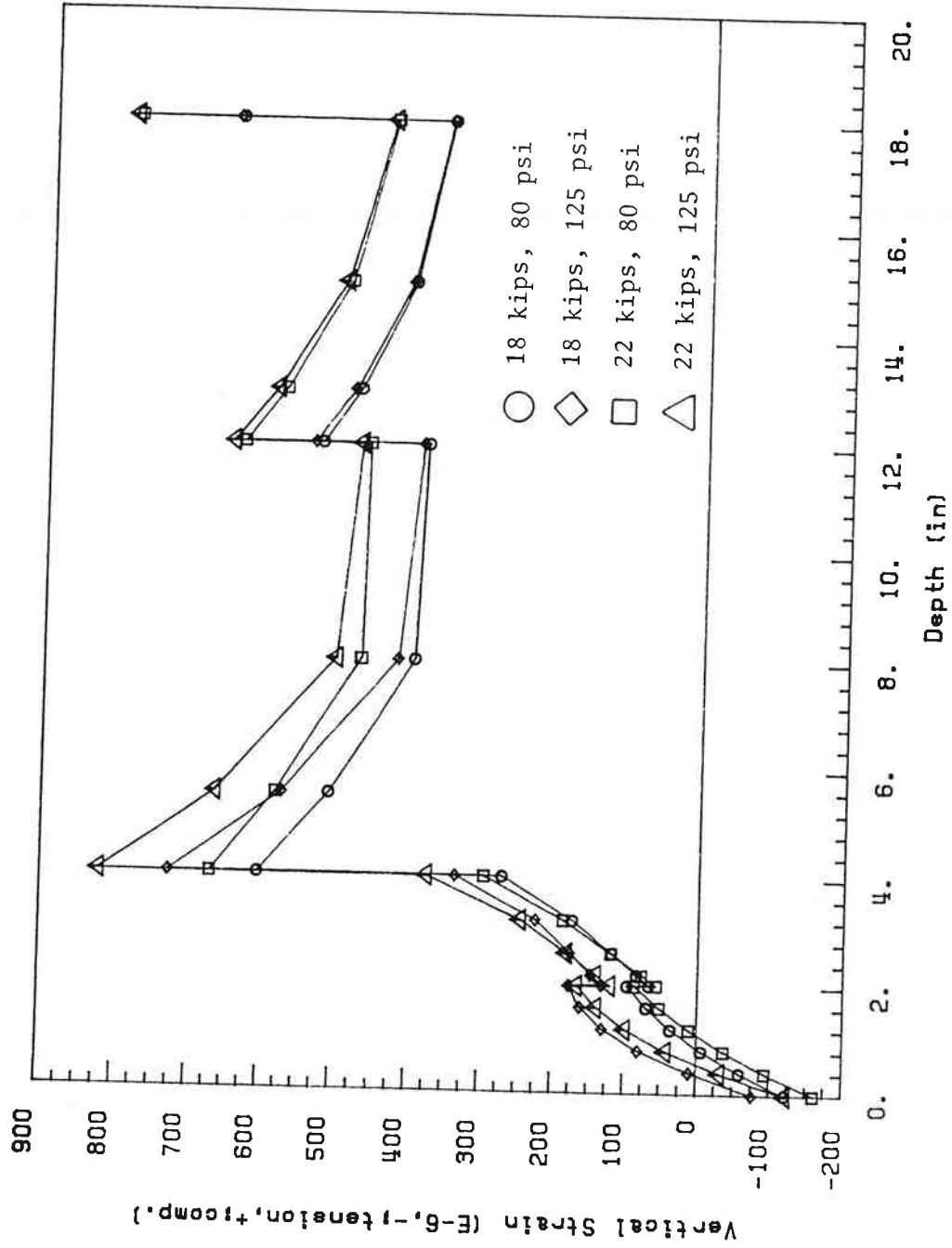
(a) Single Axle, Dual Tire - Pavement A Described in Figure 4.6

Figure 5.4. Vertical Compressive Strain Through the Pavement Structure.



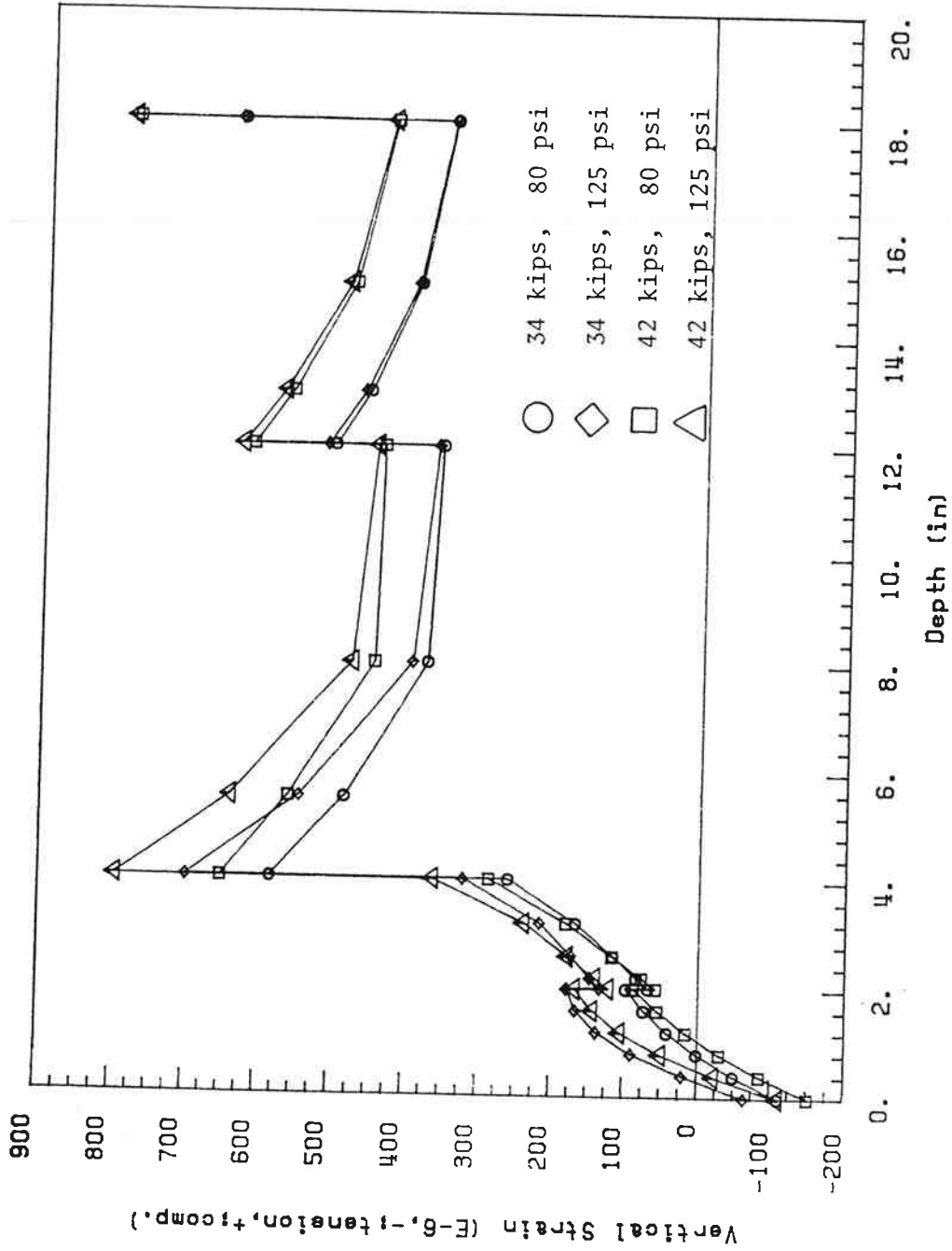
(b) Tandem Axle, Dual Tire - Pavement A Described in Figure 4.6

Figure 5.4. Vertical Compressive Strain Through the Pavement Structure (Continued).



(c) Single Axle, Dual Tire - Pavement B Described in Figure 4.6

Figure 5.4. Vertical Compressive Strain Through the Pavement Structure (Continued).



(d) Tandem Axle, Dual Tire - Pavement B Described in Figure 4.6

Figure 5.4. Vertical Compressive Strain Through the Pavement Structure (Continued).

the top of subgrade is negligible. However, the magnitude of the vertical compressive strain at the top of the untreated subgrade in Pavement A, which has a stiffer subgrade and thinner structure depth than Pavement B, is greater than that in Pavement B.

5.4.2 Equivalency Factors

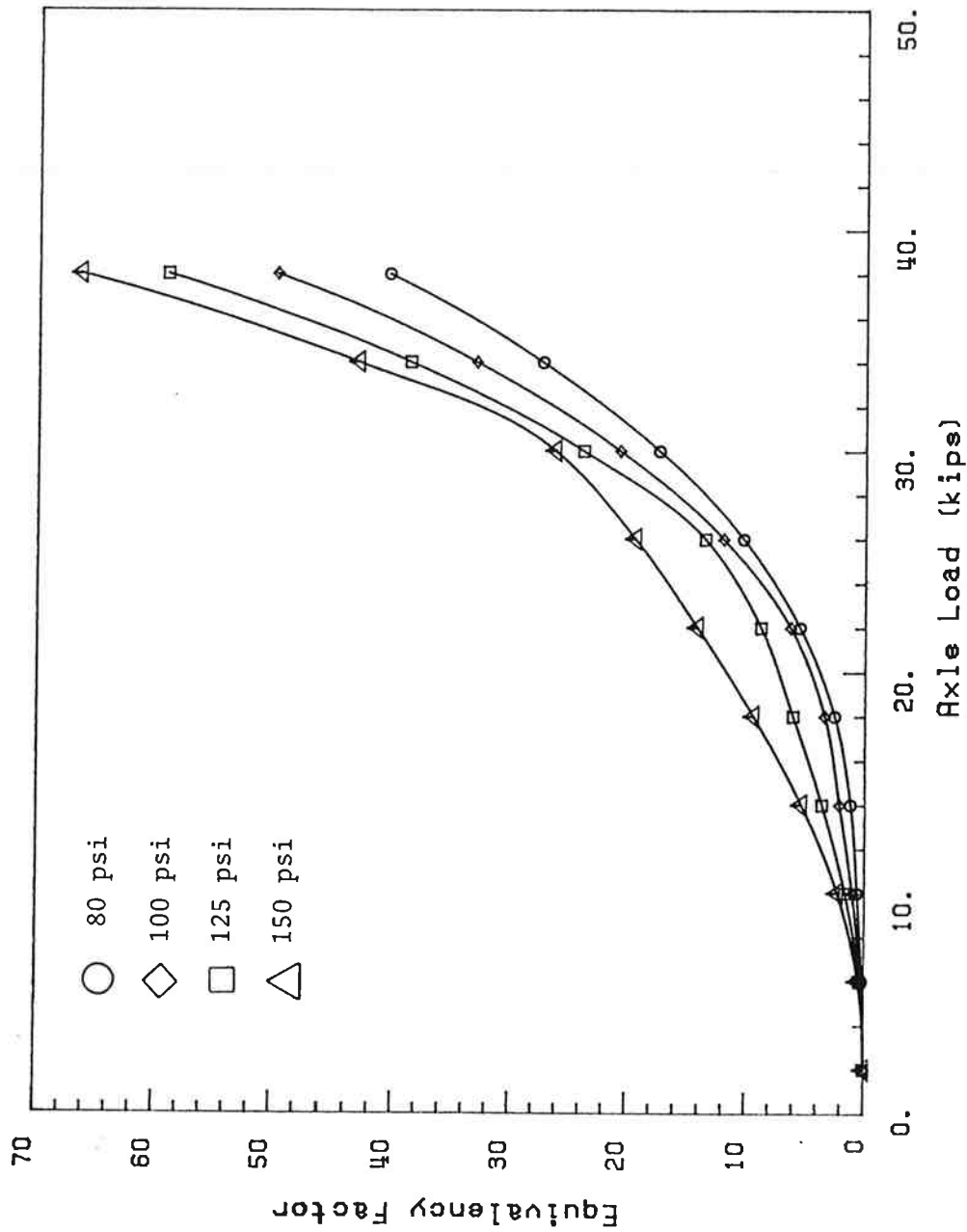
As reviewed in Section 2.2, one method of assessing the destructive effects of increased tire pressure is through the use of load equivalency factors.

In most previous research studies (6,11,12,13,14), only the effect of increased axle load was investigated. In this study, tire pressure is added as another variable.

As a standard tire pressure, axle load, and wheel configuration; 80 psi, an 18-kip load and a single axle with dual tires were used. The theoretical equivalency factors with reference to this tire pressure and axle load can be computed easily from the maximum tensile strain or maximum vertical compressive strain in the pavement structure. These factors are presented in Tables 4.9 and 4.10 and are calculated from the results of ELSYM5. The procedure to calculate the equivalency factor is presented in Appendix C.

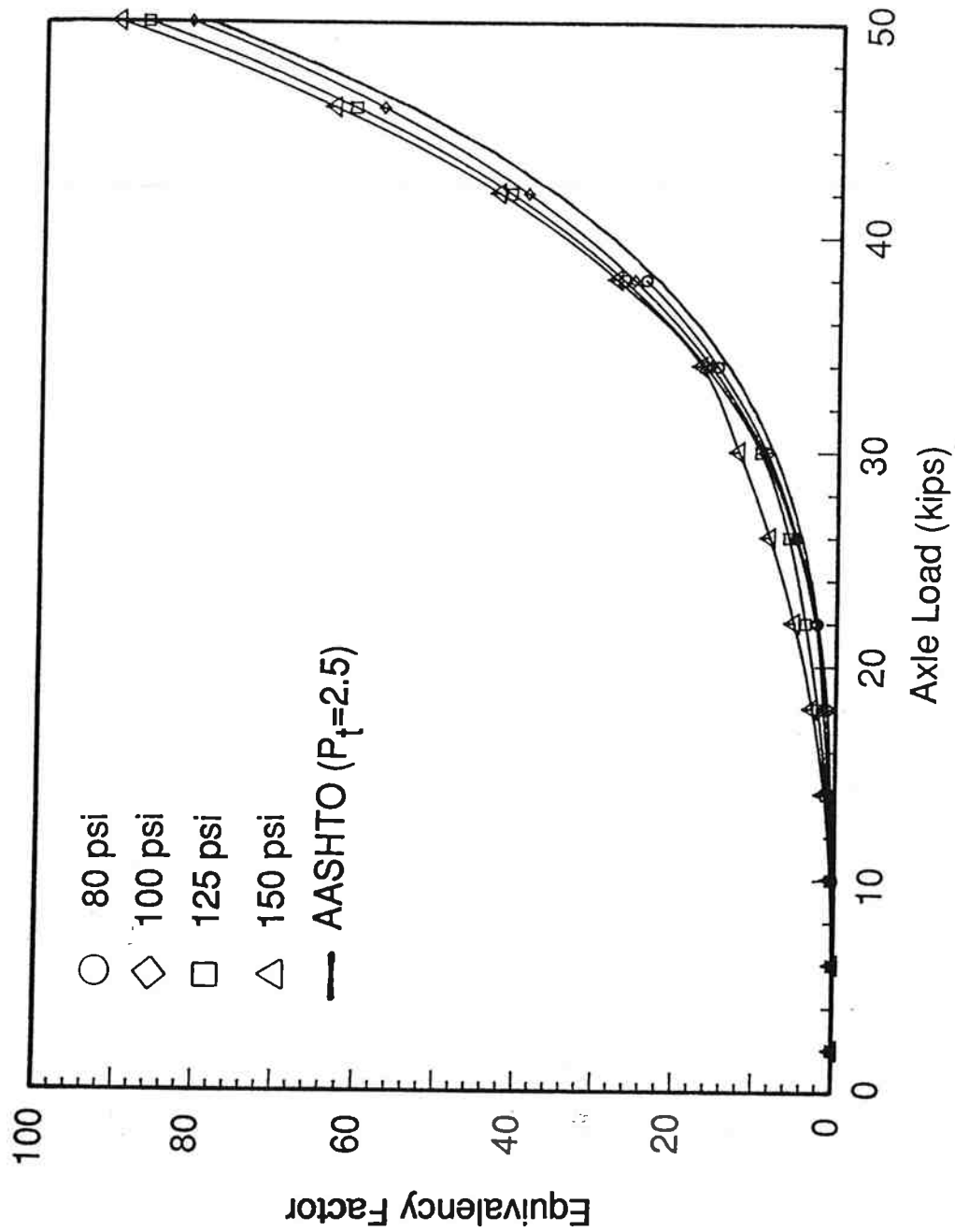
Figures 5.5 and 5.6 present equivalency factors for the two asphalt concrete pavements shown in Figure 4.6. Maximum compressive strains at the top of the subgrade and maximum tensile strains at the bottom of the asphalt concrete base layer were calculated. The greater equivalency factor from either the maximum tensile strain or from the maximum compressive strain was selected for the determination of the load equivalency factor.

For the single axle, the change of equivalency factor for tire pressures between 80 psi and 100 psi is relatively small in the range of axle loads from 0 to 26 kips. However, in this same load range, the change in equivalency



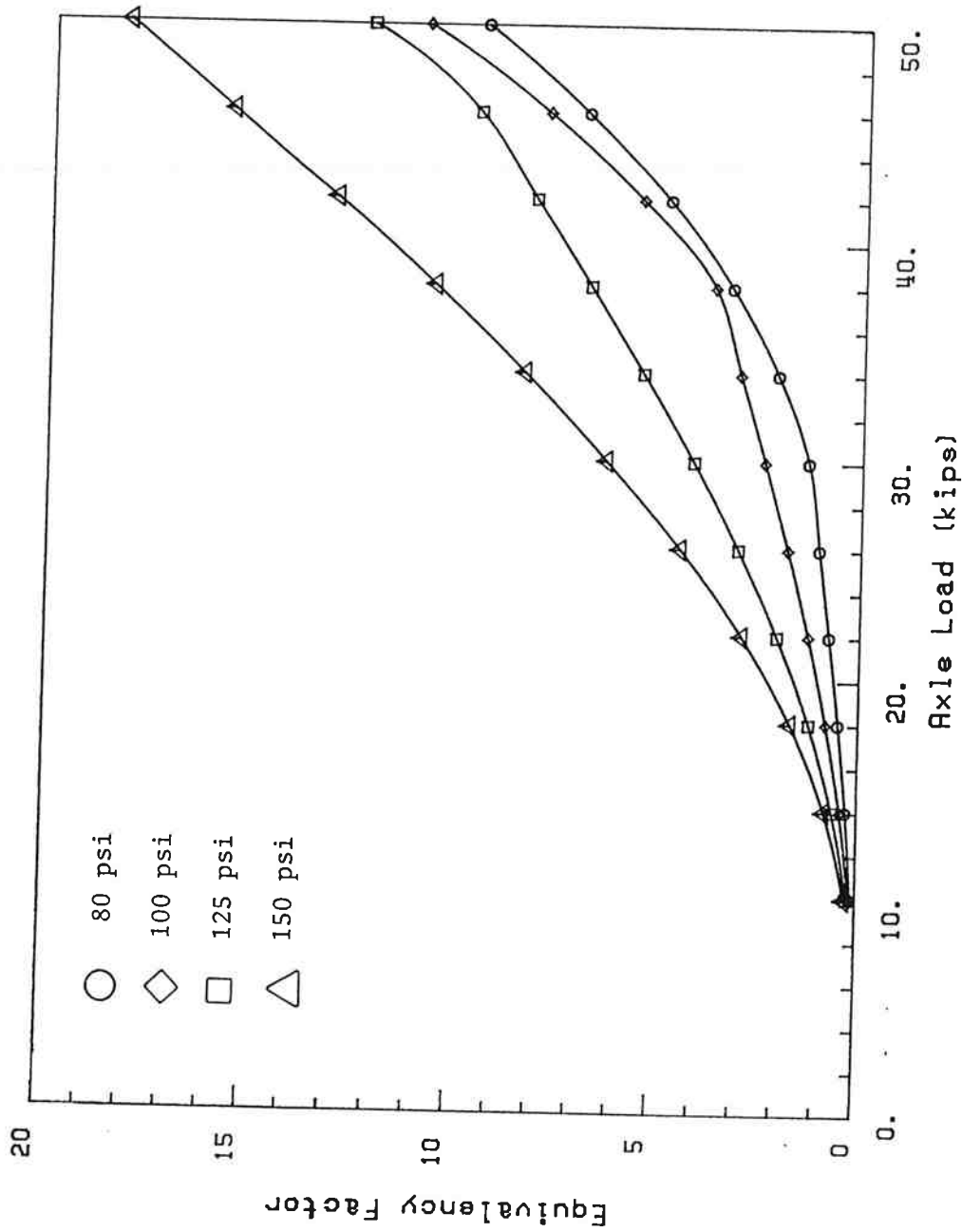
(a) Single Axle, Single Tire

Figure 5.5. Equivalency Factors for Pavement A.



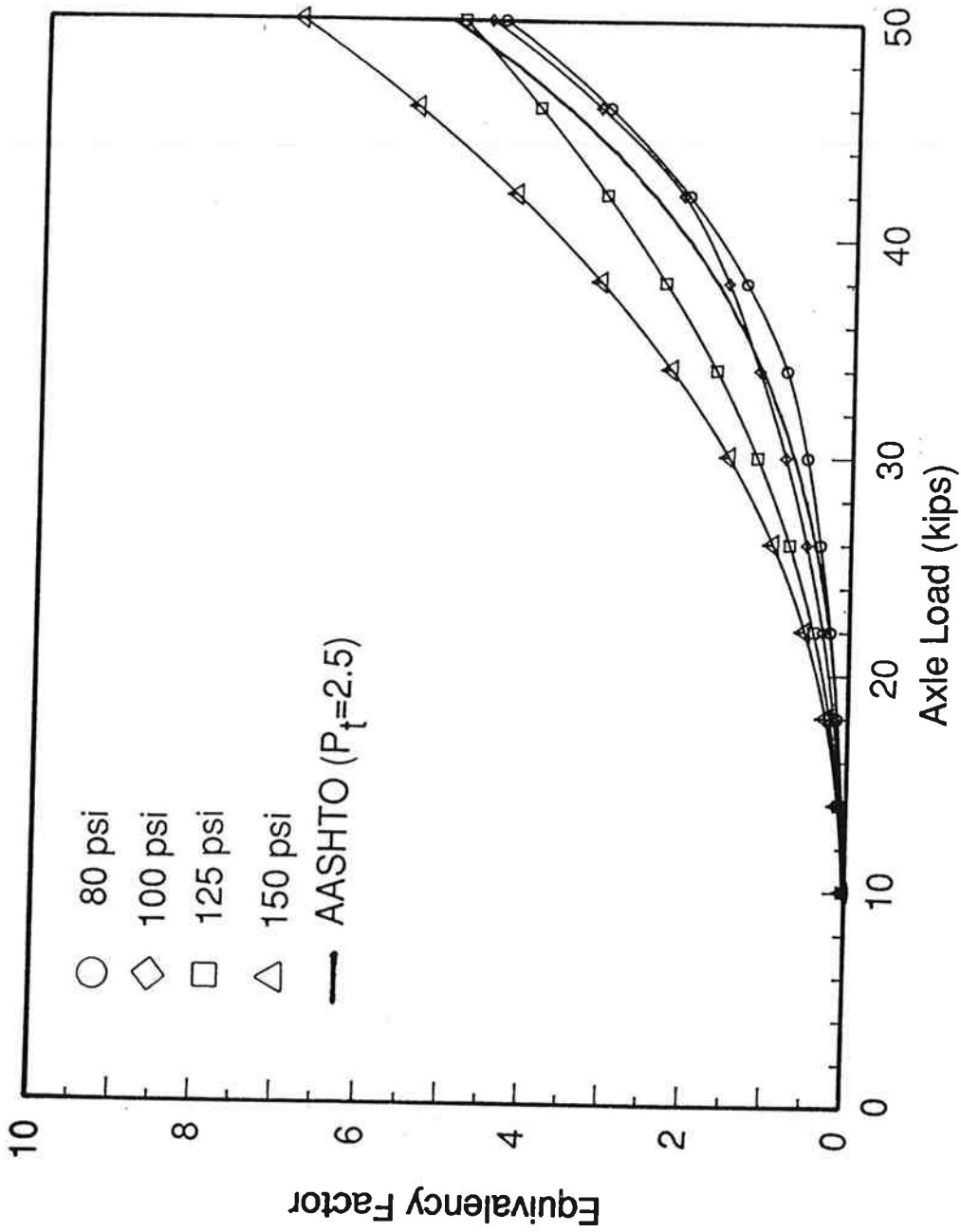
(b) Single Axle, Dual Tire

Figure 5.5. Equivalency Factors for Pavement A (Continued).



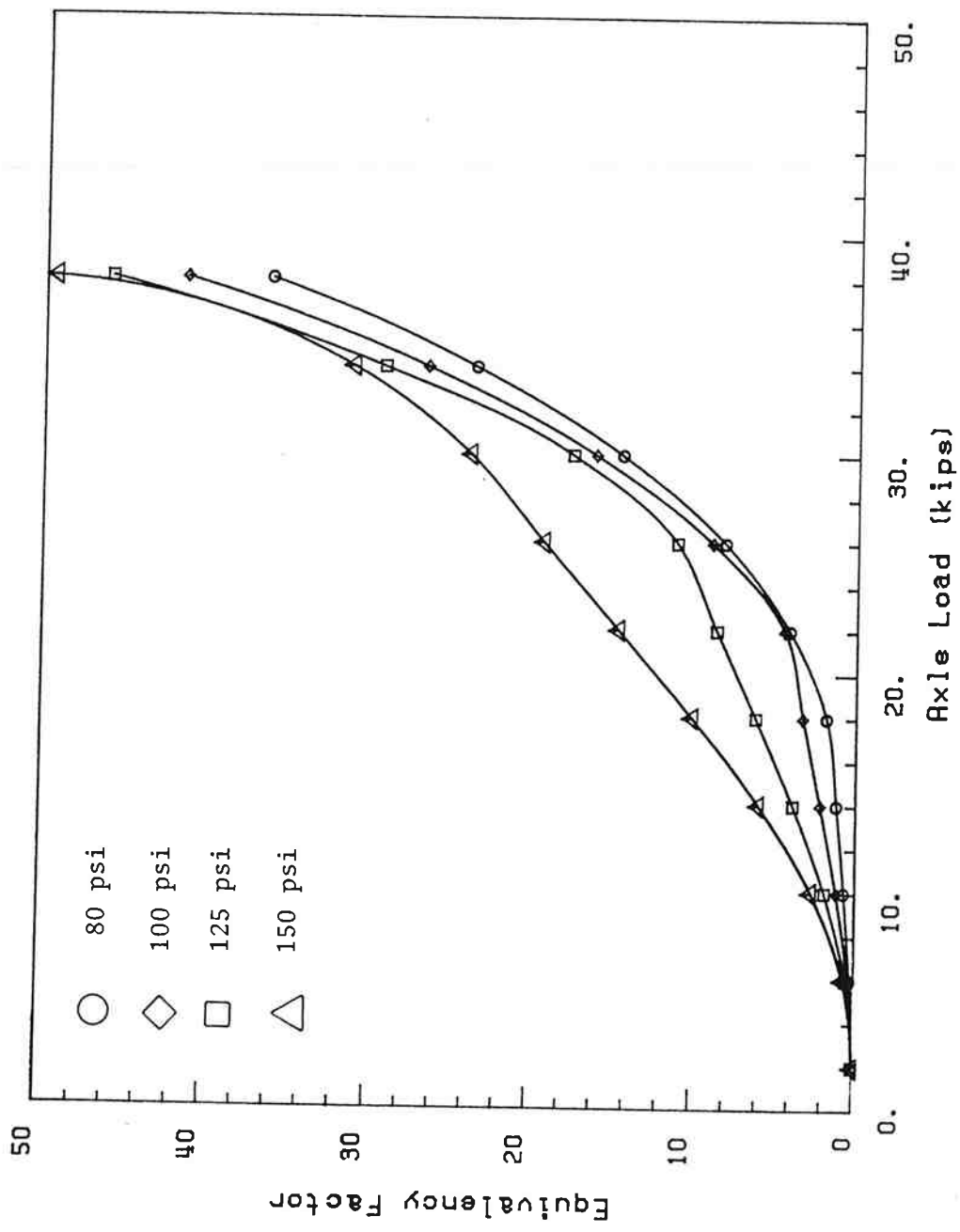
(c) Tandem Axle, Single Tire

Figure 5.5. Equivalency Factors for Pavement A (Continued).



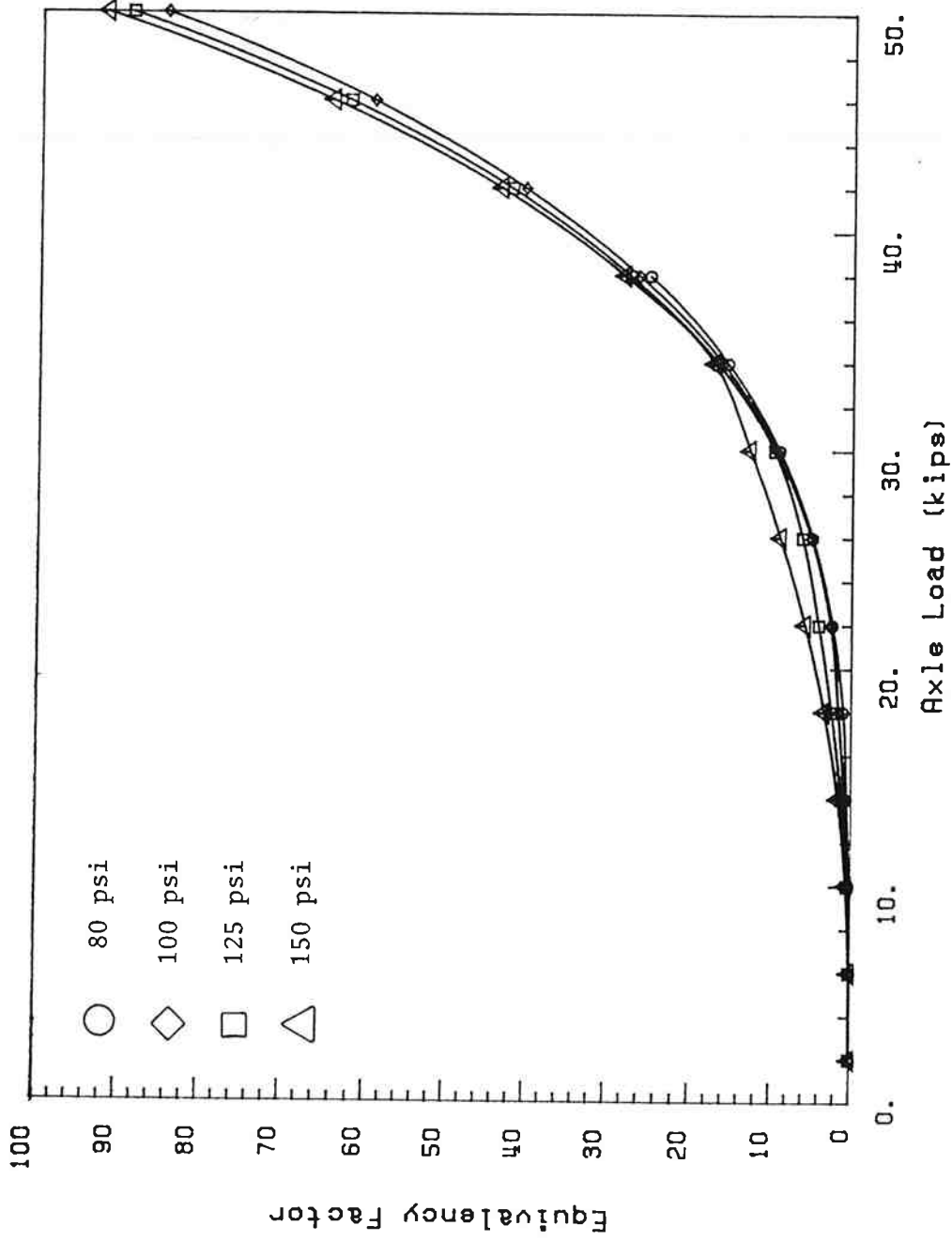
(d) Tandem Axle, Dual Tire

Figure 5.5. Equivalency Factors for Pavement A (Continued).



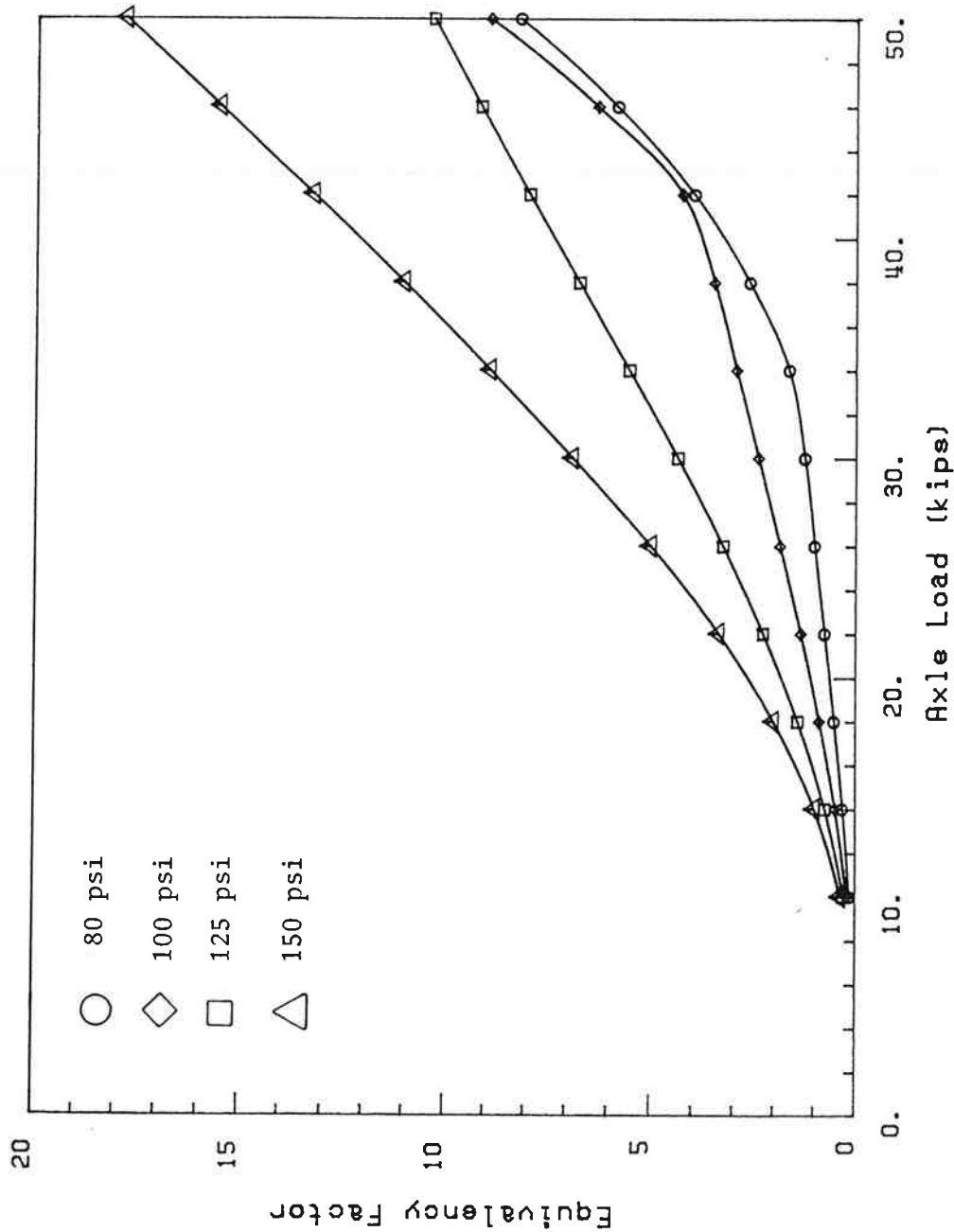
(a) Single Axle, Single Tire

Figure 5.6. Equivalency Factors for Pavement B.



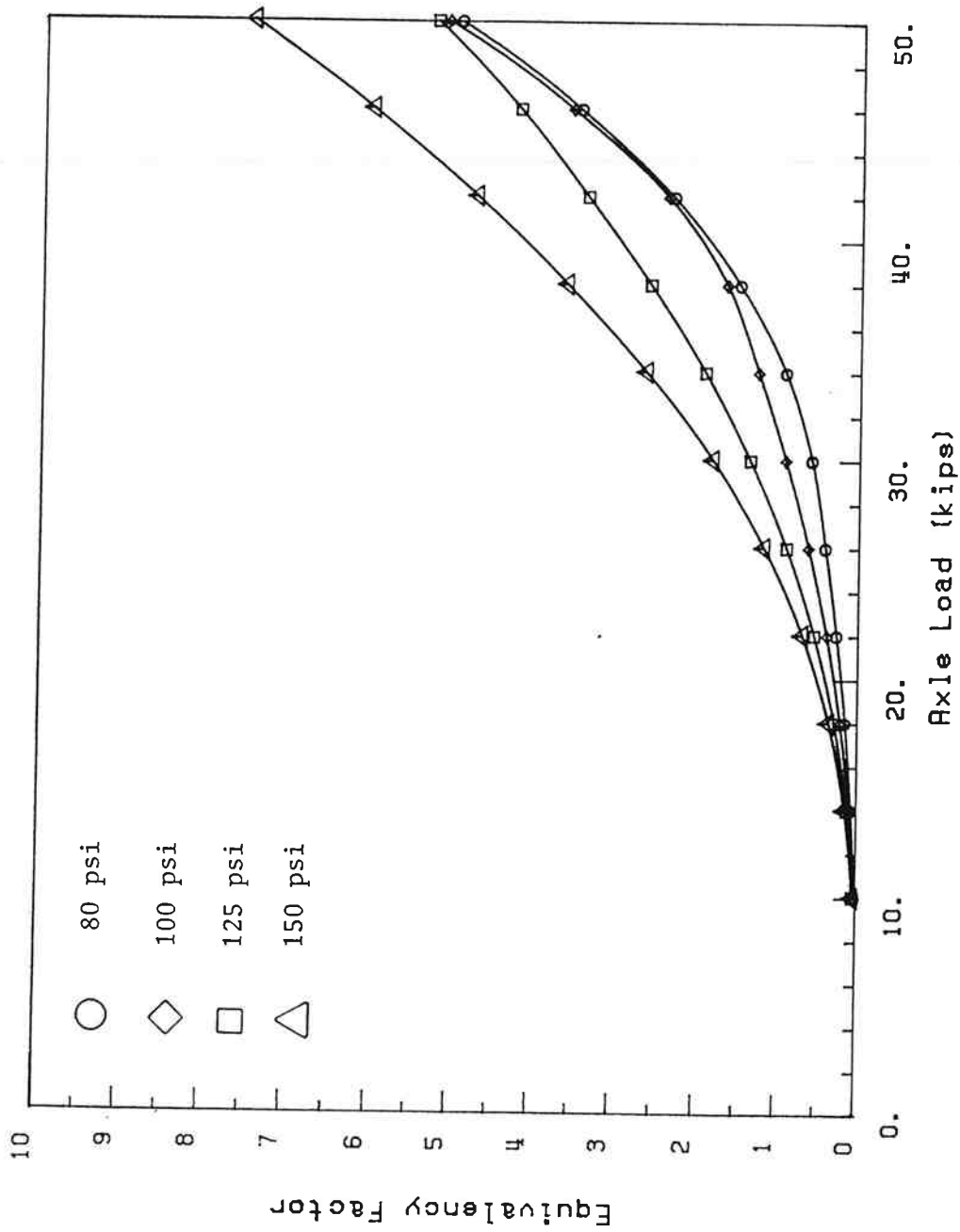
(b) Single Axle, Dual Tire

Figure 5.6. Equivalency Factors for Pavement B (Continued).



(c) Tandem Axle, Single Tire

Figure 5.6. Equivalency Factors for Pavement B (Continued).



(d) Tandem Axle, Dual Tire

Figure 5.6. Equivalency Factors for Pavement B (Continued).

factor becomes bigger as the tire pressure increases from 125 psi or 150 psi. A similar trend occurs for the tandem axles in the range of axle loads from 34 kips to 50 kips.

The results indicated that a 25% increase in tire pressure (80 psi to 100 psi) could result in a 40 to 60% increase in the equivalency factor for dual tired single axle with an 18-kip load and dual tired tandem axle with a 34-kip load. However, this theoretical analysis needs to be verified by further field studies.

In general, the equivalency factors for a tandem axle with dual tires are the smallest. That is, tandem axles and/or dual tires do less damage to the asphalt concrete pavement than single axles and/or single tires.

A comparison of the theoretical equivalency factors developed in this study and AASHTO factors (14) is illustrated in Figure 5.5(b) and (d). For single axle dual tires, the theoretical equivalency factors developed in this study are significantly greater than the AASHTO factors for the given axle load and tire pressure ranges. For tandem axle dual tires, however, the AASHTO equivalency factors are greater for a tire pressure of 80 psi and 100 psi (above an axle load of 34 kips). The equivalencies developed in this study for tandem axle dual tires and pressures of 125 and 150 psi are greater than the AASHTO equivalencies.

It can be concluded that the effect of increased tire pressure on asphalt concrete pavement is significant. Fatigue failure of the asphalt layer seems to be the main distress type due to the increased tire pressure. This means that the equivalency factor based on the tensile strain at the bottom of the asphalt concrete base layer is greater than that based on the compressive strain at the top of the subgrade, except for the range of

extremely heavy axle loads. However, it should be noted that the analysis used here does not account for increased asphalt concrete layer deformation. This problem is addressed below.

5.4.3 Rut Depth

In order to predict the rut depth due to the increased tire pressure, the results from creep test, physical properties of asphalt cement used, vertical compressive stress (shown in Figure 5.2), and the pavement structures given in Figure 4.6 were used. The Shell method was employed to predict the rut depth of the given pavement structures under tire pressure of 80 psi (i.e., assumed tire pressure used in previous pavement design) and 125 psi (possible tire pressure for future pavement design).

According to Van de Loo (37), the permanent deformation in the asphalt layer can be calculated by the following equation;

$$\Delta = C_M H_o \frac{\sigma_{avg}}{S_{mix}} \quad (5-1)$$

where Δ = reduction in layer thickness,
 C_M = correction factor for the so-called dynamic effect, which takes into account the differences between static (creep) and dynamic (rutting) behavior [this factor depends on the type of asphalt concrete mix and must be determined empirically],
 H_o = design thickness of the asphalt layer,
 σ_{avg} = average stress in the pavement under the moving wheel, and
 S_{mix} = value of stiffness of the mix at $S_{bit} = S_{bit,visc}$.

The rut depth increases as either the average stress increases or the S_{mix} decreases, according to Eq. (5-1).

As indicated by Van de Loo (40), it is essential that the creep curve which is used as an input into the calculation procedure is representative of the mix as it will be present in the pavement. Since the creep behavior (i.e., slope of the curve) of laboratory prepared specimens may be quite different from that obtained on cores from pavements, core samples should be obtained shortly after construction and used for the creep test. Because of this, the prediction of rut depth with laboratory fabricated specimens may not be representative. However, laboratory prepared specimens can be used to determine the ranking of different mixes. The procedure to calculate the rut depth according to the Shell method is illustrated in Appendix E in detail. As demonstrated in Appendix E, the percent increase in rut depth of asphalt layer is approximately the same as percent increase in tire inflation pressure.

6.0 CONCLUSIONS AND RECOMMENDATIONS

6.1 Summary

The existing operating characteristics of Oregon's trucks, including levels of tire pressures and tire sizes, were surveyed and analyzed. The results of the survey showed that 87% of the tires were of radial construction. The average measured (hot) tire pressures of the radial and bias tires were 102 and 82 psi, respectively. The size of most tires was 11 in. wide with a rim diameter of 24.5 in. (i.e., 11/80 R 24.5 or 11-24.5). The average tread depth of the radial tires was slightly greater than that of the bias tires.

In order to evaluate the mix design criteria used by OSHD, aggregate from four different sources was used. Six different aggregate gradations including the Fuller maximum density gradation were tested. A simple method of creep testing which used a data acquisition system and a personal computer was performed on mix samples. These creep test results were used with the Shell method to predict rutting performance of hypothetical pavement structures. Correlation analyses were made for the mix samples between the creep behavior and the mix design criteria.

A pavement analysis program (ELSYM5) for microcomputers was used to investigate the effect of higher truck tire pressures on asphalt pavements. Theoretical equivalency factors were developed taking into account observed levels of tire pressure and typical asphalt concrete pavement structures found in Oregon.

6.2 Conclusions

The major conclusions of this study are:

- 1) Radial tires are most often used on long-haul trucks. In this study nearly 90% of the truck tires checked were of the radial type.
- 2) Average tire pressures (hot) currently used on long-haul trucks are generally close to the average of the tire manufacturer's maximum recommended tire pressures (cold).
- 3) Many trucks operate with tire pressures greater than those used in the 1959 AASHO road test. Of the tires sampled in this study, 67% had measured (hot) tire pressures over 100 psi (assumed maximum hot inflation pressure of tires used in the AASHO road test), and 93% had manufacturer's maximum recommended cold inflation pressures exceeding 80 psi (assumed maximum of manufacturer's recommended cold inflation pressures for tires used in the AASHO road test).
- 4) Fatigue failure due to tensile strain is a major type of distress in asphalt concrete pavements that results from increased tire pressure. For this study, tensile strain effects were determined using load equivalency factors determined by a computer program using a five-layer elastic analysis system.
- 5) Theoretical load equivalency factors increase 40 to 60% from a tire pressure increase of 25% (from 80 to 100 psi) for either a tandem axle with dual tires and a 34-kip load, or a single axle with single tires and an 18-kip load. For this study, reference was to a single axle with dual tires, an 18-kip load, and 80 psi tire pressure.
- 6) Hveem Stabilometer test results have little relationship to creep stiffness values. Creep tests made for this study have shown that a

mix with a high Hveem stability may not have better resistance to creep deformation than a mix with low stability.

- 7) Creep stiffness test results have some relationship to asphalt concrete mix gradations. In this study, the creep stiffness increased when either the voids in the mineral aggregate increased or the percentage of fines passing the #200 sieve decreased. For the aggregates without lime treatment, the creep stiffness increased when either the percent of rock passing the #10 sieve increased or the percent of aggregate passing the 1/4-in. screen decreased. For the aggregates with lime treatment, the creep stiffness increased when either the percent passing the 1/4-in. screen increased or the percentage of aggregate passing the #10 screen decreased.
- 8) The Fuller maximum density gradation is not acceptable for use in asphalt concrete paving mixtures subject to high tire pressures and loads. In this study, mixtures with gradations at or near the Fuller gradation:
 - a. had low stiffness,
 - b. had unacceptably low voids in mineral aggregate (VMA) values, and
 - c. had durability characteristics based on the Index of Retained Strength and/or Resilient Modulus Ratio lower than the acceptable minimum.
- 9) The rut depth predicted in an asphalt concrete surface layer becomes greater as the tire pressures increase. In this study the Shell method was used for the theoretical analysis of the effects of increased tire pressures on rut depth.

6.3 Recommendations

In order to control the effects of increased tire pressures on asphalt concrete pavements, the following recommendations are made:

- 1) This study has shown that the average hot tire pressure on long-haul trucks is approximately equal to the average of the manufacturer's maximum recommended cold inflation pressures. Consequently, limiting the maximum cold inflation pressure may be effective in limiting the average hot inflation pressure. Further study is needed to find this limiting value.
- 2) Dual tires, rather than single tires, are recommended for both single and tandem axles. In this study, load equivalency factors indicate that for a given load, and regardless of tire width; dual tires spread heavy loads over the pavement more effectively and reduce pavement damage.
- 3) Creep testing should be investigated and applied in the design of asphalt concrete mixtures. This will require a study to determine a minimum acceptable creep test value for the design of mixtures. This minimum allowable creep value should be specified for future pavement mixture designs.
- 4) Target gradations for the design of Oregon Class "B" and "C" dense-graded asphalt concrete mixtures should be modified. The percentages of aggregate passing the 1/2-in. and 1/4-in. sieves should be equal to or less than the Fuller's maximum density gradation. This will require a change in the asphalt concrete mixture specification grading requirements. Changes are needed for both the 3/4-

in. to 1/4-in. stockpiled coarse aggregates and the percentage of rock passing the 1/2-in. screen.

- 5) Specified gradations for all asphalt concrete mixtures should be limited to a maximum of 7.0% passing the #200 sieve.
- 6) More investigation is needed to determine the effect of asphalt grade, asphalt modifiers, and mix additives on the resistance to pavement deformation of asphalt concrete mixtures.
- 7) Pavement structural sections for asphalt concrete surfacing and heavy traffic loading should be evaluated for predicted rut depth using the Shell procedures.

7.0 REFERENCES

1. Druhan, W.T., "Federal Weight-Distance Tax: An Old Tax as Modern as Today," AASHTO Quarterly, Vol. 63, No. 3, July 1984.
2. _____, "Rolling Thru Oregon," Oregon Department of Transportation, Salem, 1985.
3. Paxon, D.S. and J.P. Glickert, "Values of Overweighting to Intercity Truckers," TRB Record 889, pp. 33-37, Washington, DC, 1982.
4. Asa Sharp, III, "Truck Tire Pavement Interaction," Proceedings, A Symposium/Workshop on High Pressure Truck Tires, Austin, TX, February 1987.
5. Roberts, F.L. and R.L. Lytton, "Summary of Findings from Texas Studies on Tire Pressures," Texas Transportation Institute, January 1985.
6. Wang, M.C. and R.P. Anderson, "Load Equivalency Factors of Triaxle Loading for Flexible Pavements," TRB, Transportation Research Record 810, 1981, pp. 42-49.
7. Terrel, R.L. and S. Rimsritong, "Pavement Response and Equivalencies for Various Truck Axle and Tire Configurations," TRB, Transportation Research Record 602, 1976, pp. 33-38.
8. Yoder, E.J. and M.W. Witczak, "Principles of Pavement Design, 2nd Edition," John Wiley & Sons, Inc., 1975.
9. Marshek, K.M., H.H. Chen, R.B. Connell, and C.L. Saraf, "Effect of Truck Tire Inflation Pressure and Axle Load on Flexible and Rigid Pavement Performance," TRB, Transportation Research Record 1070, 1986, pp. 14-21.
10. Marshek, K.M., H.H. Chen, R.B. Connell, and W.R. Hudson, "Experimental Determination of Pressure Distribution of Truck Tire-Pavement Contact," TRB Transportation Research Record 1070, 1986, pp. 9-14.

11. Deacon, J.A., "Load Equivalency in Flexible Pavements," Proceedings, the Association of Asphalt Paving Technologist, Vol. 38, 1969.
12. Southgate, H.F., R.C. Deen, and J.H. Havens, "Analysis of Tandem Axle Loads by Elastic Theory," TRB, Transportation Research Record 671, 1978, pp. 57-63.
13. Halim, A.O.A. and F.F. Saccomanno, "Axle Load Limits in Ontario: Long Term Analysis," TRB, Transportation Research Record 1038, 1985, pp. 26-33.
14. _____, "AASHTO Guide for Design of Pavement Structures: 1986," American Association of State Highway and Transportation Officials, Washington, DC, 1986.
15. Bell, C.A. and M. Krukar, "Selected Results from the First Three Years of the Oregon Automatic Vehicle Monitoring Demonstration Project," Paper for Presentation and Publication at the Transportation Research Board Annual Meeting, 1987.
16. Havens, J.H., H.F. Southgate, and R.C. Deen, "Fatigue Damage to Flexible Pavements under Heavy Loads," TRB, Transportation Research Record 725, 1979, pp. 15-22.
17. Hicks, R.G., R.D. Layton, and S. Glover, "Evaluation of Increased Truck Size and Mass on Pavement Life and Design Thickness," TRB, Transportation Research Record 671, 1978, pp. 46-53.
18. Monismith, C.L., N. Markevich, and R. Yüce, "An Analysis of Pavement Damage Resulting from Increased Axle Loads and Tire Pressures," Paper presented at Twenty-First Paving and Transportation Conference, The University of New Mexico, Albuquerque, NM, January 10-11, 1984.

19. Barker, W.R. and Y.T. Chou, "Improving the Distribution and Reducing the Magnitude of Pavement Damage," Report No. FHWA/RD-80/025, U.S. Army Waterways Experiment Station, Vicksburg, MS, August 1980, 68 pp.
20. Southgate, H.F., R.C. Deen, and J.G. Mayes, "Strain Energy Analysis of Pavement Designs for Heavy Trucks," UKTRP-82-23, November 1982.
21. Finn, F.N., C.L. Monismith, and N.I. Markevitch, "Pavement Performance and Asphalt Concrete Mix Design," Proceedings, The Association of Asphalt Paving Technologists, Vol. 52, pp. 121-150, 1983.
22. Shell International Petroleum Company Limited, "Shell Pavement Design Manual," London, 1978.
23. Hicks, R.G. and C.A. Bell, "Evaluation of Oregon State Highway Division Asphalt Mix Design Procedures," Transportation Research Report 85-1, Oregon State University, February 1985.
24. WASHTO, "Asphalt Pavement Rutting in the Western States," Western Association of State Highway and Transportation Officials, May 1984.
25. Epps, J.A., J.W. Button, and B.M. Gallaway, "Paving with Asphalt Cements Produced in the 1980s," TRB, NCHRP Report 269, December 1983.
26. Brown, S.F., "An Introduction to the Analytical Design of Bituminous Pavements," Department of Civil Engineering, University of Nottingham, England, 1980.
27. Gough, V.E., "Structure of the Pneumatic Tire," Mechanics of Pneumatic Tires, National Highway Traffic Safety Administration, U.S. Department of Transportation, Washington, DC, 1981, pp. 217.
28. Cooper, L.C., "Radial Truck Tire Trends," SAE Technical Paper Series 851463, 1985.

29. Wong, J.Y., "Theory of Ground Vehicles," John Wiley & Sons, Inc., New York, 1978, p 5.
30. Chbukgil, A., R. Ridout, and D. Ross, "Recent Developments in Truck Technology: Potential for Improved Energy Efficiency in Long-Haul Trucking," Transportation Forum, Vol. 2-3, p. 57.
31. Van de Loo, P.J., "Creep Testing, A Simple Tool to Judge Asphalt Mix Stability," Proceedings, The Association of Asphalt Paving Technologists, Vol. 43, 1974, pp. 253-284.
32. Hills, J.F., "The Creep of Asphalt Mixes," Journal of the Institute of Petroleum, Vol. 59, No. 570, November 1973, pp. 247-262.
33. Grob, H., "Recommendations for the Performance of Unconfined Statical Creep Test on Asphalt Specimens," Auszug aus der Mitteilung Nr. 37, Colloquium 77, Institut für Strassen-, Eisenbahn- und Felsbau an der Eidgenössischen Technischen Hochschule Zürich, September 1977.
34. Björklund, "Some Studies of the Behaviour of Asphalt Mixes with Reference to Compaction, Heat Transfer and Repeated Loading," Bulletin 1984:1, Department of Highway Engineering, Royal Institute of Technology, Stockholm, Sweden, 1984.
35. Brown, S.F. and M.S. Snaith, "The Permanent Deformation Characteristics of a Dense Bitumen Macadam Subjected to Repeated Loading," Proceedings, Association of Asphalt Paving Technologists, Vol. 43, 1974, pp. 224-252.
36. Bolk, H.J.N.A., "Prediction of Rutting in Asphalt Pavements on the Basis of the Creep Test," Proceedings, Fifth International Conference on the Structural Design of Asphalt Pavements, The University of Michigan and the Delf University of Technology, August 1982, pp. 303-320.

37. Van de Loo, P.J., A Practical Approach to the Prediction of Rutting in Asphalt Pavements: The Shell Method," TRB, Transportation Research Record 106, 1976, pp. 15-21.
38. Laboratory Manual of Test Procedures, Laboratory Manual, Vol. 1, Material and Research Section, Highway Division, Oregon Department of Transportation, Salem, March 1978.
39. The Asphalt Institute, "Mix Design Methods for Asphalt Concrete," MS-2, May 1984.
40. Van de Loo, P.J., "The Creep Test: A Key Tool in Asphalt Mix Design and in the Prediction of Pavement Rutting," Proceedings, the Association of Asphalt Paving Technologists, Vol. 47, 1978, pp. 522-557.
41. _____, "Firestone Light Truck Tire Sales Handbook,"
42. Kopperman, S., G. Tiller and M. Tseng, "ELSYM5: Interactive Microcomputer Version," User's Manual: IBM-PC and Compatible Version, Report to Federal Highway Administration, Office of Implementation, FHWA-RD-85, September 1985.
43. Brown, James L., "Tire Pressure Issues - State Highway Agencies Viewpoint," Proceedings, A Symposium/Workshop on High Pressure Truck Tire, Austin, TX, February 1987.

APPENDIX A

CREEP TEST PROCEDURE

This section documents the creep testing equipment and procedures used in the acquisition of data required for this report. Equipment available in the laboratory where the testing was performed was used wherever possible. It is the opinion of the authors that the equipment and procedures described in this appendix were adequate for this experiment, though they may not be the most efficient for the creep test procedure. Indeed, many diverse combinations of testing machinery and methods may achieved satisfactory results.

1.0 SCOPE

1.1 This test provides information about the creep characteristics of asphalt concrete mixtures. Creep is axial strain due to elastic and plastic deformation in a cylindrical pavement specimen under a constant axial load.

2.0 APPARATUS

- 2.1 Abrasive powder for the lapping of test specimen ends. For this experiment HALCO medium grade aluminum dredge powder was used.
- 2.2 A smooth flat plate for the lapping of the test sample ends. An 18-in. long by 16-in. wide by 1/4-in. thick glass plate was used in this study.
- 2.3 A grease capable of lubricating the sample end to platen interface. Vacuum grease was utilized in this study.
- 2.4 An instrument capable of measuring the sample height to the nearest

- 0.01 mm (0.001 in.). In this study a caliper with a dial readout was used.
- 2.5 Smooth flat platens. The lower or movable platen should be of at least 25 mm (1 in.) larger diameter than the sample to be tested. For this experiment standard platens used in soil consolidation testing were utilized.
- 2.6 A stand capable of holding the tip of the transducer over the face of the movable platen. A stand was fabricated from miscellaneous laboratory hardware for this study.
- 2.7 A device capable of exerting a constant .1 MPa (14.5 psi) \pm 3% axial pressure on the test specimen for at least 3 hours. For the tests performed for this report, a Karol-Warner Model 352 pneumatic soil consolidation loading device with an integral air pressure regulator was used.
- 2.8 A means of measuring the axial deformation in the test sample. For this study, a TransTek Model 351-000 gaging transducer provided a voltage output proportional to the axial displacement of the sample.
- 2.9 A means of measuring the internal temperature of a sample. In this experiment, a YSI Model 44004 thermistor provided a resistance value inversely proportional to sample core temperature.
- 2.10 A data collection and processing system capable of performing periodic calculations on the outputs from both the transducer and the thermistor. This equipment should provide the sample's temperature and deformation values at discrete time intervals. In this study, either a Hewlett-Packard Model 3421A or Model 3497A data acquisition

unit was used in conjunction with a Hewlett-Packard Model 85A microcomputer.

- 2.11 An environmental cabinet capable of containing and maintaining the soil consolidation device and several samples at 40°C (104°F) $\pm 1^{\circ}\text{C}$. A portal in the cabinet wall was required to pass the wires and air line from the sensors and consolidation apparatus within the cabinet to the data acquisition unit and air pressure source located externally. This experiment used a "Precision Low Temperature Incubator" manufactured by GCA Corporation. The incubator housing resembled a refrigerator and internal temperatures could be regulated between -10°C (14°F) and 50°C (122°F).
- 2.12 A source capable of supplying air at a minimum pressure of 0.1 MPa (14.5 psi) for a minimum duration, for each sample tested, of 3-1/2 hours. For this experiment the laboratory compressed air source was used.
- 2.13 An air pressure regulator and gauge capable of measuring and regulating the incoming air from the supply source to output pressures of 0 kPa, 2 kPa (0.3 psi), and $0.1\text{ MPa} \pm 3\%$ (14.5 psi). In this study the pressure regulator for a soil compaction device was used.

3.0 CALIBRATION OF TRANSDUCER

In order to determine the movement of the lower platen, and consequent axial deformation of the sample, the relationship between the voltage drop across the transducer and the displacement of the transducer tip was established. In this report the relationship will be called the LVDT calibra-

tion coefficient. It will be described as the voltage drop across the transducer in volts for displacement of the transducer tip in inches.

The LVDT calibration coefficient was determined as follows:

- 3.1 The LVDT was mounted firmly over an immobile platen.
- 3.2 The transducer leads were inserted into the data acquisition unit. This device displayed the voltage drop across the transducer.
- 3.3 Feeler gages of various thicknesses were inserted between the transducer tip and the platen. The voltage drop across the LVDT was recorded for each tip displacement.
- 3.4 A graph was plotted indicating the voltage drop in volts across the transducer on the Y-axis for the tip displacement in inches on the X-axis.
- 3.5 A linear regression was performed on the data collected in the previous step. The slope of the regression line was the LVDT calibration coefficient. For example, the LVDT used in the program shown in Figure A.1 had a calibration coefficient of 21.9103 volts/in. of tip travel. This is shown on Line 240 of Figure A.1.

4.0 TEST SPECIMENS

- 4.1 Samples were prepared for the various mix designs using the method described in AASHTO T247. No tests were performed on the samples prior to the creep test.
- 4.2 1 tablespoon of water and 1 teaspoon of aluminum dredge powder were placed on the glass plate and mixed into a paste.
- 4.3 A sample end was placed on the paste and the end was lapped in a figure-eight motion across the plate until a uniform end surface was


```

5  OPTION BASE 1
10  DIM B(3), T(20,3)
20  SETTIME 0,0
30  Q1=0.00146668
40  Q2=0.000238497
50  Q3=0.000000100533
51  IMAGE 3X,"TIME",2X,"TEMP1",
    ,2X,"TEMP2",2X,"TEMP3,"
52  PRINT USING 51
53  IMAGE 3X,"SEC",4X,"DEG C",3X
    ,"DEG C",3X,"DEG C"
54  PRINT USING 53
60  FOR I=1 TO 20
70  OUTPUT 709 ;"TWO3-5"
80  FOR J=1 TO 2
90  ENTER 709 ; B(J)
100  Q4=LOG(B(J))
110  T(I,J)=1/(Q1+Q4*(Q2+Q3*Q4*Q4
    )-273.15
120  NEXT J
130  OUTPUT 709 ;"OPN"
135  BEEP
140  PRINT USING 150 ; T1,T(I,J-3
    ),T(I,J-2),T(I,J-1)
150  IMAGE 2X,5D,3X,2D.2D,3X,2D.2
    D,3X,2D.2D
160  T1=TIME
170  IF T1>20*I THEN 200
180  DISP "RUNNING NOW"
190  GOTO 160
200  NEXT I
210  END

```

Figure A.1. Computer Program to Record Temperature (HP Model No. 3421A).

obtained. On a typical sample this lapping took 8 to 10 minutes per end. After lapping the sample ends were washed with water and allowed to dry.

- 4.4 The sample heights were measured in four different locations, to 0.001 in., using the calipers. These measurements were averaged to get the height of the sample.
- 4.5 The sample ends were coated with a thin film of grease.
- 4.6 One additional sample, called a dummy sample, was prepared by the guidelines in step 4.1. A small hole was drilled into the center of this sample and the thermistor inserted. The thermistor hole was sealed with yellow clay.
- 4.7 One additional dummy sample was used for setting up the loading device.

5.0 PROCEDURE

- 5.1 The loading device was placed in the environmental cabinet. A dummy sample was placed in the loading device. The external and loading device regulators were set to totally block air flow. An air line, called the source air line, was connected between the air source and the external regulator. Another line, called the regulated air line, was placed between the external and loading device regulators. The air source valve was opened, and consequently, the source air line was pressurized. The external regulator was fully opened, and as a result the regulated air line was pressurized. The loading device regulator was opened until a 0.1 MPa (14.5 psi) axial pressure was placed on the sample. This was the loading device

regulator setting for the remainder of the tests. The external regulator was closed and the dummy sample was removed from the loading device.

- 5.2 The LVDT was mounted near, but not touching, the lower platen. The LVDT leads were plugged into the data collector. The dummy sample containing the thermistor was placed in the cabinet and the thermistor leads were also plugged into the data collector.
- 5.3 The applicable program was programmed into the computer. Figure A.1 shows a program for the HP 3421A data collector. Figure A.2. shows a program for an HP 3497A machine. These programs instructed the computer to read the thermistor resistance and transducer voltage at regular time intervals. Procedures were also included in the program to tell the computer to perform calculations required to determine the sample temperature and displacement. The output, on paper tape, consisted of the time since the 0.1 MPa load was initiated in minutes in the first column, the sample temperature in the second column, and the axial displacement of the sample in the third column.
- 5.4 The environmental cabinet door was closed and the temperature control set to 40°C (104°F). The computer program was started. The time and temperature were recorded on the output tape while the deformation values remained static. The time required for the sample to reach 40°C was recorded. This interval was the time needed to heat additional samples to the test temperature.
- 5.5 When the dummy sample reached a core temperature of 40°C the cabinet was opened. The thermistor was removed from the dummy sample and

```

5  OPTION BASE 1
10  DIM B(3), T(181,3), D(181)
15  CLEAR 709
16  OUTPUT 709 ;"VR3AI10"
17  ENTER 709 ; R0
18  DISP R0
20  SETTIME 0,0
30  Q1=0.00146668
40  Q2=0.000238497
50  Q3=0.000000100533
51  IMAGE 3X,"TIME,",2X,"TEMP1,"
    ,2X,"DEFORM"
52  PRINT USING 51
53  IMAGE 3X,"SEC",4X,"DEG C",3X
    ," in."
54  PRINT USING 53
60  FOR I=1 TO 181
70  OUTPUT 709 ;"AF09AL10VR3VC2"
80  FOR J=1 TO 2
85  OUTPUT 709 ;"ASVT3"
90  ENTER 709 ; B(J)
94  IF J=2 THEN 111
95  B(J)=B(J)*10000
100  Q4=LOG(B(J))
110  T(I,J)=1/(Q1+Q4*(Q2+Q3*Q4*Q4))-273.15
111  D(I)=(B(J)-R0)/21.63 ! DISPL
    ACEMENT CALIBRATION
112  OUTPUT 709 ;"VC0"
120  NEXT J
130  OUTPUT 709 ;"VC0"
135  BEEP
140  PRINT USING 150 ; T1,T(I,1),
    D(I)
150  IMAGE 2X,5D,2X,4D.1D,2X,2D.D
    DDD
160  T1=TIME
170  IF T1>60*I THEN 200
180  DISP "RUNNING NOW"
190  GOTO 160
200  NEXT I
210  END

```

Figure A.2. Computer Program to Record Temperature and Deformation of a Specimen (HP Model No. 3497A).

attached with clay to the side of the sample to be tested. The sample to be tested was placed on the lower platen, and the upper platen was laid on the top of the sample. The air valve on the external regulator was opened just enough to cause the lower platen to rise and barely put pressure on the sample. The transducer was positioned so that its tip barely touched the lower platen, as shown in Figure A.3.

- 5.6 The environmental cabinet was closed and the internal air and sample temperature allowed to reach 40°C. This took 5 to 10 minutes.
- 5.7 Using the external regulator, a preloading stress of 2 kPa (0.3 psi) was applied to the sample for one minute.
- 5.8 The computer program was started and the 0.1 MPa (14.5 psi) pressure was applied simultaneously. This action resulted in an output tape with columns indicating the time since 0.1 MPa load application, the sample temperature, and the axial deformation of the sample.
- 5.9 After three hours under load, the external regulator was closed, the environmental cabinet opened, the LVDT lifted, and the test sample removed. A new preheated sample was placed in the loading device and the testing procedure repeated. A sketch of the layout of the testing apparatus is shown in Figure A.4.

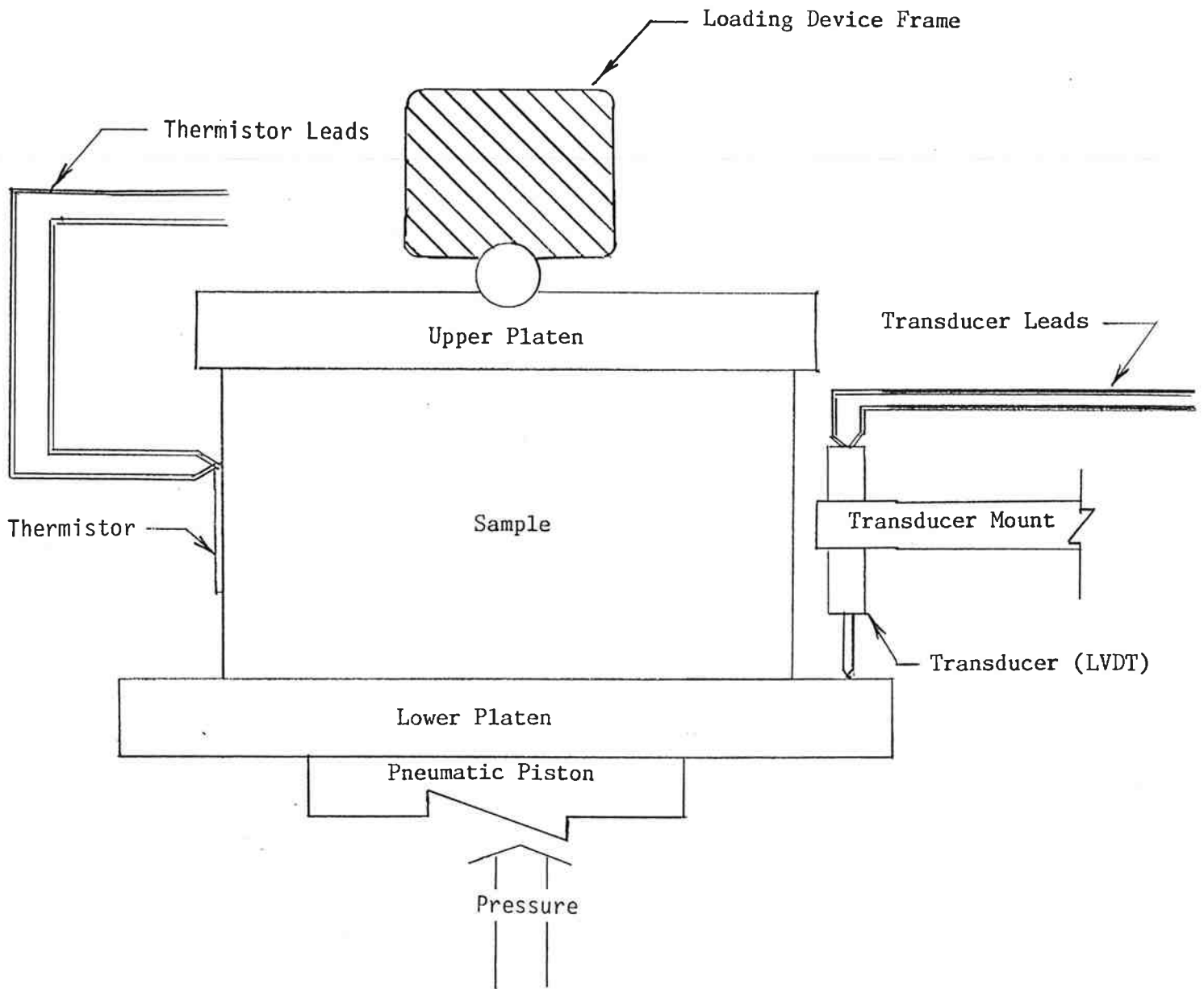


Figure A.3. Loading Device and Transducer Setup

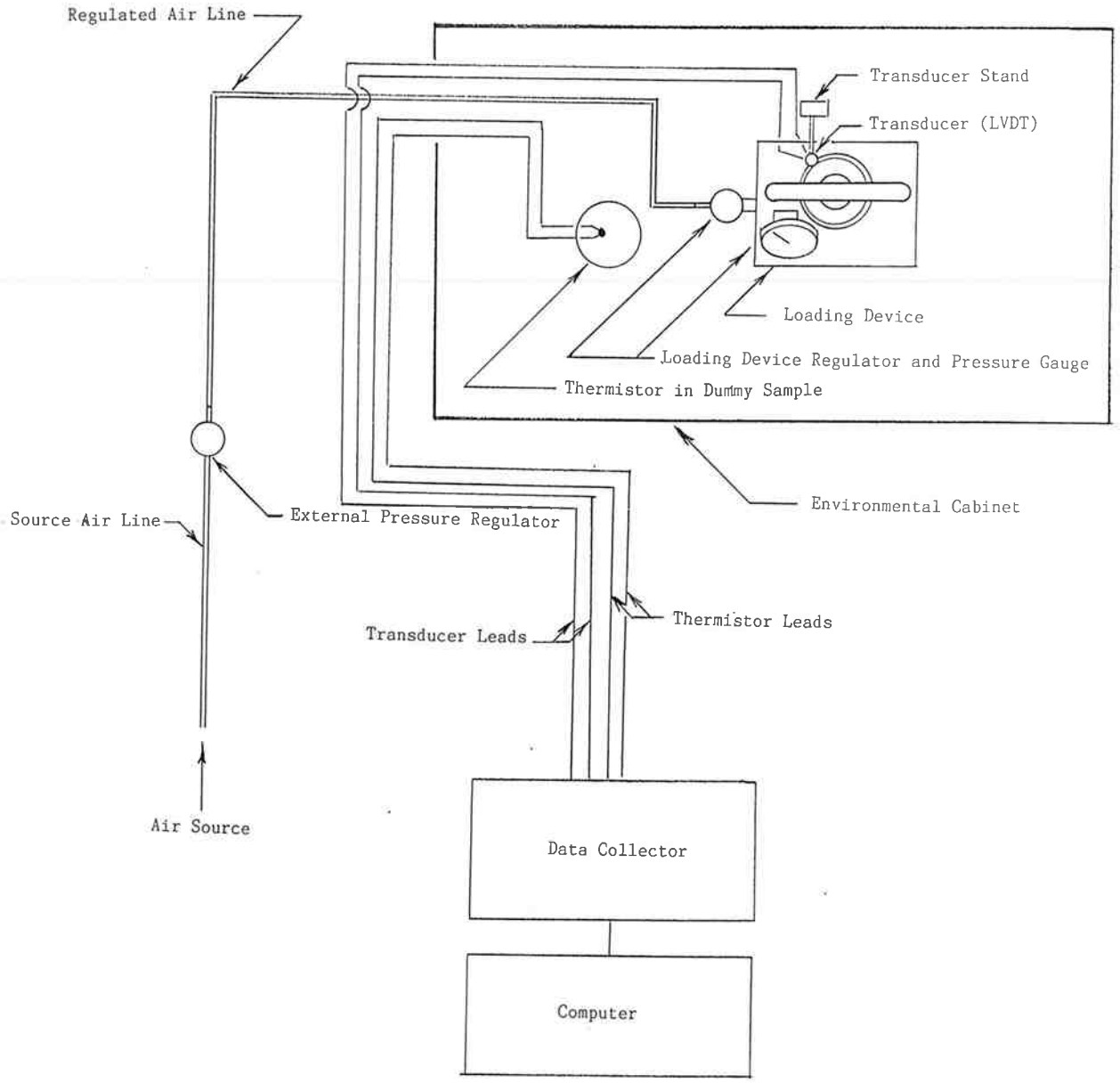


Figure A.4. Apparatus Layout

-Plan View-

COMMENTS ON APPARATUS AND PROCEDURE

If a sufficiently accurate external regulator is used, there may be no need for a pressure regulator on the loading device. All air pressure regulation could occur outside of the environmental cabinet. As a result, the loading device regulator setting procedures in step 5.1 could be eliminated.

Instead of using one transducer to monitor the movement of the lower platen, three transducers spaced 120° apart on the lower platen edge are recommended. The average value of the displacements recorded by each transducer could be calculated by a revised computer program. This average displacement value could help compensate for errors in both the linear approximation of the individual LVDT calibration coefficients and possible instrument or apparatus-induced error.

If asphalt concrete samples using large coarse aggregates are to be tested, samples larger than the 4-in. wide by 2-1/2-in. high cylinders used in this experiment may be desired. With the smaller cylinders, platen-rock-rock-platen contact may occur. This direct contact between hard and solid materials may cause unrealistically low creep test values.

The creep test as outlined in this study may not be applicable for polymer modified asphalt concrete mixtures. The large amounts of elastic deformation present in some of these mixtures may yield erroneously high creep values. If mixtures with substantial elastic properties are to be tested, considerations need to be made for elastic deformation. One approach could be to separate the reversible (elastic) and irreversible (plastic) portions of the total deformation.

The loading pressure of 0.1 MPa presently used in the creep test may not be representative of the stresses placed on pavement at the present time.

This 0.1 MPa testing pressure was standardized during 1977 in Europe. During the last decade changes in pavement construction, materials, and traffic characteristics may have made this testing pressure obsolete.

APPENDIX B
TIRE PRESSURE DATA

I. Recommended Pressure by Manufacturer.

(a) Radial Tire

	Single Tire Steering Axle		Single Tire Non-Steering Axle		Dual Tire Non-Steering Axle		Total		Accum. %
	Freq.	%	Freq.	%	Freq.	%	Freq.	%	
Pressure (psi)									
65	-	-	6	6.7	2	0.1	8	0.3	0.3
70	-	-	-	-	-	-	-	-	-
75	2	0.4	-	-	21	1.2	23	1.0	1.3
80	2	0.4	-	-	-	-	2	0.1	1.4
85	-	-	-	-	30	1.7	30	1.3	2.7
90	-	-	1	1.1	4	0.2	5	0.2	2.9
95	6	1.2	3	3.4	549	31.6	558	24.1	27.0
100	125	25.2	11	12.4	586	33.8	722	31.1	58.1
105	220	44.4	17	19.1	287	16.5	524	22.6	80.7
110	67	13.5	3	3.4	125	7.2	195	8.4	89.1
115	11	2.2	32	36.0	49	2.8	92	4.0	93.1
120	58	11.7	10	11.2	75	4.3	143	6.2	99.3
125	-	-	2	2.2	1	0.1	3	0.1	99.4
130	4	0.8	4	4.5	6	0.3	14	0.6	100.0
Total	495	100	89	100	1735	100	2319	100	
Mean	106		108		101				
Standard Deviation	7		14		8				
100% Tile	130		130		130				
90	120		120		110				
75	110		115		105				
50	105		115		100				
25	100		105		95				
10	100		95		95				
0	75		65		65				

I. Recommended Pressure by Manufacturer (Continued).

(b) Bias Tire

	Single Tire Steering Axle		Single Tire Non-Steering Axle		Dual Tire Non-Steering Axle		Total		Accum. %
	Freq.	%	Freq.	%	Freq.	%	Freq.	%	
Pressure (psi)									
60	4	8.7	-	-	4	1.4	8	2.3	2.3
65	-	-	-	-	-	-	-	-	-
70	-	-	-	-	6	2.1	6	1.8	4.1
75	1	2.2	-	-	133	46.7	134	39.2	43.3
80	2	4.3	4	36.4	3	1.1	9	2.6	45.9
85	35	76.1	6	54.5	116	40.7	157	45.9	91.8
90	-	-	-	-	5	1.7	5	1.5	93.3
95	0	0	1	9.1	4	1.4	5	1.5	94.8
100	2	4.3	-	-	8	2.8	10	2.9	97.7
105	2	4.3	-	-	6	2.1	8	2.3	100.0
Total	46	100	11	100	285	100	342	100	
Mean		84		84		81			
Standard Deviation		9		4		8			
100% Tile		105		95		105			
90		86		85		85			
75		85		85		85			
50		85		85		75			
25		85		80		75			
10		75		80		75			
0		60		80		60			

II. First Measured Pressure.

(a) Radial Tire

Pressure (psi)	Single Tire Steering Axle		Single Tire Non-Steering Axle		Dual Tire Non-Steering Axle		Total		Accum. %
	Freq.	%	Freq.	%	Freq.	%	Freq.	%	
25	-	-	-	-	1	0.1	1	0.0	-
30	-	-	-	-	2	0.1	2	0.1	0.1
35	-	-	-	-	1	0.1	1	0.0	-
40	-	-	-	-	-	-	-	-	-
45	-	-	-	-	-	-	-	-	-
50	1	0.2	-	-	3	0.2	4	0.2	0.3
55	1	0.2	-	-	6	0.3	7	0.3	0.6
60	-	-	-	-	7	0.4	7	0.3	0.9
65	2	0.4	1	1.1	6	0.3	9	0.4	1.3
70	-	-	3	3.3	12	0.7	15	0.6	2.0
75	1	0.2	2	2.2	17	1.0	20	0.9	2.9
80	7	1.4	-	-	59	3.4	66	2.8	5.7
85	5	1.0	1	1.1	58	3.4	64	2.7	8.4
90	24	4.8	6	6.6	183	10.6	213	9.1	17.5
95	24	4.8	4	4.4	160	9.3	188	8.0	25.5
100	103	20.7	13	14.3	398	23.1	514	21.9	47.4
105	93	18.7	14	15.4	206	11.9	313	13.4	60.8
110	121	24.3	17	18.7	384	22.3	522	22.3	83.1
115	60	12.0	6	6.6	135	7.8	201	8.6	91.7
120	43	8.6	14	15.4	87	5.0	144	6.1	97.8
125	10	2.0	3	3.3	20	1.2	33	1.4	99.2
130	3	0.6	5	5.5	7	0.4	15	0.6	99.8
135	-	-	2	2.2	3	0.2	5	0.2	100.0
Total	498	100	91	100	1566	100	2344	100	
Mean	106		107		102				
Standard Deviation	10		15		12				
100% Tile	132		134		136				
90	118		124		115				
75	112		118		110				
50	106		108		102				
25	100		102		95				
10	95		90		88				
0	52		64		26				

II. First Measured Pressure (Continued).

(b) Bias Tire

	Single Tire Steering Axle		Single Tire Non-Steering Axle		Dual Tire Non-Steering Axle		Total		Accum. %
	Freq.	%	Freq.	%	Freq.	%	Freq.	%	
Pressure (psi)									
30	-	-	-	-	1	0.3	1	0.3	0.3
35	-	-	-	-	1	0.3	1	0.3	0.6
40	-	-	-	-	4	1.4	4	1.1	1.7
45	1	2.2	-	-	2	0.7	3	0.9	2.6
50	1	2.2	-	-	2	0.7	3	0.9	3.5
55	1	2.2	-	-	4	1.4	5	1.4	4.9
60	1	2.2	-	-	19	6.5	20	5.7	10.6
65	3	6.5	-	-	10	3.4	13	3.7	14.3
70	1	2.2	-	-	27	9.2	28	8.0	22.3
75	3	6.5	-	-	23	7.9	26	7.4	29.7
80	7	15.2	2	18.2	54	18.5	63	18.1	47.8
85	5	10.9	2	18.2	33	11.3	40	11.5	59.3
90	8	17.4	3	27.3	44	15.1	55	15.8	75.1
95	3	6.5	1	9.1	27	9.2	31	8.9	84.0
100	6	13.0	-	-	23	7.9	29	8.3	92.3
105	2	4.3	2	18.2	7	2.4	11	3.1	95.4
110	2	4.3	1	9.1	4	1.4	7	2.0	97.4
115	-	-	-	-	4	1.4	4	1.1	98.5
120	1	2.2	-	-	2	0.7	3	0.9	99.4
125	1	2.2	-	-	1	0.3	2	0.6	100.0
Total	46	100	11	100	292	100	349	100	
Mean		86		93		82			
Standard Deviation		17		10		15			
100% Tile		125		110		125			
90		105		105		100			
75		98		105		92			
50		88		90		82			
25		78		84		74			
10		64		82		62			
0		46		82		30			

III. Tread Depth (1/32 in.).

(a) Radial Tire

	Single Tire Steering Axle		Single Tire Non-Steering Axle		Dual Tire Non-Steering Axle		Total		Accum. %
	Freq.	%	Freq.	%	Freq.	%	Freq.	%	
Tread Depth									
0-4	3	0.6	-	-	57	3.3	60	2.6	2.6
4-8	35	7.1	16	18.2	315	18.0	366	15.7	18.3
8-12	109	22.0	26	29.5	500	28.6	635	27.3	45.6
12-16	218	43.9	27	30.7	517	29.6	762	32.7	78.3
16-20	130	26.2	17	19.3	254	14.5	401	17.2	95.5
20-24	1	0.2	2	2.3	72	4.1	75	3.2	98.7
24-28	-	-	-	-	31	1.8	31	1.3	100.0
Total	496	100	88	100	1746	100	2330	100	
Mean	13		12		11				
Standard Deviation	3.4		4.3		4.9				
100% Tile	20		21		27				
90	17		17.5		18				
75	16		15		15				
50	13		12		12				
25	11		8.5		8				
10	8		6		5				
0	1		4		0				

III. Tread Depth (1/32 in.) (Continued).

(b) Bias Tire

	Single Tire Steering Axle		Single Tire Non-Steering Axle		Dual Tire Non-Steering Axle		Total		Accum. %
	Freq.	%	Freq.	%	Freq.	%	Freq.	%	
Tread Depth									
0-4	1	2.2	-	-	12	4.2	13	3.8	3.8
4-8	7	15.2	1	9.1	72	25.1	80	23.3	27.1
8-12	19	41.3	4	36.4	121	42.2	144	41.9	69.0
12-16	14	30.4	3	27.2	71	24.7	88	25.6	94.6
16-20	5	10.9	3	27.3	10	3.5	18	5.2	99.8
20-24	-	-	-	-	1	0.3	1	0.3	100.0
Total	46	100	11	100	287	100	344	100	
Mean	11		12		9				
Standard Deviation	3.7		3.7		3.4				
100% Tile	18		18		20				
90	16		16		14				
75	14		16		12				
50	10		12		9				
25	9		10		7				
10	6		7.5		4				
0	1		7		1				

IV. Tire Size.

(a) Radial Tire

	Single Tire Steering Axle		Single Tire Non-Steering Axle		Dual Tire Non-Steering Axle		Total	
	Freq.	%	Freq.	%	Freq.	%	Freq.	%
7.00 R 15LT	-	-	6	6.6	-	-	6	0.3
8.25 R 15	-	-	-	-	12	0.7	12	0.5
LT235 85 R 16	2	0.4	-	-	2	0.1	4	0.2
10/17.5	-	-	-	-	4	0.2	4	0.2
9.00 R 20	-	-	1	1.1	-	-	1	0.0
10.00 R 20	10	2.0	4	4.4	54	3.1	68	2.9
11 R 20	4	0.8	-	-	1	0.1	5	0.2
14/80 R 20	2	0.4	-	-	-	-	2	0.1
10.00 R 22	10	2.0	-	-	68	3.9	78	3.4
255/70 R 22.5	-	-	2	2.2	10	0.6	12	0.5
275/80 R 22.5	19	3.9	-	-	71	4.1	90	3.9
295/75 R 22.5	11	2.2	-	-	49	2.8	60	2.6
9 R 22.5	-	-	-	-	4	0.2	4	0.2
10 R 22.5	-	-	-	-	6	0.3	6	0.3
11 R 22.5	109	22.2	18	19.8	366	21.1	493	21.3
12 R 22.5	10	2.0	30	33.0	38	2.2	78	3.3
11/80 R 24.5	228	46.5	14	15.4	852	49.1	1094	47.2
275/80 R 24.5	30	6.1	3	3.3	67	3.9	100	4.3
285/75 R 24.5	47	9.6	1	1.1	124	7.1	172	7.4
285/80 R 24.5	4	0.8	-	-	10	0.6	14	0.6
G159	2	0.4	-	-	-	-	2	0.1
R294	2	0.4	-	-	-	-	2	0.1
15 R 22.5	-	-	12	13.2	-	-	12	0.5
Total	490	100	91	100	1737	100	2318	100

(b) Bias Tire

	Single Tire Steering Axle		Single Tire Non-Steering Axle		Dual Tire Non-Steering Axle		Total	
	Freq.	%	Freq.	%	Freq.	%	Freq.	%
7.50 x 16 LT	4	7.7	-	-	4	1.3	8	2.2
8.25-20	2	3.8	-	-	8	2.6	10	2.7
9.00-20	2	3.8	5	45.5	8	2.6	15	4.1
10.00-20	8	15.4	4	36.4	90	29.8	102	27.9
10.00-22	6	11.5	2	18.2	64	21.2	72	19.7
10-24	1	1.9	-	-	2	0.7	3	0.8
11-24.5	16	30.8	-	-	93	30.8	109	29.9
13-80	2	3.8	-	-	1	0.3	3	0.8
11-20	2	3.8	-	-	1	0.3	3	0.8
11-22.5	9	17.3	-	-	30	9.9	39	10.7
G-159	-	-	-	-	2	0.7	2	0.5
Total	52	100	11	100	302	100	365	100

V. Manufacturer.

(a) Radial Tire

	Single Tire Steering Axle		Single Tire Non-Steering Axle		Dual Tire Non-Steering Axle		Total	
	Freq.	%	Freq.	%	Freq.	%	Freq.	%
Armstrong	2	0.4	-	-	10	0.6	12	0.5
Astro	-	-	-	-	-	-	-	-
ATF	-	-	-	-	-	-	-	-
Aurora	4	0.8	-	-	21	1.2	25	1.1
Bridgestone	77	15.5	22	24.2	263	15.0	362	15.5
Bulldog	-	-	-	-	4	0.2	4	0.2
Ceat	-	-	-	-	-	-	-	-
Centennial	5	1.0	-	-	15	0.9	20	0.9
Chelin	-	-	-	-	1	0.1	1	0.0
Continental	1	0.2	-	-	-	-	1	0.0
Convoy	2	0.4	-	-	5	0.3	7	0.3
Cooper	6	1.2	-	-	6	0.3	12	0.5
Datso	-	-	-	-	4	0.2	4	0.2
Dayton	-	-	-	-	1	0.1	1	0.0
Douglas	-	-	-	-	1	0.1	1	0.0
Dunlop	8	1.6	5	5.5	10	0.6	23	1.0
Dunhill	-	-	-	-	-	-	-	-
Eitios Service	-	-	-	-	-	-	-	-
Embassy	-	-	-	-	1	0.1	1	0.0
Firestone	11	2.2	1	1.1	49	2.8	61	2.6
Fleetmiler	-	-	-	-	1	0.1	1	0.0
Fuehaff	-	-	-	-	-	-	-	-
Fulda	-	-	-	-	2	0.1	2	0.1
Geat	-	-	-	-	2	0.1	2	0.1
General	13	2.6	-	-	25	1.4	38	1.6
Goodrich	2	0.4	-	-	6	0.3	8	0.3
Goodyear	109	22.0	10	11.0	398	22.7	517	22.1
Hercules	2	0.4	-	-	2	0.1	4	0.2
Highway Air Co.	-	-	-	-	-	-	-	-
Hood	-	-	-	-	-	-	-	-
Ironman	-	-	-	-	2	0.1	2	0.1
Kelly	18	3.6	2	2.2	71	4.0	91	3.9
Laser	-	-	-	-	-	-	-	-
Leat	-	-	-	-	1	0.1	1	0.0
Lee	-	-	-	-	-	-	-	-
Long/Ranger	-	-	-	-	4	0.2	4	0.2
LTR	-	-	-	-	1	0.1	1	0.0
McCreary	-	-	-	-	-	-	-	-
Metal Air Co.	-	-	-	-	-	-	-	-
Michelin	124	25.0	33	36.3	498	28.4	655	28.0
Monarch	-	-	-	-	-	-	-	-
Multimile	-	-	-	-	4	0.2	4	0.2
Natl	-	-	-	-	-	-	-	-
Nokia	-	-	-	-	8	0.5	8	0.3
Ohtsu	18	3.6	1	1.1	29	1.7	48	2.0
Orban	-	-	-	-	-	-	-	-
Pilote	1	0.2	-	-	-	-	1	0.0
Pirelli	-	-	-	-	2	0.1	2	0.1
Powerplus	-	-	-	-	1	0.1	1	0.0
Premium	2	0.4	-	-	-	-	2	0.1
Propar	-	-	-	-	1	0.1	1	0.0
Remington	8	1.6	-	-	21	1.2	29	1.2
Reynolds	-	-	-	-	-	-	-	-
Riss	-	-	-	-	-	-	-	-
Sears	-	-	-	-	4	0.2	4	0.2
Semperit	-	-	-	-	-	-	-	-
Solar	4	0.8	-	-	4	0.2	8	0.3
Stars	-	-	-	-	4	0.2	4	0.2
Sumitomo	6	1.2	2	2.2	11	0.6	19	0.8
Supermiler	4	0.8	-	-	11	0.6	15	0.6
Tayfeng	-	-	-	-	-	-	-	-
Toyo	48	9.7	14	15.4	169	9.6	231	9.9
Trison	-	-	-	-	9	0.5	9	0.4
Truckway	-	-	-	-	-	-	-	-
Union	-	-	-	-	8	0.5	8	0.3
Uniroyal	-	-	-	-	5	0.3	5	0.2
Unocal	2	0.4	-	-	8	0.5	10	0.4
YKS	-	-	-	-	-	-	-	-
Yokohama	19	3.8	1	1.1	52	3.0	72	3.1
Total	496	100	1755	100	2342	100		

V. Manufacturer.

(b) Bias Tire

	Single Tire Steering Axle		Single Tire Non-Steering Axle		Dual Tire Non-Steering Axle		Total	
	Freq.	%	Freq.	%	Freq.	%	Freq.	%
Armstrong	-	-	-	-	4	1.4	4	1.2
Astro	-	-	-	-	2	0.7	2	0.6
ATF	-	-	-	-	4	1.4	4	1.2
Aurora	-	-	-	-	8	2.8	8	2.4
Bridgestone	-	-	-	-	22	7.7	22	6.5
Bulldog	-	-	-	-	-	-	-	-
Ceat	-	-	-	-	4	1.4	4	1.2
Centennial	1	2.2	-	-	1	0.4	2	0.6
Chelin	-	-	-	-	-	-	-	-
Continental	-	-	-	-	-	-	-	-
Convoy	-	-	-	-	-	-	-	-
Cooper	4	8.7	-	-	5	1.8	9	2.6
Datso	-	-	-	-	-	-	-	-
Dayton	-	-	-	-	1	0.4	1	0.3
Douglas	-	-	-	-	-	-	-	-
Dunlop	2	4.3	-	-	11	3.9	13	3.8
Dunhill	-	-	-	-	3	1.1	3	0.9
Eitios Service	-	-	-	-	1	0.4	1	0.3
Embassy	-	-	-	-	-	-	-	-
Firestone	3	6.5	-	-	27	9.5	30	8.8
Fleetmiler	-	-	-	-	4	1.4	4	1.2
Fuehaff	-	-	-	-	1	0.4	1	0.3
Fulda	-	-	-	-	-	-	-	-
Geat	-	-	-	-	-	-	-	-
General	-	-	1	10.0	20	7.0	21	6.2
Goodrich	5	10.9	2	20.0	19	6.7	26	7.6
Goodyear	5	10.9	3	30.0	66	23.2	74	21.8
Hercules	-	-	-	-	1	0.4	1	0.3
Highway Air Co.	-	-	-	-	3	1.1	3	0.9
Hood	-	-	-	-	2	0.7	2	0.6
Ironman	-	-	-	-	-	-	-	-
Kelly	1	2.2	-	-	5	1.8	6	1.8
Laser	-	-	-	-	2	0.7	2	0.6
Leat	-	-	-	-	-	-	-	-
Lee	-	-	-	-	2	0.7	2	0.6
Long/Ranger	-	-	-	-	-	-	-	-
LTR	-	-	-	-	2	0.7	2	0.6
McCreary	-	-	-	-	-	-	-	-
Metal Air Co.	-	-	-	-	2	0.7	2	0.6
Michelin	-	-	-	-	-	-	-	-
Monarch	-	-	-	-	2	0.7	2	0.6
Multimile	4	8.7	-	-	10	3.5	14	4.1
Natl	-	-	-	-	1	0.4	1	0.3
Nokia	-	-	-	-	2	0.7	2	0.6
Ohtsu	4	8.7	2	20.0	6	2.1	12	3.5
Orban	-	-	-	-	1	0.4	1	0.3
Pilote	-	-	-	-	-	-	-	-
Pirelli	-	-	-	-	-	-	-	-
Powerplus	-	-	-	-	-	-	-	-
Premium	1	2.2	-	-	-	-	1	0.3
Propar	-	-	-	-	1	0.4	1	0.3
Remington	2	4.3	-	-	4	1.4	6	1.8
Reynolds	2	4.3	-	-	-	-	2	0.6
Riss	-	-	-	-	1	0.4	1	0.3
Sears	1	2.2	-	-	-	-	1	0.3
Semperit	-	-	-	-	1	0.4	1	0.3
Solar	-	-	-	-	-	-	-	-
Stars	-	-	-	-	-	-	-	-
Sumitomo	4	8.7	-	-	6	2.1	10	2.9
Supermiler	-	-	-	-	1	0.4	1	0.3
Tayfeng	2	4.3	-	-	-	-	2	0.6
Toyo	2	4.3	-	-	8	2.8	10	2.9
Trison	2	4.3	-	-	-	-	2	0.6
Truckway	-	-	-	-	1	0.4	1	0.3
Union	1	2.2	-	-	6	2.1	7	2.1
Uniroyal	-	-	-	-	2	0.7	2	0.6
Unocal	-	-	1	10.0	1	0.4	2	0.6
YKS	-	-	-	-	5	1.8	5	1.5
Yokohama	-	-	1	10.0	5	1.8	6	1.8
Total	46	100	10	100	284	100	340	100

VI. (First Measured Pressure - Recommended Pressure) * 100/Recommended Pressure.

(a) Radial Tire

	Single Tire Steering Axle		Single Tire Non-Steering Axle		Dual Tire Non-Steering Axle		Total		Accum. %
	Freq.	%	Freq.	%	Freq.	%	Freq.	%	
Percent									
-80	-	-	-	-	-	-	-	-	-
-75	-	-	-	-	1	0.1	1	0.0	0.0
-70	-	-	-	-	2	0.1	2	0.1	0.1
-65	-	-	-	-	1	0.1	1	0.0	0.1
-60	-	-	-	-	2	0.1	2	0.1	0.2
-55	1	.02	-	-	2	0.1	3	0.1	0.3
-50	-	-	-	-	1	0.1	1	0.0	0.3
-45	0	0.2	-	-	6	0.3	7	0.3	0.6
-40	-	-	-	-	2	0.1	2	0.1	0.7
-35	1	0.2	-	-	8	0.5	9	0.4	1.1
-30	1	0.2	-	-	6	0.3	7	0.3	1.4
-25	6	1.2	-	-	26	1.5	32	1.4	2.8
-20	14	2.8	4	4.5	54	3.1	72	3.1	5.9
-15	34	6.9	5	5.6	105	6.1	144	6.2	12.1
-10	45	9.1	5	5.6	165	9.5	215	9.3	21.4
- 5	71	14.3	17	19.1	237	13.7	325	14.0	35.4
0	104	21.0	20	22.5	284	16.4	408	17.6	53.0
5	100	20.2	26	29.2	277	16.0	403	17.4	70.4
10	70	14.1	9	10.1	236	13.6	315	13.6	84.0
15	29	5.9	3	3.4	154	8.9	186	8.0	92.0
20	9	1.8	-	-	114	6.6	123	5.3	97.3
25	6	1.2	-	-	36	2.1	42	1.8	99.1
30	2	0.4	-	-	12	0.7	14	0.6	99.7
35	1	0.2	-	-	2	0.1	3	0.1	99.8
40	-	-	-	-	1	0.1	1	0.1	99.9
Total	495	100	89	100	1734	100	2318	100	
Mean	0.3		-0.2		1.3				
Standard Deviation	10.7		8.0		12.9				
100% Tile	33.3		16.9		41.2				
90	12.4		8.2		16.2				
75	6.7		5.2		10.0				
50	0.9		1.0		1.9				
25	-5.5		-4.3		-6.0				
10	-14.3		-13.0		-14.3				
0	-56.7		-21.6		-75.2				

VI. (First Measured Pressure - Recommended Pressure) * 100/Recommended Pressure.
(Continued).

(b) Bias Tire

	Single Tire Steering Axle		Single Tire Non-Steering Axle		Dual Tire Non-Steering Axle		Total		Accum. %
	Freq.	%	Freq.	%	Freq.	%	Freq.	%	
Percent									
-65	-	-	-	-	1	0.3	1	0.3	0.3
-60	-	-	-	-	-	-	-	-	0.3
-55	-	-	-	-	1	0.3	1	0.3	0.6
-50	-	-	-	-	2	0.7	2	0.6	1.2
-45	-	-	-	-	3	1.1	3	0.9	2.1
-40	-	-	-	-	2	0.7	2	0.6	2.7
-35	1	2.3	-	-	3	1.1	3	1.2	3.9
-30	1	2.3	-	-	7	2.5	8	2.4	6.3
-25	1	2.3	-	-	6	2.1	7	2.1	8.4
-20	1	2.3	-	-	23	8.1	24	7.1	15.5
-15	2	4.5	-	-	14	4.9	16	4.7	20.2
-10	3	6.8	-	-	19	6.7	22	6.5	26.7
- 5	7	15.9	1	9.1	33	11.6	41	12.1	38.8
0	6	13.6	2	18.2	23	8.1	31	9.1	47.9
5	6	13.6	2	18.2	42	14.7	50	14.7	62.6
10	5	11.4	-	-	25	8.8	30	8.8	71.4
15	7	15.9	3	27.3	20	7.0	30	8.8	80.2
20	3	6.8	1	9.1	23	8.1	27	7.9	88.1
25	1	2.3	2	18.2	13	4.6	16	4.7	92.8
30	-	-	-	-	3	1.1	3	0.9	93.7
35	-	-	-	-	11	3.9	11	3.2	96.9
40	-	-	-	-	4	1.4	4	1.2	98.1
45	-	-	-	-	3	1.1	3	0.9	99.0
50	-	-	-	-	2	0.7	2	0.6	99.6
55	-	-	-	-	2	0.7	2	0.6	100.0
Total	44	100	11	100	285	100	340	100	
Mean	2.5		10.0		2.2				
Standard Deviation	14.6		9.6		19.9				
100% Tile	29.4		23.3		53.3				
90	19.0		23.6		26.7				
75	13.9		17.5		14.7				
50	4.9		12.5		4.0				
25	-5.9		1.2		-9.4				
10	-17.5		-2.4		-20.0				
0	-36.4		-3.5		-64.7				

APPENDIX C

CALCULATION FOR EQUIVALENCE FACTORS

The following two equations referring, to tensile strain and compressive strain, are used to calculate equivalency factors from the results presented in Tables 4.9 and 4.10.

$$\text{Equivalency Factor} = \left(\frac{\epsilon_{tij}}{\epsilon_{tss}} \right)^m \quad (\text{C-1})$$

and

$$\text{Equivalency Factor} = \left(\frac{\epsilon_{cij}}{\epsilon_{css}} \right)^b \quad (\text{C-2})$$

where ϵ_{tij} = the tensile strain of the i axle load and j tire inflation pressure
 ϵ_{tss} = the tensile strain of the standard axle load (18 kips, single axle) and the standard tire pressure (80 psi)
 ϵ_{cij} = the compressive strain of the i axle load and j tire inflation pressure
 ϵ_{css} = the compressive strain of the standard axle load (18 kips, single axle) and the standard tire pressure (80 psi)
m = 4.5
b = 4.48

The following sections explain the background of Eqs. (C-1) and (C-2).

1. Fatigue Criteria

The relationship between fatigue failure and tensile strain can be expressed by the following equation,

$$N_f = K \left(\frac{1}{\epsilon_t} \right)^m \quad (C-3)$$

where N_f = number of repetitions to failure,
 ϵ_t = tensile strain at bottom of the asphalt concrete layer,
and
 K, m = coefficients

For the same material, the equivalency factor based on fatigue can be expressed as the ratio of N_f to n_f :

$$E.F. = \frac{N_f}{n_f} = \frac{K \left(\frac{1}{\epsilon_{tss}} \right)^m}{K \left(\frac{1}{\epsilon_{tij}} \right)^m} = \left(\frac{\epsilon_{tij}}{\epsilon_{tss}} \right)^m \quad (C-4)$$

where n_f = number of repetitions to failure at the initial tensile strain of ϵ_{tij} .

Since a common value of m ranges from 2 to 5, m value of 4.5 was chosen in this study.

2. Rutting Criteria

For a given stress state and material properties, there is a linear relationship on a $\log \epsilon_c$ (compressive strain) - $\log N$ (repetition) for soils.

So

$$N = a \left(\frac{1}{\epsilon_c} \right)^b \quad (C-5)$$

where N = number of load applications,
 ϵ_c = vertical compressive strain at the top of subgrade, and
 a, b = coefficients.

Since the equivalency factor is the ratio of the number of standard load applications (N), to the number of arbitrary load applications (n),

$$E.F. = \frac{N}{n} = \frac{a \left(\frac{1}{\epsilon_{css}} \right)^b}{a \left(\frac{1}{\epsilon_{cij}} \right)^b} = \left(\frac{\epsilon_{cij}}{\epsilon_{css}} \right)^b \quad (C-6)$$

To determine b, Eq. (C-5) is rewritten.

$$\epsilon_c = \ell \left(\frac{1}{N} \right)^m \quad (C-7)$$

$$\begin{aligned} \log \epsilon_c &= \log \ell + m \log \left(\frac{1}{N} \right) \\ &= \log \ell - m \log N \end{aligned} \quad (C-8)$$

So,

$$m \log N = \log \ell - \log \epsilon_c = \log \frac{\ell}{\epsilon_c} \quad (C-9)$$

Therefore,

$$\log N = \frac{1}{m} \log \left(\frac{\ell}{\epsilon_c} \right) \quad (C-10)$$

Finally,

$$N = \left(\frac{\ell}{\epsilon_c} \right)^{1/m} = \ell^{1/m} \left(\frac{1}{\epsilon_c} \right)^{1/m} \quad (C-11)$$

From Eqs. (C-5) and (C-11)

$$b = \frac{1}{m}$$

Shook, et al. (5th International Conference on the Structural Design of Asphalt Pavements, Proceedings, Volume 1, p. 22) list the values for ℓ and m in three methodologies:

Methodology	ℓ	m
Shell	2.8	0.25
Chevron	1.05	0.223
Nottingham	2.16	0.28

Since the Chevron method is more conservative, an m value of 0.223 is chosen in this study. So,

$$b = \frac{\ell}{m} = \frac{1}{0.223} = 4.48$$

APPENDIX D

EQUIVALENCY FACTORS FOR PAVEMENTS A AND B IN FIGURE 4.6

Table D.1. Equivalence Factors Based on Tensile Strain at the Bottom of Asphalt Concrete Base Layer.

(a) Pavement Type A in Figure 4.6

Axle Load (kips)	Single Axle			Single Axle			Tandem Axle			Tandem Axle		
	80	150	125	80	150	125	80	150	125	80	150	125
2	0.0058	0.0070	0.0082	0.0092	0.0086	0.0087	0.0007	0.0007	0.0008	0.0008	0.0008	0.0008
6	0.1803	0.2677	0.3787	0.4868	0.0382	0.0481	0.0585	0.0673	0.0673	0.0673	0.0673	0.0673
10	0.6039	1.0033	1.5878	2.2274	0.1960	0.2689	0.3545	0.4327	0.1105	0.1579	0.2153	0.2683
14	1.1610	2.0805	3.5437	5.2825	0.5147	0.7484	1.0470	1.3375	0.2683	0.4124	0.6028	0.7942
18	1.7602	3.3323	6.0048	9.3609	1	1.5181	2.2182	2.9354	0.4839	0.7846	1.2139	1.6698
22	2.3468	4.6405	8.7384	14.138	1.6429	2.5762	3.8966	5.3127	0.7405	1.2567	2.0285	2.8936
26	2.8899	5.9385	11.591	19.322	2.7749	3.9157	6.0851	8.4917	1.0233	1.8016	3.0202	4.4371
30	3.3704	7.1685	14.451	24.715	4.4793	5.7947	8.7652	12.471	1.3210	2.3985	4.1500	6.2619
34	3.7931	8.3017	17.235	30.148	6.8017	8.8100	11.928	17.235	1.6260	3.0359	5.3918	8.3188
38	4.1450	9.3234	19.873	35.502	9.6945	12.780	16.536	22.777	1.9303	3.6917	6.7214	10.574
42	--	--	--	--	--	--	--	--	--	--	--	--
46	--	--	--	--	--	--	--	--	--	--	--	--
50	--	--	--	--	--	--	--	--	--	--	--	--

(b) Pavement Type B in Figure 4.6

Axle Load (kips)	Single Axle			Single Axle			Tandem Axle			Tandem Axle		
	80	150	125	80	150	125	80	150	125	80	150	125
2	0.0080	0.0099	0.0118	0.0133	0.0088	0.0088	0.0009	0.0010	0.0011	0.0011	0.0011	0.0011
6	0.2128	0.3289	0.4830	0.6356	0.0467	0.0600	0.0756	0.0882	0.0882	0.0882	0.0882	0.0882
10	0.6433	1.1192	1.8498	2.6853	0.2211	0.3147	0.4290	0.5366	0.1329	0.1970	0.2781	0.3556
14	1.1512	2.1638	3.8657	5.9752	0.5433	0.8249	1.2005	1.5828	0.3023	0.4851	0.7383	1.0018
18	1.6513	3.2814	6.2040	10.062	1.0000	1.5906	2.4298	3.3319	0.5168	0.8809	1.4214	2.0223
22	2.1050	4.3774	8.6522	14.557	1.5751	2.5929	4.1045	5.8026	0.7571	1.3491	2.2852	3.3784
26	2.4919	5.3948	11.070	19.202	2.5289	3.7987	6.1890	8.9670	1.0090	1.8674	3.2814	5.0096
30	2.8125	6.3019	13.375	23.797	4.0397	5.3213	8.6522	12.800	1.2600	2.4082	4.3774	6.8664
34	3.0637	7.0879	15.496	28.243	6.0850	8.0028	11.463	17.230	1.5042	2.9570	5.5304	8.8875
38	3.2541	7.7503	17.430	32.434	8.6135	11.512	15.163	22.220	1.7386	3.5062	6.7217	11.023
42	--	--	--	--	--	--	--	--	--	--	--	--
46	--	--	--	--	--	--	--	--	--	--	--	--
50	--	--	--	--	--	--	--	--	--	--	--	--

Table D.2. Equivalence Factors Based on Compressive Strain at the Top of Subgrade.

(a) Pavement Type A in Figure 4.6

Axle Load (kips)	Single Axle			Single Axle			Tandem Axle			Tandem Axle			
	80	100	125	80	100	125	80	100	125	80	100	125	150
2	0.0002	0.0002	0.0002	0.0002	0.0000	0.0000	0.0000	0.0000	0.0000	0.0000	0.0000	0.0000	0.0000
6	0.0252	0.0258	0.0264	0.0271	0.0079	0.0080	0.0081	0.0081	0.0081	0.0081	0.0081	0.0081	0.0081
10	0.2265	0.2381	0.2465	0.2518	0.0764	0.0776	0.0785	0.0792	0.0819	0.0122	0.0126	0.0130	0.0037
14	0.9131	0.9901	1.0506	1.0881	0.3346	0.3419	0.3481	0.3519	0.0517	0.0532	0.0545	0.0556	0.0168
18	2.4988	2.7831	3.0251	3.1857	1.0000	1.0283	1.0518	1.0677	0.1525	0.1590	0.1636	0.1670	0.0510
22	5.4404	6.2211	6.9009	7.3852	2.3808	2.4644	2.5335	2.5807	0.3556	0.3765	0.3920	0.4014	0.1236
26	10.252	11.955	13.514	14.701	4.8766	5.0798	5.2472	5.3539	0.7110	0.7640	0.8051	0.8301	0.2573
30	17.370	20.645	23.759	26.176	8.9658	9.3908	9.7625	10.004	1.2741	1.3886	1.4814	1.5402	0.4811
34	27.301	32.971	38.609	42.981	15.227	16.068	16.787	17.263	2.1042	2.3251	2.5095	2.6299	0.8301
38	40.438	49.641	58.993	66.406	24.242	25.736	27.073	27.917	3.2655	3.6561	3.9870	4.2143	1.3454
42	--	--	--	--	--	39.313	41.483	42.981	4.8168	5.4622	6.0301	6.4169	2.0741
46	--	--	--	--	--	57.619	61.103	63.565	6.8487	7.8086	8.7118	9.3576	3.1814
50	--	--	--	--	--	81.589	87.082	90.706	9.3908	10.834	12.198	13.164	4.3959

(b) Pavement Type B in Figure 4.6

Axle Load (kips)	Single Axle			Single Axle			Tandem Axle			Tandem Axle			
	80	100	125	80	100	125	80	100	125	80	100	125	150
2	0.0001	0.0001	0.0002	0.0002	0.0000	0.0000	0.0000	0.0000	0.0000	0.0000	0.0000	0.0000	0.0000
6	0.0153	0.0157	0.0164	0.0172	0.0078	0.0079	0.0079	0.0080	0.0080	0.0080	0.0080	0.0080	0.0080
10	0.1448	0.1478	0.1505	0.1531	0.0756	0.0766	0.0774	0.0779	0.0080	0.0083	0.0088	0.0094	0.0041
14	0.6221	0.6452	0.6611	0.6708	0.3328	0.3388	0.3437	0.3473	0.0350	0.0357	0.0368	0.0382	0.0184
18	1.8023	1.9067	1.9810	2.0244	1.0000	1.0236	1.0424	1.0556	0.1060	0.1079	0.1099	0.1123	0.0560
22	4.1373	4.4576	4.7055	4.8463	2.3944	2.4625	2.5204	2.5583	0.2553	0.2610	0.2655	0.2696	0.1361
26	8.1576	8.9283	9.5699	9.9793	4.9332	5.0883	5.2471	5.3395	0.5267	0.5431	0.5542	0.5618	0.2841
30	14.408	16.035	17.448	18.341	9.1383	9.4969	9.7916	9.9793	0.9730	1.0127	1.0398	1.0556	0.5329
34	23.498	26.506	29.191	31.064	15.602	16.255	16.872	17.273	1.6551	1.7382	1.7973	1.8305	0.9220
38	36.107	41.304	45.941	49.380	25.006	26.265	27.324	27.992	2.6408	2.7978	2.9137	2.9812	1.4991
42	--	--	--	--	--	40.288	41.993	43.278	4.0016	4.2784	4.4900	4.6154	2.3179
46	--	--	--	--	--	59.233	62.154	64.216	5.8209	6.2824	6.6330	6.8562	3.4432
50	--	--	--	--	--	84.466	88.720	91.860	8.1576	8.8937	9.4606	9.8289	4.9332

APPENDIX E

PROCEDURE USING THE SHELL METHOD TO PREDICT THE RUT DEPTH IN ASPHALT CONCRETE PAVEMENTS

The following steps are used for prediction of rut depth in pavements constructed with asphalt concrete mixes according to the modified Shell method.

1. Carry out a creep test on a core sample at 40°C and apply a compressive stress of 0.1 MPa.
2. Record the deformation (Δ) with time.
3. Calculate strain (ϵ_t) and S_{mix} (see Figure E.1),

$$\epsilon_t = \frac{\Delta}{l}$$

$$S_{mix} = \frac{\sigma_o}{\epsilon_t}$$

where: l = thickness of the sample, and

$$\sigma_o = 0.1 \text{ MPa (14.5 psi).}$$

4. Determine S_{bit} at the same values of time (t) used Step 2, using Van der Poel's nomograph.
5. Plot S_{mix} vs. S_{bit} (see Figure E.2)
6. Determine the asphalt viscosity ($N \cdot s/m^2$) at the mean annual air temperature (MAAT) for the asphalt layer (see Figure E.3).
7. Calculate the viscous component of the asphalt stiffness,

$$S_{bit,vis} = \frac{3\eta}{n \cdot t_w}$$

where: η = asphalt viscosity, $N \cdot s/m^2$,

N = total number of applications of loads, and

t_w = loading duration, sec.

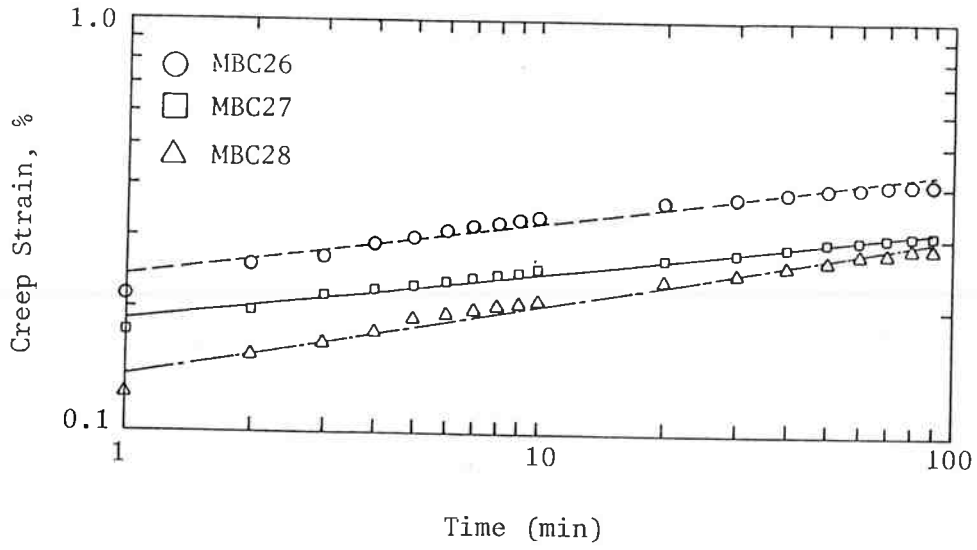


Figure E.1. Strain vs. Time

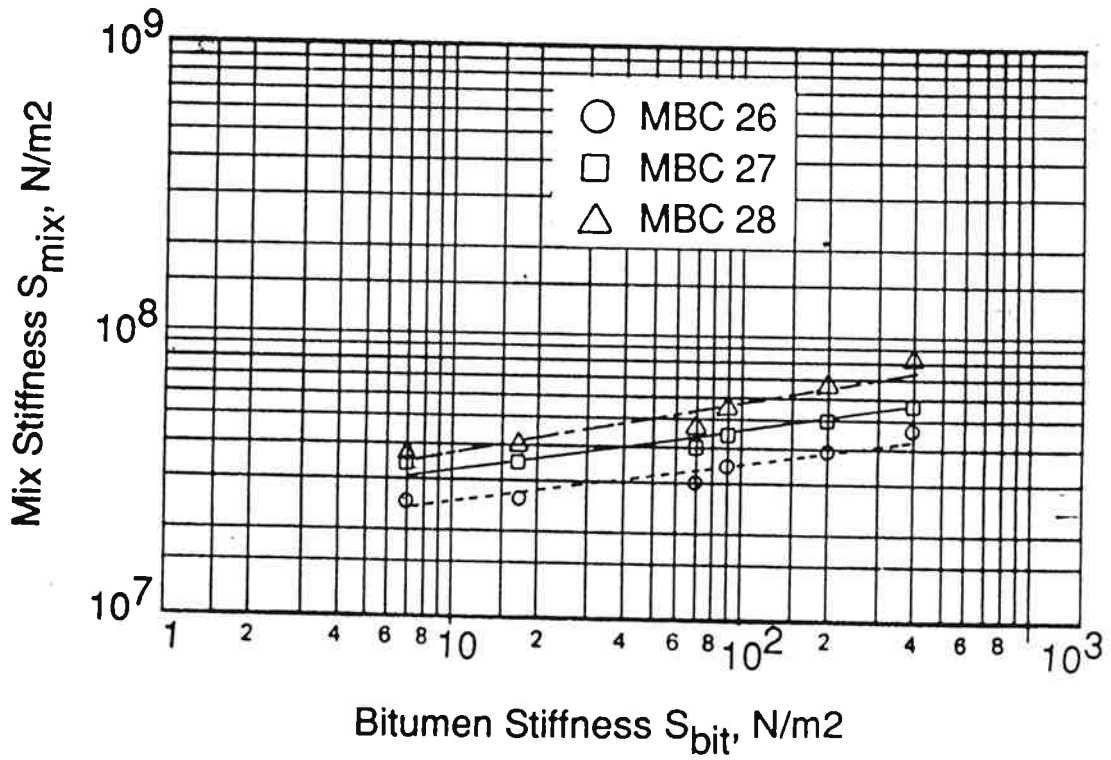


Figure E.2. S_{mix} vs. S_{bit} .

Viscosity, Ns/m^2

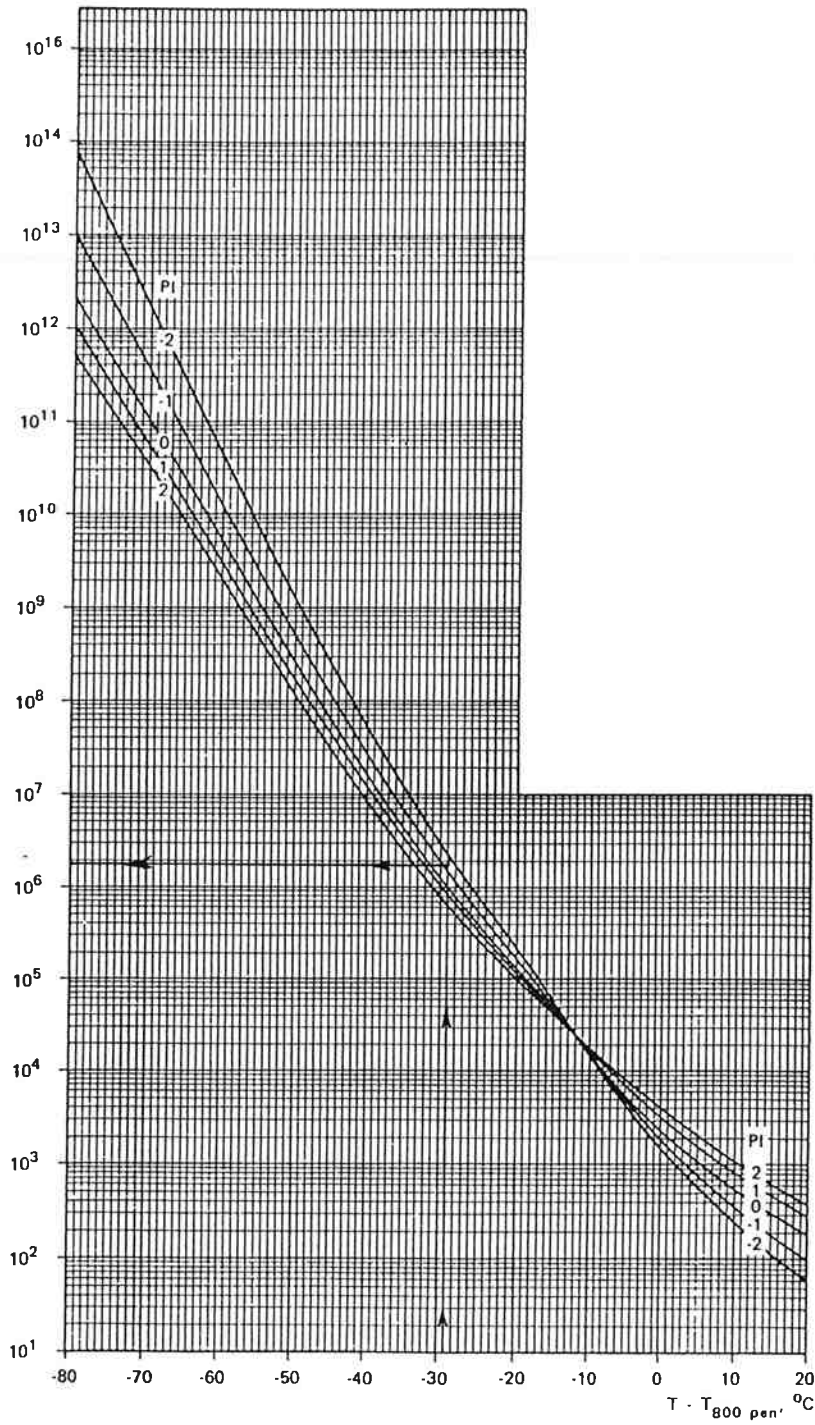


Figure E.3. Viscosity as a Function of the Temperature Difference $MAAT - T_{800 \text{ pen}}$

8. Input $S_{bit,vis}$ to the S_{mix} vs S_{bit} plot (Figure E.2) and read off S_{mix} .
9. Calculate the average vertical compressive stress in the asphalt layer using the output of ELSYM5 (see Table E.1).
10. Calculate the in-service deformation,

$$\delta_H = C_M \cdot h \cdot \frac{\sigma_{avg}}{S_{mix}}$$

where: C_M = correction factor (Table E.2) and
 σ_{avg} = average vertical compressive stress.

Example

It is assumed that the asphalt cement property of cores is the average of the original asphalt and after the rolling thin film oven test, as demonstrated in Figure E.4.

Asphalt Cement: AR-4000W, Morse Brothers Pit (Table 3.3)

$P_{25} = 51$ $SP = 49^\circ C$ $PI = -1.4$
 $N = 10^6$ $t_w = 0.0125 \text{ sec}$ (Speed = 50 mph)
 $MAAT = 20^\circ C$ $C_M = 1.2$ $h = 2 \text{ in.}$
 $\eta = 1.8 \times 10^6 \text{ N}\cdot\text{s}/\text{m}^2$

$$S_{bit,vis} = \frac{3\eta}{N \cdot t_o} = \frac{3 \cdot 1.8 \cdot 10^6}{10^6 \cdot 0.0125} = 432 \text{ Pa}$$

From Step 5, $\log S_{mix} = a + b \log S_{bit}$.

For MBC27, the coefficients of a and b are 1.401 and 0.129, respectively, from the regression analysis done on the data shown in Figure E.2. Therefore, S_{mix} is 55.1 MPa (7990 psi) at S_{bit} of 432 Pa.

From Table E.1,

$\sigma_{avg} = 70 \text{ psi}$ for a tire pressure of 80 psi

Table E.1. Average Vertical Compressive Stress in Asphalt Surface Layer (psi).

(a) Single Axle, Dual Tires

	18 kips		22 kips	
	80 psi	125 psi	80 psi	125 psi
Pavement A in Figure 4.6	70.7	108.2	71.8	109.4
Pavement B in Figure 4.6	72.6	112.8	72.9	113.2

(b) Tandem Axle, Dual Tires

	34 kips		42 kips	
	80 psi	125 psi	80 psi	125 psi
Pavement A in Figure 4.6	70.4	107.6	71.1	108.8
Pavement B in Figure 4.6	72.4	112.4	72.7	112.8

Table E.2. The Correction Factor for Dynamic Effects for Various Mix Types.

	Mix Type	C_{m-i}
Open	Sand sheet and lean sand mixes	1.6-20.0
	Lean open asphalt concrete	
	Lean bitumen macadam	1.5-1.8
Dense	Asphaltic concrete	1.2-1.6
	Gravel sand asphalt	
	Dense bitumen macadam	
	Mastic types	1.0-1.3
	Gu asphalt	
	Hot rolled asphalt	

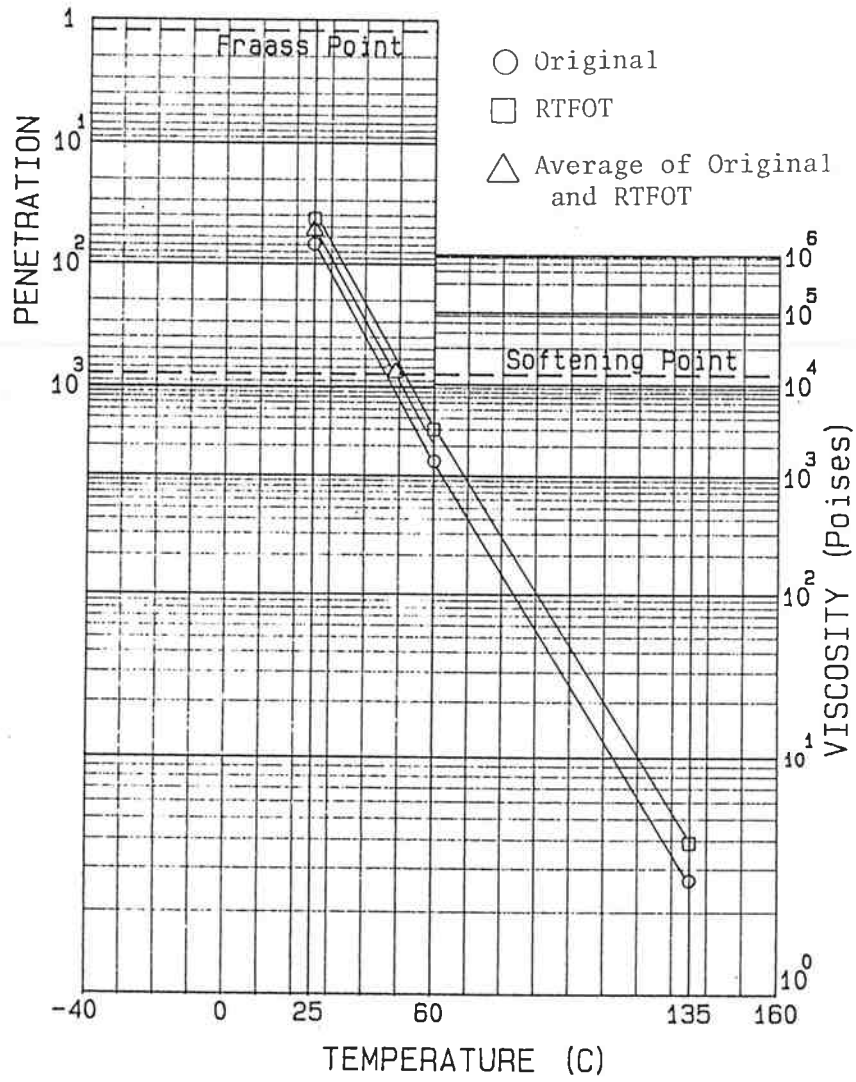


Figure E.4. Bituminous Test Data Chart.

$\sigma_{\text{avg}} = 108$ psi for a tire pressure of 125 psi
for Pavement A in Figure 4.6

$$\delta_{80} = 1.2 \times 2.0 \times \frac{70}{7990} = 0.021 \text{ in.}$$

and

$$\delta_{125} = 1.2 \times 2.0 \times \frac{108}{7990} = 0.032 \text{ in.}$$

The rut depth of asphalt surface layer increases by 52% as the tire inflation pressure increases by 56%.